Mineralium Deposita

Structural controls and metallogenic model of polyphase uranium mineralization in the Kiggavik area (Nunavut, Canada)

--Manuscript Draft--

Manuscript Number:	
Full Title:	Structural controls and metallogenic model of polyphase uranium mineralization in the Kiggavik area (Nunavut, Canada)
Article Type:	Regular Articles
Corresponding Author:	Alexis Grare, Ph.D Sorbonne Universite Paris, FRANCE
Corresponding Author Secondary Information:	
Corresponding Author's Institution:	Sorbonne Universite
Corresponding Author's Secondary Institution:	
First Author:	Alexis Grare, Ph.D
First Author Secondary Information:	
Order of Authors:	Alexis Grare, Ph.D
	Antonio Benedicto
	Julien Mercadier
	Olivier Lacombe
	Anna Trave
	Marie Guilcher
	Antonin Richard
	Patrick Ledru
	Mario Blain
	John Robbins
	Philippe Lach
Order of Authors Secondary Information:	
Funding Information:	
Abstract:	The Kiggavik area is located on the eastern border of the Paleo- to Mesoproterozoic Thelon Basin (Nunavut, Canada) and hosts major uranium mineralization in Archean basement rocks. These mineralizations display a strong structural control and share many similarities with the world-class unconformity-related U deposits of the coeval Athabasca Basin (Saskatchewan, Canada). An innovative cross-disciplinary study combining macro- to micro-scale characterization was applied to define the uranium mineral system in the Kiggavik area: observation, characterization and measurement of fractures in the field and from drillcores, petrographic and cathodoluminescence identification of fracture cements, analysis of fluid inclusions, and analysis of uranium oxides and related mineral phases through SEM, LA ICP-MS and SIMS. The analysis of fluid inclusions coupled with oriented measurements of fluid inclusions planes they constitute allow allows to link fluid circulation to a tectonic stress and therefore to bridge the gap between the micro and the macro-scales. Our results show that the first order fault/fracture network in the Kiggavik area is mainly oriented ENE-WSW and NE-SW and consists of polyphased fault zones initiated during the Thelon and Trans-Hudsonian orogenies (ca. 1900-1800 Ma). These faults were subsequently U mineralized in four stages referred to as U0, U1, U2 and U3. These different U stages,

	yield distinctive fracture, alteration and mineralization patterns, indicating different conditions of formation. U0, inferred to be of magmatic-volcanic origin, likely occurred at ca. 1830 Ma and is related to micro-brecciation and weak clay-alteration under a WSW-ENE compressional stress. This event predates intense quartz brecciation, iron oxidation and veining at ca. 1750 Ma. This silicifying event, called Quartz Breccia (QB), predates the deposition of the Thelon Basin and is of magmatic-epithermal origin, associated with anorogenic rifting and emplacement of the Kivalliq igneous suite. Circulation of Si-bearing magmatic derived fluids caused pervasive silicification of former fault zones, which in turn controlled subsequent fracture development and behaved as barriers for later U mineralizing fluids (U1 to U3). Both the U0 mineralization and the subsequent QB silicifying event reflect the importance of pre-Thelon Basin fracturing and fluid circulation events in controlling the development and location of later U mineralizing stages. U1, U2 and U3 postdate deposition of the Thelon Basin. U1 is characterized by polymetallic mineralization in reduced narrow fault zones and U2 is characterized by monometallic mineralization in oxidized wider fault zones. These two mineralization episodes are characterized by illite and sudoite crystallization and occurred under a regional strike-slip stress regime, with the direction of $\sigma 1$ evolving from WNW-ESE (U1) to NE-SW /ENE-WSW (U2); both formed between ~1500-1330 Ma and are related to circulations of Thelon-derived U-bearing basinal brines similar to the mineralizing brines at the origin of the 1600-1270 Ma unconformity-related U deposits in the Athabasca Basin. A post U2, but pre-Mackenzie dikes, NE-SW extensional stress caused normal-dextral offset of the orebodies by reactivating NNW-SSE and E-W faults. This fracturing event triggered circulation of hot (~300°C), probably acidic fluids, dequartzcifying, illitizing and bleaching the host-rock. U3 is a redistribution/reconcentration of the previous U mineralization along redox fronts, postdating MacKenzie dike (ca. 1270 Ma) and occurred through weak reopening of the pre-existing fracture network enhancing percolation of low temperature meteoric fluids during two main events at ca. 550 and 350 Ma. Our study shows that U deposits and prospects in the Kiggavik area are of mixed type: a pre-basin magmatic-volacnic U stock (U0) remobilized by post-basin basinal brines to form unconformity-related mineralization (U1 and U2), which were lately altered and remobilized by massive percolations of meteoric waters (U3). This zone demonstrates thus a mobility of U during more than 1.5 billion years and had an evolution similar to that of the world-class U district of the Athabasca Basin. A significant difference with the Athabasca Basin is however that the strongest clay alteration event, formed by illite and linked to the MacKenzie dike intrusions, postdates the main stages of mineralization (U0 to U2).
Suggested Reviewers:	Eric Potter, Doctor Research scientist, Geological survey of canada, Ottawa eric.potter@canada.ca His research interest is focused on the formation of uranium-bearing ore deposits in Canada
	Charlie Jefferson Section Head, Research Scientist, Natural Resources Canada charlie.jefferson@canada.ca Charlie Jefferson is interested about mineral resources system and spent a lot of time working on the Kiggavik area and around the Thelon basin dealing with cartographic, structural and geochemical data.
	Guoxiang Chi, Professor University of Regina guoxiang.chi@uregina.ca His research interest is focused on Mineral Deposits Geology and Geochemistry. He is specifically specialised on fluid inclusions and he worked on the Kiggavik area.

STRUCTURAL CONTROLS AND METALLOGENIC MODEL OF POLYPHASE URANIUM MINERALIZATION IN THE KIGGAVIK AREA (NUNAVUT, CANADA)

Alexis Grare[a,b] , Antonio Benedicto[c], Julien Mercadier[d], Olivier Lacombe[a], Anna Trave[e], Marie Guilcher[d], Antonin Richard[d], Patrick Ledru[b], Mario Blain[b], John Robbins[b], Philippe Lach[f]

[a] Sorbonne Université, CNRS-INSU, Institut des Sciences de la Terre de Paris, ISTeP UMR 7193, F-75005 Paris, France

[b] *AREVA Resources Canada Inc. 817-45th St West Saskatoon. SK S7L 5X2. Canada*

[c] *Université Paris Sud, UMR GEOPS, 91405 Orsay. France*

[d] *Université de Lorraine, CNRS, CREGU, GeoRessources lab, Campus Aiguillettes, Faculté des Sciences et Technologies, rue Jacques Callot, Vandoeuvre-lès-Nancy, 54506 France*

[e] *Universitat de Barcelona, Departament de Mineralogia, Petrologia i Geologia Aplicada, Facultat de Ciències de la Terra. 08028 Barcelona. Spain*

[f] *BRGM French Geological Survey, 3 avenue Claude Guillemin, BP 36009, 45060 Orléans Cedex 2, France*

Abstract

The Kiggavik area is located on the eastern border of the Paleo- to Mesoproterozoic Thelon Basin (Nunavut, Canada) and hosts major uranium mineralization in Archean basement rocks. These mineralizations display a strong structural control and share many similarities with the world-class unconformity-related U deposits of the coeval Athabasca Basin (Saskatchewan, Canada). An innovative cross-disciplinary study combining macro- to micro-scale characterization was applied to define the uranium mineral system in the Kiggavik area: observation, characterization and measurement of fractures in the field and from drillcores, petrographic and cathodoluminescence identification of fracture cements, analysis of fluid inclusions, and analysis of uranium oxides and related mineral phases through SEM, LA ICP-MS and SIMS. The analysis of fluid inclusions coupled with oriented measurements of fluid inclusions planes they constitute allow allows to link fluid circulation to a tectonic stress and therefore to bridge the

gap between the micro and the macro-scales. Our results show that the first order fault/fracture network in the Kiggavik area is mainly oriented ENE-WSW and NE-SW and consists of polyphased fault zones initiated during the Thelon and Trans-Hudsonian orogenies (ca. 1900-1800 Ma). These faults were subsequently U mineralized in four stages referred to as U0, U1, U2 and U3. These different U stages, yield distinctive fracture, alteration and mineralization patterns, indicating different conditions of formation. U0, inferred to be of magmatic-volcanic origin, likely occurred at ca. 1830 Ma and is related to micro-brecciation and weak clay-alteration under a WSW-ENE compressional stress. This event predates intense quartz brecciation, iron oxidation and veining at ca. 1750 Ma. This silicifying event, called Quartz Breccia (QB), predates the deposition of the Thelon Basin and is of magmatic-epithermal origin, associated with anorogenic rifting and emplacement of the Kivalliq igneous suite. Circulation of Si-bearing magmatic derived fluids caused pervasive silicification of former fault zones, which in turn controlled subsequent fracture development and behaved as barriers for later U mineralizing fluids (U1 to U3). Both the U0 mineralization and the subsequent QB silicifying event reflect the importance of pre-Thelon Basin fracturing and fluid circulation events in controlling the development and location of later U mineralizing stages. U1, U2 and U3 postdate deposition of the Thelon Basin. U1 is characterized by polymetallic mineralization in reduced narrow fault zones and U2 is characterized by monometallic mineralization in oxidized wider fault zones. These two mineralization episodes are characterized by illite and sudoite crystallization and occurred under a regional strike-slip stress regime, with the direction of σ1 evolving from WNW-ESE (U1) to NE-SW /ENE-WSW (U2); both formed between ~1500-1330 Ma and are related to circulations of Thelon-derived U-bearing basinal brines similar to the mineralizing brines at the origin of the 1600-1270 Ma unconformity-related U deposits in the Athabasca Basin. A post U2, but pre-Mackenzie dikes, NE-SW extensional stress caused normal-dextral offset of the orebodies by reactivating NNW-SSE and E-W faults. This fracturing event triggered circulation of hot (~300°C), probably acidic fluids, dequartzcifying, illitizing and bleaching the host-rock. U3 is a redistribution/reconcentration of the previous U mineralization along redox fronts, postdating MacKenzie dike (ca. 1270 Ma) and occurred through weak reopening of the pre-existing fracture network enhancing percolation of low temperature meteoric fluids during two main events at ca. 550 and 350 Ma.

Our study shows that U deposits and prospects in the Kiggavik area are of mixed type: a pre-basin magmatic-volacnic U stock (U0) remobilized by post-basin basinal brines to form unconformity-related mineralization (U1 and U2), which were lately altered and remobilized by massive percolations of meteoric waters (U3). This zone demonstrates thus a mobility of U during more than 1.5 billion years and had an evolution similar to that of the world-class U district of the Athabasca Basin. A significant difference with the Athabasca Basin is however that the strongest clay alteration event, formed by illite and linked to the MacKenzie dike intrusions, postdates the main stages of mineralization (U0 to U2).

Keywords

Uranium; deposit; structural control; uranium dating; clay alteration; fracture; Thelon Basin; Kiggavik; unconformity-related; brines

1. introduction

Numerous uranium (U) occurrences have been discovered since the 1970s in the Thelon-Baker Lake area in the Nunavut Territory, northern Canada (Curtis and Miller 1980; Miller 1980, 1982, 1995; Miller and LeCheminant 1985; Miller et al. 1986). In this area, the Paleo- to Mesoproterozoic Thelon Basin presents direct similarities whether in term of sedimentology, geology, structural evolution, and diagenetic history with the Athabasca Basin (Saskatchewan, Canada), located further south and which hosts the largest number of high grade unconformity-related uranium (URU) deposits in the world (Miller and LeCheminant 1985; Fuchs et al. 1986; Weyer et al. 1987; Friedrich et al. 1989; Fuchs and Hilger 1989; W Jefferson et al. 2007). Based on this knowledge, the Thelon Basin and its related basement have been considered as prospective for the discovery of URU deposits and thus have been explored since the 80s. Among the different prospective zones, the Kiggavik area, located on the eastern border of the Thelon’s Aberdeen sub-basin (Fig. 1), has been explored since the 1980s and several uranium orebodies of economic interest were discovered: Kiggavik (Main Zone, Center Zone, East Zone), Bong, Andrew Lake, End, which are deposits, and Granite grid, 85W, Sleek, Jane and Contact, which are prospects (Fig. 2; Fuchs et al. 1986; Riegler et al. 2014; Chi et al. 2017; Roy et al. 2017).

Various scientific studies have been carried out on these orebodies to characterize the specific key parameters which controlled the formation of these U mineralization, with the objective to compare them with those controlling the formation of the world-class URU deposits in the Athabasca Basin (Jefferson et al. 2007; Cuney and Kyser 2009). Previous studies about the Kiggavik area mainly focused on the characterization of mineralizing fluids and their alteration products throughout analysis of fluid inclusions and geochemical analysis and age-dating of U oxides and related clay minerals (Farkas 1984; Riegler et al. 2014; Sharpe et al. 2015; Chi et al. 2017; Shabaga et al. 2017). The tectonic history, the related structural controls and the relative timing of the deposits have not been studied in detail and are consequently weakly understood although they are key parameters for the URU deposits in the Athabasca Basin. A recent work on the Contact prospect (Grare et al. 2018a), has provided the first detailed picture of the successive pre- and syn/post-Thelon fracturing/faulting events at different scales and their role in the formation of U mineralization within this prospect. A major difference, in contrast to the Athabasca Basin where ductile to brittle tectonics involving Hudsonian graphitic-rich shear zones reactivated exerted a major structural and metallogenic control on the formation of the deposits (Polito et al. 2005; Pascal et al. 2015; Martz et al. 2017), is that the tectonic style of deformation and mineralization in the Kiggavik area is dominantly brittle, as exemplified by prevailing cataclastic to ultracataclastic fault rocks (Grare et al. 2018a). Graphite is almost absent from the basement lithologies and faults within the Kiggavik area.

Based on the study of fluid inclusions in quartz-carbonate veins spatially associated with U mineralization at End deposit, Chi et al. (2017) proposed that a ca. 1300 Ma U mineralization initially formed from high-salinity (> 30 wt% NaCl), 80-200°C Na- to Ca-rich basinal brines derived from the Thelon Basin, which is slightly higher in salinity than original Na-dominated diagenetic fluids defined within the Thelon Basin (Renac et al. 2002). These Na- to Ca-rich basinal brines are similar in terms of P-T of circulations and chemistry to the mineralizing fluids in the URU deposits of the Athabasca Basin (Pagel 1975; Derome et al. 2005; Richard et al. 2010, 2016; Chu and Chi 2016; Martz et al. 2018). For Bong deposit, Sharpe et al. (2015) proposed a five-stage metallogenic model with primary U mineralization occurring at ca. 1500 Ma, followed by different U mineralizing stages/remobilizations almost until the present time, for which the structural parameters are poorly known. The nature of the mineralizing fluids are unconstraint for the first stage and those related to the second stage of mineralization (at 1100 Ma) are isotopically closer to meteoric fluids rather than to basinal brines. Shabaga et al. (2017) proposed, based on chemical characterization and age-dating study of alteration products and U mineralization, that three events of mineralizing fluids (ca. 1030 Ma, 530 Ma and <1 Ma) were active at Andrew Lake and dominantly meteoric and oxidizing then acidic, meteoric and oxidizing. Illite-chlorite-U oxide association is commonly observed (Riegler et al. 2014; Sharpe et al. 2015; Chi et al. 2017; Shabaga et al. 2017) for the primary stage of mineralization in the whole Kiggavik area. The hydrothermal chlorite has a dominant sudoitic composition, as observed for the hydrothermal chlorite linked to U mineralization in the Athabasca Basin (Hoeve and Quirt 1984; Kotzer and Kyser 1995).

Anand and Jefferson (2017) recently released a structural synthesis for the Kiggavik area, based on satellite and geophysical map interpretation, and on field data. This model presents a district-scale structural evolution from ca.

2760 to 447 Ma and emphasizes multiple reactivation of a Riedel shear system. Their approach contrasts with the detailed sequence of fracturing/faulting events published by Grare et al. (2018a) for the Contact prospect that was reconstructed on the basis of both macroscopic (drill core and field data) and microscopic (optical microscopy, cathodoluminescence and SEM) paragenetic observations, and on a precise appraisal of chronological constrains.

This review of previous works highlights that the nature of the U mineralization at Kiggavik and their controls (structural, fluid, timing and physico-chemical) are still under debate. Despite the work by Anand and Jefferson (2017) that provides insights into the succession of regional tectonic events, the link between the macroscale and the microscale fractures and U mineralization, and the 3D architecture of faults zones in the Kiggavik area remains also unconstrained. These points need however to be carefully addressed for building a complete metallogenic model of U mineralization in the Kiggavik area. For this purpose, we propose here a specific and innovative work combining (1) the evolution of the structural framework controlling the U mineralization in the Kiggavik area with (2) mineralogical, geochemical and dating observations and measurements to fully depict the U system in this zone. Such work will facilitate the comparison with the world-class URU mineralization from the Athabasca Basin.

The aims of this contribution are therefore:

(1) to depict the brittle tectonic stages leading to the formation of the fault/fracture network that controls the U mineralization in the Kiggavik area and to determine its spatial-temporal evolution on the basis of multi-scale observations: review of the existing drill core information, coupled with structural analysis of oriented data from both outcrops and drill core, integrating samples from new drill holes from various deposits and prospects. Our work uses as a starting point the characterization of the sequence of brittle structural events established at the Contact prospect (Grare et al. 2018a). Oriented measures of fluid inclusions planes were also used to constrain the related tectonic stress at the time of fluid circulations.

(2) to establish the nature of the paleo-fluids and their conditions and timings of circulation through the identified fracture networks and tectonic episodes by the analysis of the resulting fluid-rock interactions, i.e. the fluid inclusions, the fracture infill products (cements, clays, ore minerals), and U mineralization. For this purpose, new mineralogical observations have been made, coupled with chemical characterization of fluid inclusions, alteration products and U oxides. New U/Pb isotopic and geochemical measurements on U oxides were also performed to define the physico-chemical conditions and ages of formation/alteration.

They are compared with published data for the Kiggavik area to better constrain the timing and conditions of the mineralizing events.

As an outcome of this multi-faceted approach, we finally propose an integrated structural and metallogenic model for the formation of the U deposits and prospects in the Kiggavik area. This model includes both pre-Thelon and post-Thelon Basin U ore formation, and for the first time fully illustrates the genesis and evolution of U mineralization of the prospective Kiggavik area and related Thelon Basin.

2. Geological setting

2.1 Regional setting

The Thelon Basin (ca. 1670–1540 Ma, (Hiatt et al. 2003; Davis et al. 2011) and the Athabasca Basin (1740–1540 Ma, Ramaekers et al. 2007) are Proterozoic intracratonic basins (Gall et al. 1992) hosted by the Churchill Province, which resulted from the collisional amalgamation of the Rae and Hearne cratons along the Snowbird Tectonic Zone (STZ), either in the Neoarchean or during the Snowbird orogenesis at ~1.9 Ga (Hoffman 1988; Corrigan et al. 2009; Fig. 1). These basins are located between the eroded remnants of the Trans-Hudson orogenic belt to the Southeast (ca. 2070-1800 Ma, overall NW-SE shortening) and the Thelon-Taltson orogenic belt to the west (ca. 2020-1900 Ma, overall E-W shortening). The Thelon Basin mainly consists of the Thelon Formation, an 1800-meter-thick sedimentary pile of conglomerates and coarse-grained sandstones, overlain by the ca. 1540 Ma shoshonitic basalts of the Kuungmi Formation (Chamberlain et al. 2010) and marine dolomites of the Lookout Point Formation (Gall et al. 1992) of the Barrensland Group (Fig. 1).

The Thelon Formation unconformably overlies a complex set of sedimentary and bi-modal volcanic-sedimentary rocks that filled up the Baker Lake Basin which developed between 1850 Ma and 1750 Ma (Rainbird et al. 2006; Rainbird and Davis 2007). The Baker Lake Basin formed as a result of (retro-arc) extensional to transtensional rifting tectonics related to the pre/syn-collision between the Churchill province and the Superior province (the Trans-Hudsonian orogeny). It was followed by uplifting, extensive erosional peneplanation and regolith formation, over which deposited the Thelon formation, linked to thermal subsidence (Rainbird et al. 2003; Rainbird and Davis 2007; Hadlari and Rainbird 2011). The Barrensland, Wharton and Baker Lake groups are parts of the Dubawnt Supergroup (Peterson, 2006) (Fig. 1) which overlies the metamorphosed Archean basement : the latter comprises ca. 2870 Ma granitic gneisses (Davis et al. 2006), 2730–2680 Ma supracrustal rocks of the Woodburn Lake Group (Pehrsson et al. 2013) and a distinctive package of 2620–2580 Ma felsic volcanic and related hypabyssal rocks known as the Snow Island suite (Jefferson et al. 2011; Peterson 2015; Johnstone, 2016). They are overlain by the Paleoproterozoic (2300–2150 Ma, Rainbird et al. 2010) orthoquartzite of the Ketyet River Group (Fig. 2). These rocks, especially the Woodburn Lake Group, host the uranium mineralization in the Kiggavik area (Fig. 2).

The Archean to Paleoproterozoic rocks of the Churchill province were intruded by three intrusive suites: (i) the late syn-orogenic (ca. 1830 Ma) Hudson suite (Peterson et al. 2002), (ii) the Dubawnt minette suite (contemporaneous of the Hudson suite), with ultrapotassic rocks, minette dikes and lamprophyres, and (iii) the rapakivi-style Nueltin granite of the anorogenic (ca. 1750 Ma) Kivalliq igneous suite (Hoffman 1988; Breemen et al. 2005; Peterson et al. 2015; Scott et al. 2015). Minor uranium mineralization are hosted in fractures and faults developped in Hudson granitoids at the 85W prospect. Dikes of the giant Mackenzie diabase swarm (1267±2 Ma; LeCheminant and Heaman 1989; Heaman and LeCheminant 1993) form prominent linear aeromagnetic features trending NNW-SSE (Tschirhart et al. 2013, 2017); they cut across all of the previous rocks and represent the last magmatic-tectonic event in the region.

2.2 Local setting, main fault structures and tectonic evolution

In the Kiggavik area, the previously described basement rocks are intruded by the Schultz Lake Intrusive Complex (SLIC) (Scott et al. 2015). The SLIC comprises rocks from the two intrusive suites previously described (Scott et al. 2015): (i) the “Hudson granite” consists of non-foliated granitoid sills, syenites and lamprophyre dikes of the late syn-orogenic Hudson suite. (ii) The “Nueltin granite” comprises anorogenic granite to rhyolite of the Kivalliq igneous suite (Peterson et al. 2015). Uranium and thorium primary enrichment were described to be associated with bostonite dikes (Peterson et al. 2011) and pegmatites attributed to emplacement of the Dubawnt minette (ca. 1830 Ma) and Kivalliq igneous suite, respectively. Such bostonite dikes were observed near the Kiggavik Main Zone (Anand and Jefferson 2017). These rocks are unconformably overlain by the Thelon Formation, which crops out in the Northern part of the Kiggavik property (Fig. 2). Several dikes of the Mackenzie swarm form NNW-SSE lineaments observed in the area.

The main structural features in the Kiggavik area are the ENE-trending Thelon fault (TF) and the Main Zone fault (MZF) in the northern part of the property, the ENE-trending Judge Sissons fault (JSF) in the central part, and the NE-trending Andrew Lake Fault (ALF) in the southwestern part (Fig. 2). The MZF hosts 85W, Granite grid and Kiggavik (Main, Central and East Zones). End is hosted by the JSF, while Andrew Lake, Jane and Contact occur along the ALF (Fig. 2) (see also Grare et al. 2018a).

Tectonic initiation of these faults likely dates back to the convergence of cratonic blocks during the latest stage of Trans-Hudsonian orogeny. The TF constitutes the boundary between the siliciclastic sedimentary rocks of the Thelon Formation to the north and the metamorphosed basement rocks to the south (Fig. 2). South of the TF, magnetic maps show that the SLIC is crosscut by numerous ENE-trending parallel and sub-parallel faults with apparent right-lateral displacement (Tschirhart et al. 2017). It has been observed on discontinuous outcrops and in drill holes that the JSF dips steeply to the north. The ALF constitutes the mapped boundary between the Hudson granite to the west and the metamorphosed basement rocks to the east (Fig. 2). The ALF is delineated from interpretation of aeromagnetic and ground gravity maps (Fig.2) (Roy et al. 2017; Tschirhart et al. 2017), as outcrops are almost absent.

The recent study of the Contact prospect (Grare et al. 2018a) gave new insights into the structural evolution of the ALF, an evolution which also included a post-Thelon U mineralizing event. Grare et al. (2018a) highlighted the presence of an extensive silicification event along the ALF, characterized by a quartz-healed breccia, termed the Quartz Breccia (QB) in the literature (Grare et al. 2018b). This structure is a main feature of both the JSF and the ALF: it is observable on outcrops (Anand and Jefferson 2017) and is systematically intersected by drill holes (Grare et al. 2018b). Finally, the main stages of fracturing/ mineralization recognized by Grare et al. (2017; 2018a, summarized in Fig. 3) at Contact include brittle tectonic activity along the Andrew Lake fault (fracturing stage 1 or f1), development of the quartz-cemented breccia (QB, f2), the first stage of U mineralization (f5), the second stage of U mineralization (f6), faulting associated with strong clay alteration and bleaching of the host rock (f8), and late U mineralization remobilization linked to the circulation of meteoric fluids (f9).

3. Methodology

3.1 Collection of data from field and drill cores

One hundred and forty samples were collected from drill cores obtained during 2014 and 2015 exploration campaigns done by Areva Resources Canada (ARC, now Orano Canada); 28 samples come from Andrew Lake, 5 from End, 14 from Kiggavik Center Zone, 66 from Contact and 27 from 85W (see location of deposits and prospects in Fig. 2). In addition to classical drilling realized during the exploration campaigns, two double tubing exploration drill holes (named CZ-15-01 and AND-15-01) allowing for a better preservation of the drill cores were done and studied. One was drilled at the Andrew Lake deposit and one at Kiggavik Center Zone deposit. Several drill holes (~50) from previous exploration campaigns were also re-observed in detail (fracture orientations, crosscutting relationships, cements and associated alteration and mineralization).

Field observations of faults, joints and veins were also made on outcrops and, when possible, compared and combined with previous field observations made by ARC geologists. Fault zones were characterized in drill cores by the identification of fault cores with occurrence of fault rocks such as breccias or gouges. Fault damage zones (Chester and Logan 1986; Wibberley et al. 2008; Faulkner et al. 2010) were documented by the associated veins (mode I or mixed mode I-mode II), joints (mode I) and undifferentiated fractures; an "undifferentiated fracture" in this case relates to a fracture plane which cannot be unambiguously classified as vein, joint or fault/micro-fault (no kinematic indicator). Fracture corridors and isolated veins, joints and undifferentiated fractures were also systematically reported.

Oriented data from the complete Kiggavik area's ARC database were collected and processed. Orientations of ~2,000 fractures and foliation planes were measured from oriented drill cores. Drill cores were oriented using a Reflex ACT III digital core orientation tool (Bright et al. 2014), and then a protractor was used to measure angles between fractures and the core axis (alpha angle). The angle between the bottom of the hole and the inflection line (beta angle) was also measured for calculation of true dip/dip direction data. Acoustic televiewer probing ABI40 (Williams and Johnson 2004) was run through several holes providing accurate oriented data in faulted core intervals. The mesostructural data were processed to their true orientation and plotted with Dips 6.0 software by Rocscience. Uncertainty on orientation measurements is usually about 10° as estimated from the comparison between oriented core-measurements and acoustic televiewer data.

3.2 Optical microscopy observations and scanning electron microscope (SEM) analysis

Microscopic observations were carried out to compare with and complete the mineralogical observations made by previous authors on the deposits of the Kiggavik area but also to bring new insights into the genetic link between fractures, alterations and U mineralization. Thin sections made on veins and fault rocks were studied under a Motic BA310 POL Trinocular, using transmitted and reflected lights, and a HIROX SH-3000 Scanning electron microscope (SEM) equipped with a back-scattered electron detector and a nitrogen free Energy Dispersive Spectrometer (EDS) BRK D351-10 with digital mapping capabilities at Orano la Defense site. The SEM was operated at low accelerating voltage (10 kV), 100 nA filaments current and 600 Å beam width for a working distance between 8 and 39 mm. Complementary observations on mineralogical observations and U mineralization were performed at Service Commun de Microscopie Electronique et de Microanalyses (SCMEM) of GeoRessources lab (Vandoeuvre-lès-Nancy, France), using a JEOL J7600F Scanning electron microscope equipped with an energy dispersive spectrometer.

3.3 Cathodoluminescence

The different generations of carbonate vein cements were characterized using a Technosyn Cold Cathodoluminescence device (model 8200 MkII), operating between 10 and 12 kV gun potential and between 150 and 350 µA beam current. Observations were carried out at the University of Barcelona, Spain (Departament de Mineralogia, Petrologia i Geologia Aplicada, Facultat de Ciències de la Terra).

3.4 Electron microprobe analysis (EMPA) and geothermometry of clay minerals

The chemical composition for major elements in U oxides and clay minerals (mainly chlorites and illite) were measured using a CAMECA SX-100 Electron Microprobe Analyser also at SCMEM. The analytical conditions were an accelerating voltage of 15 kV and 10 nA current. The calibration used natural and synthetic oxides and/or alloys (orthoclase, albite, $LaPO_4$, $CePO_4$, wollastonite, UO_2, $PbCrO_4$, olivine, $DyRu_2$). The counting times were 10s (K, Na, Ca), 20s (Ce, U, Si), 40s (Dy), 50s for Pb, and 60s for La. Complementary measurements on U oxides and clay minerals were made on 6 thin sections with a CAMECA SX-50 electron microprobe and conducted at the Camparis service in Sorbonne Université (Paris), based on the same analytical conditions as used at SCMEM.

In the Kiggavik area, clay minerals such as chlorite and illite are a common product of host-rock alteration. They are also found in fractures as neo-formed minerals. Variations in the chemical composition (Tschermark, di-trioctahedral, Fe-Mg exchange, Fe^{3+}/Fe^{2+} ratio) of chlorites are a powerful tool for estimating the crystallization temperature of the clay minerals, which is referred to as chlorite geothermometry. Temperatures were calculated following the equation of Cathelineau (1988), Zang and Fyfe (1995) and Kranidiotis and McLean (1987). White mica crystals were selected from the main altering and/or mineralizing stages for electron microprobe analysis, and the determined major element compositions (site occupancy and end-member mineral data) were used to calculate the precipitation temperatures. Temperatures were calculated following the equation of Cathelineau (1988). Micas coating or cementing fractures and filling pores were selected rather than replacement micas in order to minimize the influence of precursor minerals, hence to ensure their representativity of the selected fracturing stages.

3.5 Secondary ion mass spectrometry (SIMS) and LA-ICP-MS for U-Pb dating and geochemical tracing of U oxides

The Pb/Pb and U–Pb isotopic compositions of U oxides was determined using a CAMECA ims 1280-HR Secondary Ion Mass Spectrometer (SIMS) at CRPG-CNRS (Nancy, France). The O^{-} primary ion beam was accelerated at 13 kV, with an intensity ranging between 3.5 and 5 nA, and focused on a spot of ca. 15 µm diameter. The primary beam was set in Gaussian mode with a raster of 10 µm. The field aperture was set to 2,000 µm and the transfer optic magnification was adjusted to 80. Rectangular lenses were activated in the secondary ion optics to increase the transmission at high mass resolution. The energy window was opened at 30 eV, and centred on the low energy side, 5 eV before the maximum value. An offset of 50 eV was applied during the analyses in order to avoid matrix effects due to mixtures of uranitite and silicate in natural samples. Ions were measured by peak jumping in monocollection mode using the axial Faraday cup (FC) for ^{238}U and ^{238}UO and the axial electron multiplier (EM) for ^{204}Pb, ^{206}Pb, ^{207}Pb, ^{208}Pb, and ^{248}ThO. Each analysis consisted of 8 successive cycles. Each cycle began with measurement at masses 203.5 and 203.6 to obtain the background measurements for the FC and EM. Counting times were 4 s for 203.5, 203.6, ^{208}Pb and ^{238}U; 3 s for ^{248}ThO and ^{238}UO; 6 s for ^{206}Pb; 10 s for ^{204}Pb; and 20 s for ^{207}Pb (waiting time of 1 s). The standard used was an uraninite sample from Zambia (concordant age of 540 ± 4 Ma; Cathelineau et al. 1990), analysed before and after each sample for sample bracketing calibration. The error on the calibration curve is reported in the error given for each analysis. The $^{204}Pb/^{206}Pb$ ratio were low (<0.00001) for standard and unknowns, indicating that common lead was not incorporated at the time of crystallization, except for sample 9850 (0.000019-0.004619). A correction for common lead was however made for each analytical spot for all samples by precisely measuring the ^{204}Pb amount and by calculating the composition of the common lead at the time of crystallization, based on the $^{207}Pb/^{206}Pb$ measured age and using the Pb isotopic composition calculated from Stacey and Kramers (1975) model. Ages and error correlations were calculated using the ISOPLOT flowsheet of Ludwig (Ludwig 2007). Uncertainties in the ages are reported at the 1σ level.

The Rare Earth Elements-REE (La, Ce, Pr, Nd, Sm, Eu, Gd, Tb, Dy, Ho, Er, Tm, Yb, Lu) concentrations in the different U oxides were quantified using a LA-ICP-MS system (GeoLas excimer laser (ArF,193 nm, Microlas) coupled to Agilent 7500c quadrupole ICP-MS at GeoRessources lab) with a 16-24µm spot size. The detailed instrumentation and methodology are described in Lach et al. (Lach et al. 2013).

3.6 Fluid inclusions (FI) and fluid inclusion planes (FIP)

Secondary FIs (trapped after the formation of the quartz host crystals) organized in FIP were studied in primary magmatic quartz, to define the properties of fluids and the tectonic stress under which they circulated, as FIPs are considered as mode I fractures containing fluid inclusions, FIPs being supposed to have formed perpendicular to the least principal stress axis σ3, i.e. in the plane that favours the maximal decrease of the total energy of the system (Lespinasse and Pêcher 1986; Gueguen et al. 1995; Lespinasse 1999; Lespinasse et al. 2005). In our study, directions of the different FIPs were measured, FIPs being mainly subvertical fractures. The work focused on FIPs rather than on primary FIs in order to link a fluid circulation to a tectonic stress and therefore to bridge the gap between the micro and the macro-scales. Sampling for FI studies was carried out from drill core obtained during the 2014 and 2015 summer field campaigns. A selection of four oriented samples was collected at 85W and Contact (only locations where oriented samples were available) and attention was paid to take samples not too close to fault zones, when possible, in order to avoid local perturbation of the stress field. A thin section and a wafer were prepared on a horizontal plane from selected zone of the oriented drill core in order to have a “map view” of the subvertical FIPs. FIP orientations were measured under transmitted light microscope using the AnIma software (Lespinasse et al. 2005). More than 100 orientation measurements were done per sample, on a restrained zone (~25 mm^2), to provide a statistical representativity of the data proposed.

Microthermometry was carried out on fluid inclusions (FI) from the FIPs using a Linkam® MDS600 heating-cooling stage, adapted to an Olympus® microscope at the GeoRessources lab. A total of 99 secondary fluid inclusions from FIPs were studied for microthermometry. The following microthermometric parameters were measured for liquid-dominated FIs: First melting temperature (Te), melting temperatures of ice and hydrohalite (Tm ice and Tm hyd), halite dissolution (Ts NaCl), and homogenization temperature (Th) (Liq. + Vap. → Liq. or Liq. + Vap. + NaCl → Liq. + NaCl or Liq. + Vap. + NaCl → Liq. + Vap. → Liq.). The temperatures of phase changes have a precision of about ± 5 °C for Te, ±0.1 °C for Tmice, Tmhyd and ±1 °C for TsNaCl and Th. Fluid inclusions (FIs) were classified following Derome et al. (2005), the nomenclature based on both the Tm ice ranges (Tm ice < -30°C: Lw' and Lwh'; -30°C < Tm ice < -15°C: Lw1, Lw2 and Lwh; -15°C < Tm ice: Lw"), the last observed phase to melt at low temperature upon heating (ice: Lw1, Lw' and Lw"; hydrohalite: Lw2, Lwh), and the homogenisation sequence of halite-bearing inclusions (Liq. + Vap. + NaCl → Liq. + NaCl → Liq. : Lwh'; Liq. + Vap. + NaCl → Liq. + Vap. → Liq.: Lwh). FIs that do not nucleate any ice even at -190°C were assigned to Lw' type (Derome et al. 2005). Salinity is estimated from microthermometry (in wt.% NaCl equiv.).

Gas species in the vapor phase of fluid inclusions were determined at room temperature with a Labram Raman microspectrometer equipped with a Edge filter, a holographic grating with 1800 grooves per millimetre and a liquid nitrogen cooled CCD detector at GeoRessources (Nancy, France) (Dubessy et al. 1989). The exciting radiation at 514.5nm provided by an ionized Argon laser (Spectra physics) was focused on the vapor phase of the fluid inclusions using a X80 objective (Olympus). Using this setup, neither limits of detection nor absolute concentrations of trace gases, can be determined. However the relative proportions of the different gas species at room temperature can be estimated qualitatively (Dubessy et al. 1989). The targeted gas species were those commonly found in FIs from URU deposits (H_2, O_2, CO_2, CH_4, N_2, C_2H_6) (Richard 2017).

The quantification of the chemical composition (major, minor and trace elements) of water dominated FIs was tempted using the LA-ICP-MS system composed of a GeoLas excimer laser (ArF,193 nm, Microlas) coupled to an Agilent 7500c quadrupole ICP-MS at GeoRessources lab (Leisen et al. 2012). The isotopes analysed were: ^{23}Na, ^{11}B, ^{24}Mg, ^{39}K, ^{44}Ca, ^{55}Mn, ^{57}Fe, ^{63}Cu, ^{66}Zn, ^{88}Sr, ^{55}Cs, ^{137}Ba, ^{208}Pb, and ^{238}U, using an integration time of 0.01 s per mass channel for a total cycle time of 0.22 s. The laser was run at 5 Hz with a fluence of ~ 10 J/cm^2. The diameters for ablation vary from 16 to 32 µm. The reference materials NIST SRM610 and 612 were used for the standardization and calibration of the instruments. The instrument was tuned to have the maximum sensitivity for the whole mass range, keeping Th/U~1 and ThO/Th<0.5%. The signal integration and data calculation were performed using the Matlab®-based SILLS program using a charge-balance approach (Guillong et al. 2008). The analytical precision for most elements is within 20-30% RSD (Allan et al. 2005). LOD are different for each element measured, however a LOD of ~1ppm is a reasonable approximation for elements with a mass to charge ratio superior to 60.

4. Results

4.1 Characterization of fracturing/faulting events

4.1.1 Macro/mesoscopic observations

The approach and methods adopted in the present work are similar to those of Grare et al. (2018a) and for the sake of clarity, the presentation of the results follows the sequence of fracturing events defined by these authors (Fig.3). The aim is to establish whether or not the events and timing recognized at Contact can be also recognized in the other deposits and prospects and whether the chronology of events remains the same. Grare et al. (2018a) recognized 10 fracturing events at Contact among which 3 resulted in fracture-controlled U mineralization (Fig.3).

Fracture stage 0 (f0) and oldest stage of U mineralization (U0, Fig. 3). This stage is named f0 and U0 in order to respect the annotation from f1 to f10 presented in Grare et al. (2018a). This stage f0 predates the stage f1/U1 observed at Contact. Indeed, a first fracturing event, unrecognized at Contact was identified at End, Andrew Lake, Kiggavik Main Zone and Bong. This fracturing event is characterized by U-mineralized microbreccia usually displaying a dense network of millimetre-wide greenish microfractures (Fig. 4A), in breccia zones up to a 10m-thick (e.g. in End). U mineralization is observed within the microfractures and is weakly disseminated within the host rock. The mineralization is usually weak but can reach several thousands of counts per second (CPS, AREVA SPPɣ®) in some breccia zones displaying stronger brecciation. Whatever the grade, the brecciated and mineralized host rock is barely clay altered (Fig. 4B). This mineralized event is crosscut and partially overprinted by the QB (Fig. 4A).

Stage f1, pre-Thelon fracturing event (Fig. 3). At Contact, this stage is marked by faults with proto- to ultra-cataclastic fault rocks along the ALF (Grare et al. 2018a), showing later silicification and crosscut by white quartz veins and mosaic breccia of to the QB.

Stage f2 (Fig. 3): This stage is characterized in all deposits and prospects by the QB (Grare et al. 2018b) with its characteristic mosaic white quartz-sealed veins and breccia, along major fault zones: at Bong and Kiggavik Main Zone along the ENE-WSW trending MZF, at Jane along the NE-SW trending ALF and at End along the ENE-WSW trending JSF. U mineralization (all stages) is always found in the hanging wall and footwall of the QB but not within the breccia core. F1 and f2 fracturing stages, and the structural control exerted by the QB on later U mineralization were described in details by Grare et al. (2018a, b).

Stage f3 (Fig. 3): This stage is represented by cm-thick dolomite veins and micro-breccias, and was observed in all deposits and prospects of the Kiggavik area.

Stage f4 (Fig. 3): This stage is represented by calcite veins that crosscut, thus postdate emplacement of the QB. Described by Grare et al (2018a) as mixed mode-I mode-II shear fractures; they are observed at each deposit of the Kiggavik area, sometimes close to U-mineralized fault zones (f5), and may exhibit calcite-cemented steps and proto-breccia textures.

Stage f5 (Fig. 3): This mineralizing event is an U mineralizing event (also called U1, Fig. 4C) that postdates deposition of the Thelon Basin. It is characterized by grey-greenish coloured, clay-altered (illite mainly and chlorite) narrow fault zones (Fig. 4C-Andrew Lake) which were also observed in all deposits and prospects of the Kiggavik area. This fracturing event shows strongly mineralized fault zones with protocataclastic to cataclastic fault rocks (Fig. 4C-Bong and Kiggavik MZ) and re-opened, micro-fractured quartz veins from which the mineralization leaks into the foliation (Fig. 4C-End deposit; see also Chi et al. 2017). At 85W, the U mineralization is completely hosted in Hudson granitoids, mainly granites. As a consequence of the absence of foliation and of coarser size of the minerals there, the control by fractures is stronger and easier to observe. In strongly mineralized fault zones, where the mineralization is disseminated in the host rock, biotite is coated with U, which expands along the mineral cleavage (Fig. 4D). Like at Contact (Grare et al. 2018a), clay alteration (illitization mainly, but also chloritization) of the host rock is weak to moderate.

Stage f6 (Fig. 3): This stage is represented by deep red hematized fault zones and the second stage of U mineralization (U2, Fig. 5A-D). It has been recognized in all deposits of the Kiggavik area. Cataclastic, strongly clay altered (illite and chlorite) fault cores (Fig. 5B-top) and tectonic breccias are usually not mineralized. Hematite veins (Fig. 5B-bottom), millimetre-thick calcite veins (Fig. 5C-top) and microfaults host the mineralization which spreads out into the host rock as blebs surrounded by a rim of bleaching (Fig. 5A, Fig. 5C-top and bottom) in wide fracture networks of bright red oxidized damage zones (Fig. 5D). Alteration of the host rock is stronger compared to the previous stage of uranium mineralization.

Stages f7-f8 (Fig. 3): These stages represent the strongest clay alteration events in the Kiggavik area, characterized by illitization, de-quartzification and bleaching of the host rock. They are observed in all deposits and prospects. Multiple, un-mineralized, illitized faults were observed at Kiggavik Main Zone (Fig. 5E). These faults crosscut mineralized fault zones (Fig. 5F) and reworked clasts bearing U oxides are observed within cataclastic fault rocks (Fig. 5G-top and bottom). This fracturing stage, recognized for each deposit and prospect but with variable intensity, has been extensively observed at Bong. The greenish colour of some fault zones is due to the presence of retrograde metamorphic chlorite and therefore does not reflect a different fracturing process; additionally, white clay fault zones (f8) are much more frequent compared to greenish clay fault zones (f7); on the basis of these new observations, we propose to group these two fracturing events that were presented separated in Grare et al., (2018a). The strongest clay alteration event is definitively termed f7.

The Mackenzie dikes (Fig. 5H) were observed only at Kiggavik Main Zone but these dikes provide strong constraints on the timing of the fracturing events. Indeed, diabase dikes crosscut the altered and mineralized fault zones and are barely fractured and altered, and can therefore be considered as sealing the main tectonic and mineralizing history.

Stage f9 (Fig. 3): This stage is represented by weak reactivation of the fracture network and U redox fronts (U3) as described at Bong (Sharpe et al. 2015), Andrew Lake (Shabaga et al. 2017) and Contact (Grare et al. 2018a); they have also been recognized at End, Kiggavik Main Zone and 85W (Fig. 6). These remobilization fronts display the typical succession with an oxidized (goethite), un-mineralized zone, a thin black layer where uranium oxides are concentrated and a grey, non-oxidized (reduced) and mineralized zone. These redox fronts are sometime bleached by a later event described at the Contact prospect (f10) which removed iron oxides from the goethite-rich zone and therefore modified the visual aspect of the redox front.

Macroscopic re-examination of deposits and prospects in the Kiggavik area therefore confirm the structural stages previously defined by Grare et al. (2018a) at Contact, so that the sequence of fracturing events can be considered as representative of the whole Kiggavik area, although changes in lithologies may have induced differences in the mineralogy of fault rock cements between deposits and prospects. In addition, our approach has allowed for the identification of a new stage of deformation and mineralization (f0 and U0) that predates all those described in Contact and therefore also the formation of the QB, inferred to be a pre-Thelon fracturing event. This initial mineralizing stage is hereinafter characterized more in detail with microscopic observations and geochemical data.

To summarize, the fracture/mineralization history of the Kiggavik area is as follows:

- f0/U0, f1, followed by the brecciation-silicification event, the so-called Quartz Breccia (QB-f2), predate formation of the Thelon Basin.
- f3 to f7, including two stages of U mineralization (U1-f5 and U2-f6), are syn to post/post-Thelon Basin events. These fracturing/mineralization events predate emplacement of the late NNW-SSE trending Mackenzie dikes swarm that crosscut orebodies, display little to no alteration and show no offset on geophysical maps (Percival and Tschirhart 2017).
- Late events of U remobilization-reconcentration (U3) along redox fronts postdate the Mackenzie dikes in the Kiggavik area. Even though these events may have had a significant economic impact in terms of ore redistribution, they were likely linked to (weak) fracturing, and do not correspond to a main fracturing stage that significantly alter the structural architecture of deposits and prospects.

4.1.2 Geometry and kinematics of fault zones from fracture orientation measurements and kinematic data

Figure 3 shows the oriented mesostructural data collected in the prospects/deposits of the Kiggavik area (except for Jane and Sleek). The sequence of faulting/fracturing events and crosscutting relationships are displayed on the first and second columns for reference. The qualitative frequency of the fracture sets for each deposit and prospect is shown by coloured symbols; for example f7 (white clay altered fault zones) is dominant at Bong. Together with orientation data, a statistically significant number of kinematic indicators on veins and faults were also gathered mainly from outcrops located in different parts of the Kiggavik area, usually close to a known deposit or prospect, and also from drill core; they are synthetized in the last column of Fig. 3.

Oriented data for the mineralized microbreccia (f0, Fig. 3 row 0) are rare; however, data from major fractures from End collected within the mineralized microbreccia display a NE-SW trend and a steep dip to the NW. The numerous solution seams observed at the micro-scale display a NW-SE to NNW-SSE orientation (data not displayed in Fig. 3). Similarly, microstructures from the pre-QB brittle fracturing event (f1, Fig. 3-row 1), although still observable, are usually strongly silicified and overprinted by the quartz breccia (f2) precluding any reliable collection of oriented data. ENE-WSW striking faults, steeply dipping to the N (mimicking the orientation of the QB, like at Contact) would be expected for this fracturing stage that characterize the primary orientations of the JSF and the MZF, e.g., at Contact (f1, Fig. 3-row 1).

Because QB (f2, Fig. 3-row 2) has reused pre-existing main fault zones (e.g. ENE-WSW trending JSF) in the Kiggavik area (Grare et al. 2018b), the related faults/fractures display variable orientation. QB shows a NE-SW trend at Contact and Andrew Lake. Secondary ENE-WSW fracture directions are also observed at Jane and Andrew Lake. The QB displays a main ENE-WSW trend with a steep dip to the North at End and Kiggavik Main Zone. At Bong, the QB is characterized by a NNE-SSW direction and a steep dip mainly to the W and a secondary E-W direction with a steep dip to the N. At 85W, mainly small white quartz veins were observed, displaying dominant E-W directions with steep dip to the N. Quartz veins (from QB, f2) display stepped veins, associated with (Fig. 7A) or without (Fig. 7B) U oxides and arrays of mode I opening fractures (Fig. 7C). Stepped veins are usually trending WSW-ENE and NW-SE (Fig. 7D, 85W, Kiggavik and St-Tropez), while mode I opening veins display a dominant WNW-ESE direction (Fig. 7D, 85W).

Like at Contact, measurements of oriented data from calcite veins (f4) were mainly taken from Ca1 veins, as the Ca2 (Fig. 3-row 6b, no oriented data) usually displays veins too thin to be measured or to be unambiguously differentiated from those of the first stage calcite veins. Two directions are observed: E-W and NW-SE, with conjugate dip-directions. Stepped veins cemented with Ca1 (f4) and synchronous U oxides (U1) were observed only in drill core (Fig. 8A). Veins displaying kinematic indicators are rare but some stepped veins were observed and measured; they display ENE-WSW and NW-SE directions (Fig. 8B).

F5/U1 fractures (Fig. 3-row 5) follows ENE-WSW to ESE-WNW faults at Contact, dipping to the N. At Andrew Lake, mineralization is found within N-S and E-W faults, but also within reopened and/or microfractured quartz veins trending NE-SW (f2, QB stage, like at Contact). At 85W, faults and minor fractures show an ESE-WNW direction, steeply dipping mainly to the N.

F6/U2 fractures (Fig. 3-row 6a) are well observed throughout the Kiggavik area. At Contact, and Andrew Lake, they display N-S to NE-SW directions (i.e., the direction of the ALF). Contact is located on a W-dipping segment of the ALF, while Jane and Andrew Lake are located on an E-dipping segment of the ALF. Looking at the map organisation (Fig. 2), End is likely hosted within an important relay zone of the JSF; there, oxidized fault zones are trending mainly NNW-SSE to NE-SW (Fig. 3-row 6a). At Sleek, the three main faults trends are N-S, E-W and NW-SE, the latter two being visible on maps. At Bong, 85W and Kiggavik Main Zone, the fault trends are similar to those of the QB, however at Kiggavik Main Zone, like for in Contact, an E-W trend with a shallow dip to the S is also recognized. F6 is also characterized by tectono-hydraulic breccia and strongly clay altered fault zones which are both usually not mineralized (Fig. 4G). F6 fractures were observed in the field associated with radioactive anomalies. Study of relay zones allowed for the interpretation of the kinematics of the fault zone (Fig. 9A-B). Kinematic indicators were observed in the field and in drill core and are presented in Fig. 9C; faults with dominant E-W to ENE-WSW orientation show evidence for reverse and/or sinistral motion. Other faults with dextral indicators were also observed in the St-Tropez area (Fig. 9A and C), which is located 20 km to the NNE of Kiggavik Main Zone. The JSF, trending ENE-WSW, displays a reverse-sinistral slip component (Fig. 9C), which postdates the main dextral normal slip component responsible of the Hudsonian granite offset (SLIC, Fig. 2, see also Anand and Jefferson 2017).

Mineralized fractures f6c, as presented in Fig. 3-row 6c, were also observed in other deposits and prospects; they are better represented at Contact, Andrew Lake and Kiggavik Main Zone. At Andrew Lake, the third stage of U mineralization is characterized by ESE-WNW to NW-SE microfaults and by NE-SW millimetric-wide calcite veins (i.e., Ca2, measured precisely only at Andrew Lake). At End, the second stage of U mineralization is guided by NW-SE to NNW-SSE faults that mainly dip to the E. At 85W, this mineralizing stage is guided mainly by W-dipping NNE-SSW faults and by NW-SE faults as a second direction. At Kiggavik Main Zone, f6c faults are trending either ENE-WSW or NW-SE to WNW-ESE.

Finally, f7 fractures were also recognized (f7, Fig. 3-row 8). They are usually associated with NW-SE and E-W trending fault zones (i.e., 85W and End). This fracturing stage is widely encountered and dominant at Bong where it is characterized by E-W trending, N-steeply dipping fault zones. These post-ore fractures display NNW-SSE direction with evidence of strike-slip sinistral motion in End and 85W areas (Fig. 10A-C); these faults display E-W to WNW-ESE orientation, steeply dipping to the N, with a dip-slip normal kinematics. At 85W, micro-faults offset uranium mineralized fractures (f6, Fig. 10B) while at Bong the orebody is offset by E-W striking faults (Fig. 10D). The dip-slip component displacement of the U orebodies (metric to decametric) appears to be greater than the strike-slip component (centimetric to metric).

4.2 Petrological observations, chemical compositions of clays, U oxides and fluid inclusions, and U-Pb dating of U oxides

4.2.1 Optical microscopic and SEM observations

Samples of the U-mineralized microbreccia (f0, U0) is characterized by the presence of multiple irregular microstructures with interlocking pegs and sockets (Fig. 11A), usually surrounded by a millimetric halo of quartz dissolution similar to solution seams. These microstructures connect to microbreccias, within which millimetric clasts display irregular boundaries reflecting dissolution patterns (Fig. 11B). These micro-structures are cemented by dark green chlorite, ore minerals and are sharply crosscut by quartz veins of the QB (Fig. 11C-E). SEM observations and microprobe characterization show that microfractures are cemented with iron-rich clinochlore, pitchblende (containing up to several percents of thorium), brannerite, titanium oxides and sulfide minerals (mainly pyrite). These minerals are subhedral to anhedral mixed phases (Fig. 11D-F). Microprobe characterisation shows that the iron-rich clinochlore is altered into an Al-rich chlorite (Fig. 11E), close to sudoite (Table 1). Subhedral crystals of brannerite were observed in the same type of fractures/breccias on samples from Kiggavik Main Zone, associated with pitchblende-cemented microbreccia (Fig. 11F and 12A). Rutile with micro-inclusions of U-oxide and coated with anhedral U-Ti phases were observed on samples from Andrew Lake (Fig. 12B). Microfractures within magmatic quartz, cemented with rutile and colloform pitchblende were observed in samples from 85W (Fig. 12C).

Stage f5 and associated U1 is characterized by uraninite and pitchblende in fractures often cemented by calcite (Fig. 12D). U1 is spatially associated with open quartz veins displaying colloform pitchblende along the edges, with U oxides “eating away” quartz crystals (e.g. 85W, Fig. 12E). Bravoite-pyrite coated with pitchblende (Fig. 12F) was observed on samples from Jane, a mineralogical association also described at Contact for U1 (Grare et al. 2018a). Silver, gold and selenium phases were observed on samples from Andrew Lake, End and Kiggavik Main Zone. Anhedral Ag-U phases with galena were observed cementing microfractures (Fig. 12G) while gold is usually present as micro-inclusions within pitchblende (Fig. 12H). Aluminum Phosphate Sulphates (APS) were observed associated with pyrite and pitchblende in a grey-greenish fault zone at 85W (Fig. 12I). In the case of f6 and associated U2, U oxides are associated with APS in oxidized rocks at 85W (Fig. 12J). In term of clay alteration minerals, illite and sudoite were observed for U1 and U2 mineralizing stage, they are described more in detail hereinafter. Anhedral pitchblende cementing anastomosing micro-fractures characteristic of this mineralizing stage, was observed at Andrew Lake (Fig. 12K). These new observations confirm and complement previous observations made by Chi et al. (2017), Shabaga et al. (2017), Weyer et al. (1989) and Grare et al. (2018a) at End, Andrew Lake, Kiggavik Main Zone and Contact, respectively.

U3 is characterized by anhedral pitchblende, goethite and rare sulfurs (pyrite) cementing micro-fractures and coating various minerals (Fig. 12L)

4.2.2 Carbonate cements characterization under cathodoluminescence: link with U mineralization

Two generations of calcite veins are observed associated with uranium oxides. The first one, Ca1 (f4), likely formed by mixed mode I/mode II fracturing, synchronous with U1, and the second one, Ca2 (f6b), displays crack and seal textures; it crosscuts U1 and was likely formed by mode I opening.

The Ca1 spatially associated with the first stage of U mineralization (U1) shows calcite with a yellowish-orange luminescence and a darker tint when closer to U oxides. At Contact and 85W, colloform pitchblende occupies the edge of re-opened quartz-dolomite veins: dolomite and quartz display irregular boundaries in contact with calcite which separates them from U oxides (Fig. 13A). Calcite is observed cementing microbreccia on samples from 85W and End; U oxides are coating the edges of calcite crystals (Fig. 13B-C) or as subhedral colloform shapes intergrown with the calcite breccia (Fig. 13D), thus indicating synchronous precipitation of calcite and U oxides. A similar observation was made on sample from Kiggavik Main Zone.

Ca2 veining occurred during f6 and is spatially associated with U2, likely synchronous with this fracturing event. The millimetric-wide crack-seal calcite veins (Ca2) observed at Contact and associated with the second stage of U mineralization were also observed in sample from End, crosscutting U oxides of U1 (Fig. 13E). The calcite of these veins displays a dark orange luminescence (Fig. 13F). In addition to characterize two calcite cements with different orientations but also luminescence and textures, thus two calcite generations, these observations also allow concluding that f4 Calcite is synchronous with U1 (f5), these two fracturing events could therefore be gathered.

4.2.3 Composition and crystallisation temperatures of chlorites and illites

Chlorite

Chlorite in the Kiggavik area fall into three stages: retrograde metamorphic chlorite, chlorite (altered and unaltered) associated with the mineralizing stage U0, and chlorite associated with mineralizing stages U1 and U2.

They are chemographically presented in a ternary MR3-2R3-3R2 diagram in Fig. 14A (Velde 1985). Formulae of chlorite associated with U0, U1 and U2, from various locations are presented in table 1.

Representative compositions of analysed chlorites from U mineralized microbreccia samples (f0, U0) are plotted in Fig. 14B. Analyzed chlorite cements the microbreccia (Fig. 14C). Representative compositions of fresh chlorite associated with U0, with calculated temperatures, are presented in Fig. 14D, and indicate an iron-rich species of trioctahedral chlorite. Their octahedral occupancy is close to 6 atoms when the structural formulae is calculated with total Fe in the ferrous state and their XFe is generally close to 0.5. Structural formulae of chlorite linked to U1 and U2 plot toward the sudoitic pole (di-trioctahedral chlorite, Fig. 14B, complete formulae presented in table 1), characterized by an Al-Mg rich composition and an octahedral occupancy close to 5 atoms. Numerous analyses of chlorites associated with U0 reveal a mixture of variable amounts of iron-rich chlorite and sudoite, showing that neoformed dioctahedral chlorite co-genetic of U0 were altered to di-trioctahedral chlorite. This is consistent with petrographic observations showing dark green chlorite surrounded by light green chlorite (sudoite; Fig. 14C).
Temperature calculations were done using several methods (Fig. 14D) only for the Fe-rich chlorite variety linked to U0, as the geothermometers cannot be applied on low-T° di-trioctahedral chlorites like sudoite. The Cathelineau (1988) and Jowett (1991) thermometers returned temperatures ranging from 295 to 333 °C whereas Kranidiotis (1987) and Zang and Fyfe (1995) thermometers returned temperatures ranging from 130 to 159 °C. The temperatures differ considerably, and the estimation of the more likely temperature range needs to be done in the light of textural relationships, as discussed hereafter in the interpretation section.

Illite

Selected representative compositions for white micas associated with pre-ore alteration (pre-U0), with U1-f5 and U2-f6 mineralizing stages and late clay alteration micas (f7) are available as supplementary material (ESM-1) and plotted on ternary diagrams representing the average compositional fields of dioctahedral mica-like phases (Dubacq et al. 2010) (Fig. 15A). Pre-ore (pre-U1) alteration (Fig. 15B-C) is characterized by interlayered illite/smectite and smectite. Most of the white mica characterizing the alteration of U1 (Fig. 15B) is illite, as for late ore clay alteration (Fig. 15D). White mica characterizing U2 (Fig. 15C) is represented by illite and interlayered illite/smectite. The distribution of the data points in the diagram likely indicates inheritance of illite from muscovite/sericite.

Temperatures calculated using the equation of Cathelineau (1988) return an average of 224°C for pre-ore alteration, 289°C for U1, 282°C for U2 and 305°C for f7 (Fig. 15E). The method of calculation of Battaglia (2004) returns similar temperatures.

4.2.4 Composition and age of U oxides

REE signatures of uranium oxides

The REEs concentrations for U1, U2 and U3 are available as supplementary material (ESM-2). Fig. 16 displays the chondrite-normalized patterns for samples from Andrew Lake and End. Structural and macroscopic characteristics, and mineralogical associations allow defining that they represent U1 (samples 9850, 9568-38, 9568-39 and 9568-08), U2 (samples 9851, And-15-01-05), and U3 (sample And-15-01-04). U0 uranium oxides could not be analyzed by LA-ICP-MS due to their small size, anhedral shapes and mixing with Ti-U phases. Both U1 and U2 samples display bell-shaped chondrite-normalized patterns centered on Tb with a small anomaly in Eu (Fig. 16). Samples are enriched in intermediate REE (Sm to Dy) compared with light REE (LREE) and heavy REE (HREE), except for sample 9850 which is enriched in LREE compared to HREE. Samples of U1 are characterized by an HREE/LREE ratio around 1 (9568-38 and 39) or higher (sample 9568-08). Samples of U2 are slightly depleted in LREE and their HREE/LREE ratio is therefore higher. Sample AND-15-01-05 (U2) is enriched in REE compared to the other samples. Sample And-15-01-04 (U3) displays a stronger negative anomaly in Eu, higher concentrations in La compared to other LREE and a high LREE/HREE ratio (~2), comparable to sample 9850.

Sample 85W-10-04 displays a different pattern compared to the other samples of the Kiggavik area with the total concentration of REE much higher (up to a factor 10 for each element). The pattern displays a positive trend from La to Sm, centered on Sm and displays a negative pattern from Sm to Lu, this type of trend is observed only for this sample and is described for the first time in the Kiggavik area.

Age dating on U oxides

U oxides studied for REEs were also analyzed by SIMS for Pb/Pb and U-Pb isotopic dating. The dated samples come from Andrew Lake (4), End (1) and from 85W (1). Data from 9568-38 and 9568-39 are from Lach

(2012). Based on macroscopic characteristics and mineralogical associations, samples 9850, 9568-39, 9809 and 85W-10-04 are interpreted to be of U1, samples 9851, And-15-01-05 of U2 and sample And-15-01-04 of U3.

Data plot along or below the Discordia in the $^{206}Pb/^{238}U$-$^{207}Pb/^{235}U$ Concordia diagrams (Fig. 17), which suggests that most of the samples lost Pb after their crystallization. Electron microprobe analysis shows that studied uraninite and pitchblende display relatively high U contents (~75-86 wt%) but low Pb contents (0-5 wt% usually, ~10 wt% for one sample) especially for U1 and U2, indicating also a loss of Pb which confirms the Pb/U isotopic data. Three samples from Andrew Lake yielded upper intercept ages at 347 ± 58 Ma (sample 9850) and 344 ± 19 Ma (9851) for U1, 565 ±38 Ma (And-15-01-05, anchored at 0±10 Ma) for U2 and 547 ± 13 Ma (And-15-01-04) for U3. The sample from 85W yields an upper intercept age at 1073 ± 5 Ma (85W-10-04). The samples from End yields upper intercept ages at 1277±10 Ma (9568-38), 1175±23 Ma (9568-39) and 1257±58 Ma (9809). The scattering of the data for sample 9850 is linked to the presence of common lead which was corrected to calculate the upper intercept (black circles are data not considered).

4.2.5 Fluids inclusions and fluid inclusion planes characterization

Fluid inclusions composition

Different types of secondary fluid inclusions were observed as FIPs in quartz, magmatic in origin (primary quartz, in granite and granitic gneiss, predating all other quartz generations) from 85W and Contact.. Two types of FIPs were identified based on the FIs that constitute them: Type 1 and type 2 FIPs (Fig. 18A).

Type 1 FIPs are represented by monophase, vapour-only and dark fluid inclusions (rounded and sometimes "negative crystal" shape; Fig. 18B). Their size varies from 3 to 10 µm. No phase change was observed for these FIs even when they were cooled to -190°C. Analysis of the gas phase by Raman spectroscopy indicates that the FIs are filled with H_2O vapour only.

Type 2 FIPs are represented by biphase and triphase FIs. Biphase aqueous FIs are characterized by a dominant liquid phase with a vapour phase representing 10 to 20% of the FI by volume (Fig. 18C, liquid phase is H_2O). They have variable shapes with a size varying from 3 to 20 µm. They comprise three types; Lw', Lw" and Lw1. Gases other than H_2 and O_2 (CH_4, N_2) were detected very punctually and only as traces through Raman spectroscopy. Triphase aqueous FIs display a cube of halite (Fig. 18D, indicating oversaturation in NaCl), and belong to the Lwh' type. They have variable shapes and their size range from 6 to 20 µm. Liquid and vapour phases were analyzed under

Raman spectroscopy and like biphase aqueous FIs, only H_2 and O_2 were detected in the inclusions. Type 1 FIPs are crosscut by type 2 FIPs (Fig. 18E). This indicates the occurrence of at least two episodes of fluid circulation and that type 2 FIPs post-date type 1 FIPs.

A summary of microthermometric data obtained for the analysis of biphase and triphase FIs (99 FIs studied) is presented in table 2. Inclusions free of halite cube, for which the last phase to melt is ice, are referred to as Lw′ (32 FIs; −45.4 °C < Tm ice < −31.4 °C), Lw1 (2 FIs; −28.9 °C < Tm ice < −25.9 °C) or Lw″ (17 FIs; −23.9 °C < Tm ice < −1.4 °C). Except for Lw″ inclusions, the observed Te range from −85 to −60 °C, which indicates a complex composition, possibly H_2O–NaCl–$CaCl_2$ ± $MgCl_2$ – KCl. For Lw″ inclusions, the observed Te range from −65 to −38 °C and may be related to the H_2O–NaCl ± $CaCl_2$ ± $MgCl_2$ – KCl as major constituents. Considering all Lw′ and Lw1 inclusions, Tm ice display a continuous trend from −45 to −26 °C. Tm ice of Lw″ inclusions range from −24 to −1 °C. T_h varies from 62 to 245 °C and Ts NaCl range from 121 to 222 °C for Lwh′ inclusions.

The concentrations of several major, minor and trace elements in aqueous fluid inclusions (mainly Lwh' inclusions) were measured through LA-ICP-MS, and the proportions of fluid inclusions with element concentrations above the LOD (usually ~1ppm) are as follows: Na (100%), B (0%), Mg (100%), K (100%), Ca (100%), Mn (100%), Fe (38%), Cu (61%), Zn (54%), Rb (61%), Sr (100%), Cs (23%), Ba (85%), La (85%), Pb (100%), U (77%). The absolute content of every analyzed elements displays a great range of value, the highest being represented by Ca (31 000 to 80 000ppm), Na (5600 to 38 000 ppm), K (3500 to 17 000 ppm), Mg (1200 to 14 000 ppm), Fe (from LOD up to 79 000 ppm) and Sr (1000 to 6700 ppm). Metals such as Ba (LOD to 14 000 ppm), and Pb (270 to 11 000ppm) display moderate concentrations. Zn (LOD to 800 ppm), U (LOD to 1000 ppm), Cu (LOD to 400 ppm), Rb (LOD to 140 ppm), and Cs (LOD to 40 ppm), display lower concentrations compared to other elements. FIs are characterized by high concentration in Ca compared to Na, indicating that FIs studied are dominated by a $CaCl_2$-rich brines.

Fluid inclusion planes orientation (FIPs)

FIPs of each type were counted and the results plotted in rose diagrams as a function of plane strike (Fig. 20). FIPs at 85W are mainly type 1 (186 FIP measurements out of 240). In drill hole 85W-09 (samples 85W-09-07 and 85W-09-04), type 1 FIPs display main directions of N100-110. Secondary directions are N10-30 and N120-140.

For type 2 FIPs, studied samples returned a main direction of N110-120 and secondary directions around N120-130 and N40-60. For drill hole 85W-10 (sample 85W-10-04B), type 1 FIPs display main directions around N350-10, N140-160 and N110-130. Type 2 FIPs have main directions around N60-80 and N120-140. At the scale of 85W (Fig. 20, bottom part), there are therefore one main directions for type 1 FIPs: N100-110, and two minor directions: N350-10, and N140-160. Some sub-horizontal FIPs were observed at 85W; they are mainly composed by triphase FIs. Type 2 FIPs show two directions: N110-140 and N40-80.

At Contact, type 1 FIPs were also the most represented type (75 FIP measurements out of 96), these FIPs display a main N130-150 direction and secondary N110-130 direction. N0-20 is observed as a minor direction. Aqueous biphase and triphase FIPs overprint type 1 FIPs like at 85W. Type 2 FIPs display two directions: N110-120 and N80-N100. FIPs directions were also compared with reference to the orientation of the foliation of the granitic gneiss, which is sub-constant at Contact (N10/10° E).

5. Interpretation of the results and discussion

5.1 Main fracturing/mineralization events in the Kiggavik area

The fracturing events observed at Contact (Grare et al. 2018a) have been recognized in the other deposits and prospects in the Kiggavik area, confirming that the sequence of events established for this prospect can be extrapolated to the whole Kiggavik area. In addition, the present work has determined a first fracturing and magmatic-volcanic U mineralizing stage (U0). Macro- to micro-scale observations made for the Kiggavik area on outcrops and drill cores coupled to results from the multi-method approach developed are gathered and interpreted to propose for the first time a complete and global metallogenic model for this area.

Pre-Thelon fracturing and mineralization events in the Kiggavik area

Stage U0/f0

U0 is characterized macroscopically by microbrecciation (f0) of the host rock, better preserved at depth. Solution seams characteristics of this fracturing stage are traditionally observed in sedimentary environments (e.g. Rutter 1983; Benedicto and Schultz 2010) but have also been described in igneous rocks, for example in rhyolite and welded tuffs (Donald Bloss 1954; Burma and Riley 1955; Golding and Conolly 1962). Oriented data are poor for this fracturing event, making difficult to proper determine of the orientations of the associated structural features.

Fractures strike NE-SW to ENE-WSW, and dip NW, reflecting the orientation of the JSF at this location. This mineralizing stage is more represented in deposits and prospects controlled by major ENE trending faults, which highlights the role played by the major fault zones in focusing both fracturing events and fluid circulations through time for the Kiggavik area. Affected basement rocks are only weakly to non clay-altered, with Fe-rich chlorite precipitated at relatively high temperature (>300°C). Such features have not been previously depicted for U mineralization in the Kiggavik area, where mineralization are considered as associated with moderate to strongly clay-altered host rocks (Fuchs and Hilger 1989; Riegler et al. 2014; Sharpe et al. 2015; Shabaga et al. 2017) characterized by lower temperature chlorite (sudoite).

Microfracture cement is characterized, among others, by pitchblende and brannerite with Th contents of up to 7%. This mineralogy and the high Th content of U-bearing minerals is not of URU type, for which all analyzed U oxides have Th contents < 1% (Frimmel et al. 2014; Alexandre et al. 2015). This indicates that U0 is most probably related to magmatic-volcanic-related U ore systems, like those in the Beaverlodge area (Dieng et al. 2013), or the Poços de Caldas peralkaline complex (Schorscher and Shea 1992). These deposits are all related to relatively higher temperatures (>350°C) than the URU deposits (100-220°C) and with fluids with strongly different chemistries and origins. The f0 mineralized microbreccias predate veins of the QB event (ca. 1750 Ma) and is thus inferred to predate deposition of the Thelon Formation (older than 1667 Ma, Davis et al. 2011). The U0 mineralization is consequently considered to have occurred before the deposition of the Thelon Basin, at relatively high-T conditions.

QB/f2

The QB event is characterized by breccias present throughout the Kiggavik area in close association with the main fault trends (MZF, JSF, ALF). Emplacement of the QB occurred ca. 1750 Ma before the deposition of the Thelon Basin, associated with emplacement of intrusions of the Kivalliq Igneous suite (Grare et al. 2018b). QB crosscuts and postdates U0 (Fig. 4A). Main fault trends were the locus of polyphase brittle tectonic activity; they were likely first active before the QB event, and subsequently focused the circulation of Si-rich fluids (meteoric-derived fluids interacting with magmatic-derived fluids, see Grare et al. 2018b) that caused hydraulic fracturing and facilitated repeated fault reactivation. The inner zones of the breccia, much more silicified, are usually less fractured and altered compared to its outer zones; U orebodies are observed within the hangingwalls or footwalls, always out of the inner breccia zone. In addition, the clear spatial association between quartz veins of the QB (in its outer zone) and U mineralization suggests that the most silicified parts of the QB (i.e., the breccia core) was a transverse barrier for fluids but enhanced along-strike migration and entrapment through re-opening of veins in its outer zone. The QB played therefore a major role in partitioning fracturing and fluid flow through time for the different later U mineralization stages (Grare et al. 2018a, b).

Syn to post-Thelon fracturing events in the Kiggavik area and related U mineralization

U1 is hosted by relatively narrow fault zones (f5) (thickness of 5 to 20 m, damage core zones included) characterized by grey-greenish altered fault rocks (mainly illite, but sudoite was also characterized in this study and by XRD by Pacquet 1993a, b, c). Oriented data are scarce and except at Contact, they reflect the orientation of the main fault zone in which they are hosted (NE-SW trend of the ALF for the Andrew Lake deposit, WNW-ESE trend of the MZF for the 85W prospect).

U1 is usually of high grade and is not the most commonly described mineralization at Kiggavik, contrary to U2 (Sharpe et al. 2015; Shabaga et al. 2017). It can be mono and polymetallic. When monometallic, it is characterized by pitchblende and sulfide minerals (pyrite, chalcopyrite, bravoite, sometime intergrown with pitchblende), as observed at Contact. When polymetallic, it is characterized by pitchblende, sulfide minerals and Mo-Ni-As-Co-Ag-Au mineralized fault zones, as observed at Contact, Andrew Lake and Kiggavik Main Zone. Polymetallic U1 mineralization are rarer compared to monometallic mineralization. U1 is also characterized by the presence of illite and sudoite.

U2 is hosted in wider, reddish oxidized f6 fault zones associated with stronger clay alteration of the host rock, formed of illite and sudoite. This type of wide oxidized fault zones was well observed at Contact and Andrew Lake, and also recognized at End and Kiggavik Main Zone. As already observed by Grare et al. (2018a) at Contact, these oxidized faults are not always mineralized and fault cores that display strong clay alteration are usually not mineralized. U mineralization is stronger in well-developed, moderately clay-altered damage zones. These observations are in line with the classical view of fault zones (Chester and Logan 1986; Kim et al. 2004; Faulkner et al. 2010) where fracturing and fluid flow are more important in damage zones than in core zones (Caine et al. 1996).

Mineralization U2 is mineralogically characterized by pitchblende and is monometallic. Rare sulfide minerals (pyrite coated by pitchblende) are observed and relicts of ore minerals from previous stages can be observed where U1 fault zones are reworked by U2 faults. Along with the hematization of the host rock, these mineralogical differences highlight that U-bearing fluids had a different chemistry (although still being basinal brines) than those of U1, with probably slightly more elevated fO_2 and pH (see Pourbaix diagram in Romberger 1984). The orientations of U2 faults do not necessarily reflect the orientations of the main fault that hosts the deposit/prospect and which is better shown by non-mineralized oxidized faults (for example at Contact, Andrew Lake, End and Bong), whereas mineralized faults display a more complex range of orientations, sometimes with antithetic dip to the main fault (for example, NNW-SSE fractures at End, NE-SW to N-S fractures at Kiggavik). These variable orientations are typical within damage zones linking main faults and has been described in a variety of settings (Kim et al. 2004; Rotevatn and Bastesen 2014; Fossen and Rotevatn 2016). Overall, the differences (fracture orientations, intensity of clay-alteration, reduced vs. oxidized fault zones, polymetallic vs. monometallic) between mineralizing events U1 and U2 are here interpreted as the distinctive response of pre-existing and reactivated faults to a change in the regional tectonic stress field, which induced a maturation of the fault zones, thus a change in the fluids pathway, hence in contrasting fluid-rock interaction.

Main post-ore alteration event f7

The main post-ore (also called "late clay alteration") fracturing event (f7) is characterized by fault zones showing numerous narrow fault cores and strongly clay altered, dequartzified and completely bleached fault rocks. illlite is the only clay represented, sudoite were not observed under optical microscope and SEM. Fracturing/faulting is spatially and temporally dissociated of U mineralization; however this stage has a significant impact on the deposit's 3D organization because these faults offset U orebodies with a significant dip-slip and a minor strike-slip component. This is observed especially at Bong where the orebody is offset by W-E to WNW-ESE nearly dip-slip normal faults, but also at End where the orebody is offset by NW-SE to NNW-SSE faults. Moreover, observed U1 and U2 fault zones are also less mineralized when they are crosscut by white-clay altered faults, indicating remobilization of the U oxides at this stage. Only punctual relicts of pitchblende were observed in f7 fault zones (Fig. 5G). As this event corresponds to one of the latest fracturing stages, it is difficult to process oriented data in order to retrieve the "true" faults orientation, as we are facing neoformation and re-activation of fractures in complex and polyphase fault zones. An ESE-WNW to NNW-SSE trend and a steep dip to the NW appear however to be the dominant orientation of these faults in the Kiggavik area. Reactivation of faults during this stage is illustrated by NE-SW white clay-altered faults at Contact, initially belonging to the f6 stage (Grare et al. 2018a). This observation that most of the faults for this post-ore fracturing stage are inherited is consistent with models in which reactivation of faults is often easier compared to neoformation (e.g. Pinheiro and Holdsworth 1997).

Concerning mineralizing stage U3, even after careful review of drill core throughout the Kiggavik area, it was not possible to precisely link redox fronts to specific fault zone, this mineralizing event appearing associated with a weak reactivation of the fracture network without significant faulting.

5.2 Reconstruction of the temperature of the mineralizing fluids

Chlorite geothermometry

U0 is associated with chlorite crystallizing from 130-159°C up to 295-333°C, depending on the chosen geothermometer used. The evaluation of iron valence, thus the amount of Fe^{3+}, directly impacts the calculation of the temperature and has always been an analytical challenge. However, Bourdelle and Cathelineau (2015) demonstrated that the lower the temperature, the lower the impact of Fe^{3+} and a model based solely on Fe^{2+} is suitable in terms of practicability and simplicity while still giving reliable results. In our study, the high temperatures (295-333°C) obtained using Cathelineau (1988) and Jowett (1991) methods for dioctahedral chlorite of this stage appear consistent with the presence of brannerite and the high Th content of pitchblende observed in U0. The incorporation of thorium (Th^{4+}) into the uraninite structure is indeed correlated with the temperature and is commonly observed in metamorphic or magmatic uraninite (which form at T>300°C), contrary to hydrothermal uranium oxides (Depiné et al. 2013; Mercadier et al. 2013; Frimmel et al. 2014; Cuney et al. 2015) which form at T<300°C. The pre-Thelon high-temperature dioctahedral chlorites cementing f0 fractures would have likely been altered to sudoite at a later point, probably after the deposition of the Thelon Formation, by the circulation of Thelon-derived basinal brines thus crystallizing lower temperature di-trioctahedral chlorites (~100-200°C). Such a fluid circulation is considered as related to the formation of U1 and/or U2. Calculating the temperatures of formation of sudoite is not possible due to their chemistry, precluding any comparison with temperatures obtained by illite geothermometry.

Illite geothermometry

Pre-U1/f5, white mica (also called pre-ore) that crystallized at low temperatures (~200-240°C) could either represent early localized alteration along fault zones (f1) during development of the earlier Baker Lake and Wharton basins (i.e., brittle faulting and illitization prior to QB event, Grare et al. 2018b), or circulation of diagenetic fluids from the Thelon Basin (diagenetic quartz with temperatures of homogenisation of 100-160°C, peak diagenetic illite crystallized at ca. 200°C, Renac et al. 2002). White micas synchronous with U1 and U2 returned temperatures of ca. 280-290°C, but slightly higher in the case of U1. These temperatures are higher than those typically obtained for illite in the Athabasca Basin (220-280°C, Ng et al. 2013; Chu and Chi 2016), which could indicate crystallisation of illite and URU oxides at greater depth and/or an abnormally higher thermal gradient for the Thelon Basin compared to the Athabasca Basin. A higher thermal gradient, linked to magmatism associated with emplacement of the Kuungmi lavas at 1540±30 Ma (Chamberlain et al. 2010), i.e., the age proposed for the emplacement of U1 (Sharpe et al. 2015), is our preferred hypothesis, as no geological process could here explain a major increase in depth.

Post-ore illite alteration, observed in f7 fractures, returned slightly higher temperatures of 290-350°C; this increase in temperature could be linked to the emplacement of large volumes of magmas associated with the giant dike swarm of the Mackenzie event. This event could have triggered the circulation of "hot" hydrothermal fluids shortly before emplacement of the diabase dikes and "sealing" of faults, which would also be consistent with illite Ar-Ar ages obtained at ca. 1300 Ma at End, Andrew Lake, Kiggavik Main Zone and Bong (Ashcroft et al. 2017; Shabaga et al. 2017; and others, see Fig. 21).

Fluid inclusions

Temperatures obtained based on microthermometry on type 2 FIPs (syn-/post-Thelon event) observed in magmatic quartz range from 81°C to 240°C. These temperatures are comparable to those obtained in the Athabasca Basin for diagenetic-hydrothermal fluids (Richard et al. 2011, 2013), and at End (100-200°C, Chi et al. 2017) from fluid inclusions in quartz spatially associated with post-Thelon uraninite and calcite in the Kiggavik area.

The shift of ~100°C between temperatures given by fluid inclusions and those given by illite geothermometry has already been reported in the Athabasca Basin by Chu and Chi (2016). Such a difference could be related to the fact that the T_h measured for the fluid inclusions is usually lower than the temperature at the time of entrapment (i.e., at the time of fluid circulation).This difference could support a need for pressure correction of the fluid inclusion data, although it would not completely explain the shift of temperature (Richard et al. 2016).

5.3 Typology of U mineralization in the Kiggavik area

REE signatures

The REE patterns of U oxides are considered as specific to each type of U deposit, directly reflecting their conditions of formation (temperature, redox conditions, fluid composition, REE source(s); Mercadier et al. 2011; Frimmel et al. 2014; Alexandre et al. 2015). REE patterns were not obtained for the magmatic U0 because of the small size of U oxides. However their high Th contents indicate rather high T conditions and magmatic/volcanic fluids. The different U oxides from End (U1) and Andrew Lake (U2) display a bell-shape REE pattern centered on Tb which is only typical of URU systems (Bonhoure et al. 2007; Mercadier et al. 2011; Eglinger et al. 2013; Alexandre et al. 2015). Such pattern was also obtained by Fayek et al. (2017) at Kiggavik Main Zone and indicates unambiguously than U1 and U2 at Kiggavik area crystallized in rather identical physico-chemical conditions than typical unconformity-related U oxides in the Athabasca Basin (Pagel 1975; Derome et al. 2005; Richard et al. 2010; Martz et al. 2018). Most of the samples present modified bell-shaped REE patterns compared to URU-type U oxides from the Athabasca Basin, with enrichment in LREE, while concentrations of HREE remain the same (Fig. 16). This modified bell-shape REE pattern, observed for U oxides located in remobilization fronts at Kiggavik area (Fig.15A), was first described by Mercadier et al. (2011a) for U oxides in a remobilization front at Eagle Point U deposit in the Athabasca Basin, and is linked to the interaction between URU-type UO_2 and low-T (<50°C) meteoric fluids. Such modified spectrum is observed for U1 and U2 from the Kiggavik area (Fig. 16) and indicates that these initial URU-type UO_2 were chemically affected by meteoric water. This is consistent with their reset U/Pb isotopic ages (younger than 600 Ma; Fig. 17) and with macroscopic observations of redox front with goethite (AND-15-01-04 for example), inferred to have formed in low-T and low-saline conditions (Mercadier et al. 2011a). Such alteration and/or remobilization of brine-related uranium oxides by late low-T meteoric waters appears as a common and widespread features in the Kiggavik area, based on published and present data (Sharpe et al. 2015; Shabaga et al. 2017). The impact of such process is probably moreover far more developed in the Kiggavik area compared to the Athabasca Basin.

The shape of the REE patterns for the sample 85W-10-04 (85W) is quite different compared to the traditional URU bell-shaped pattern: the pattern displays comparable positive slope for LREE and negative slope for HREE, but is centered on SM and the REE concentrations are increased by a factor of 10 (Fig. 15C). A similar shape was only described for one uranium oxide in Zambia (Eglinger et al. 2013), which was considered as URU-type. Such a pattern is however not characteristic of URU oxides, as observed for all deposits in the Athabasca basins (Mercadier et al. 2011b; Alexandre et al. 2015). The REE composition and the age (post-Mackenzie dike) of this U oxide, indicate that the conditions for the crystallization of this mineralization were somewhat different than U1 and U2 U oxides. At the moment no conclusions can be made about the origin of this uranium oxide.

To summarize, when unaltered by post-crystallization alteration (End), U1 and U2 display REE patterns typical of URU-type uranium oxides from the Athabasca Basin. Such observation indicates that the physico-chemical conditions and the mineralizing fluids for the formation of U mineralization for the two districts were similar. U1 and U2 crystallized thus in URU-type conditions. These uranium oxides were strongly affected by late alteration related to meteoric waters which significantly changed their initial chemical composition and reset their U/Pb isotopic age. This alteration ultimately favored their dissolution and reprecipitation as U3 in redox front.

Fluid inclusion compositions

In contrast to what is observed in Athabasca basement (Mercadier et al. 2010; Potter and M. Wright 2015; Martz et al. 2017) no carbonic fluid inclusions were observed here. Dense arrays of dark monophase FIs are very similar to trends of retro-metamorphic fluid inclusions observed in the Athabasca Basin (Mercadier et al. 2010, Martz et al. 2017), bearing mainly CO_2, with some other gases,. The absence of CO_2 and CH_4 in our case could be explained either by the lack of graphite-rich lithologies and fault zones in the Kiggavik area, which are sources of CO_2 and CH_4 observed in retro-metamorphic FIs and in some aqueous FIs in Athabasca (Martz et al. 2017); or by a demixion at great depth that would have induced trapping of CO_2-rich liquid phase. This last hypotheses could be linked to an epithermal event, which has been characterized in/close to the Kiggavik area (Turner et al. 2001; Grare et al. 2018a, b). Such event, considered to be linked to the QB has not been described in the vicinity of the Athabasca Basin. Therefore, considering that type 1 FIPs are crosscut by type 2 FIPs, it is much more likely that these trends of vapor rich FIs characterize the QB event.

Aqueous biphase and triphase fluid inclusions observed at 85W and Contact display salinity between 24 to 39wt.% NaCl, and homogenization temperatures between 81 and 240°C. Temperatures and salinity obtained for aqueous fluid inclusions are comparable to those obtained by Chi et al. (2017) at End. Temperatures and salinity are higher compared to those obtained by Renac et al., (2002) in the Thelon sandstone out of mineralized zones: 100-160°C, ca. 17wt.% NaCl. Chi et al. (2017) also observed the absence of gases other than H_2O, H_2 or O_2, for primary monophase fluid inclusions in hydrothermal quartz. These observations, along with melting temperature of NaCl higher than homogenization temperatures and the fact that most of FIs do not freeze, indicate that aqueous biphase and triphase fluid inclusions are representative of a high salinity Ca-rich brines (Bodnar 2003; Derome et al. 2005). Such brines have been observed throughout the Athabasca Basin for all the studied U deposits. They are thought to be primarily derived from evaporated seawater and have variably mixed with with sodic brines of similar origin (Richard et al. 2011a, 2013, 2014). Ca-rich brines are supposed to derive from interaction with the basement (Derome et al. 2005; Mercadier et al. 2010; Richard et al. 2010, 2016; Martz et al. 2018). In this study, we observed only calcic brines in FIPs, while Chi et al., (2017) observed sodic and calcic brines in hydrothermal quartz veins. The sole occurrence of calcic brines and the absence of the sodic brines in some parts of the Kiggavik area would reflect a significantly long interaction of the brine with basement rocks. The slightly higher temperatures measured for the calcic brines in the Thelon Basin compared to the Athabasca Basin, in line with the temperatures calculated for the illite, could indicate a higher thermal gradient or a deeper percolation of brines within the basement. This could have well been the case in the Kiggavik area where the studied mineralized samples were located at a still unconstrained depth in the basement rocks, at the time of brine circulations (1500-1267 Ma), below a formerly overlying and now eroded cover of unknown thickness (Baker Lake and Thelon sediments).

Water-dominated fluid inclusions display similar concentrations compared to Ca-rich aqueous FIs from the McArthur River and Cigarl Lake U deposits in the Athabasca Basin (Richard et al. 2010, 2012, 2016; Martz et al. 2018), being extremely rich in metals like U, Zn, Rb, Sr, Cs, Ba, Pb. Boron was not detected in FIs of the Kiggavik area which could be linked to the lack of Mg-tourmaline in this zone compared to the Athabasca Basin. The present data indicate therefore that metal-rich (in particular U-rich) and highly-saline basinal brines circulated in the basement rocks of the Kiggavik area and were at the origin of the formation of U1 and U2 at ca. 1500-1275 Ma. These brines are rather identical to those linked to the formation of URU-type deposits in the Athabasca Basin. H_2O vapour, H_2 and O_2 were observed in some monophase and aqueous fluid, indicating radiolysis of H_2O in presence of U (Dubessy et al. 1988; Richard 2017).

5.4 Timing of mineralizing events

The pre-Thelon mineralizing event U0 is likely associated with peralkaline magmatism of the Dubawnt minette suite. Absolute age-dating was not possible on our samples due to the small size of U-oxides, but ages of ca.

1830 Ma were obtained on pitchblende within the Baker Lake Basin by (Miller and LeCheminant 1985) and Bridge et al. (2009) (Fig. 21).

Observations on U1 show that fractures associated with this mineralizing event (f5) crosscut dolomite veins formed by basinal brines derived from the Thelon Basin (Riegler et al., 2013). F6 faults constraining U2 crosscut sandstones of the Thelon Formation (Grare et al. 2018a). Absolute ages obtained for U1 are between 1293±08 Ma and 1187±20 Ma for End deposit and 354±47 Ma at Andrew Lake. The dated U2 samples display ages at 565±38 Ma and 345±19 Ma at Andrew Lake. However cross-cutting relationships indicate that these two stages occurred prior to the emplacement of the Mackenzie diabase dikes at 1267±2 Ma (LeCheminant and Heaman 1989; Heaman and LeCheminant 1993). U1 and U2 mineralization probably occurred between 1530 and 1267 Ma, interval previously proposed for the crystallization of hydrothermal UO_2 in the area (Sharpe et al. 2015; Chi et al. 2017). As previously proposed, the younger ages obtained at Andrew Lake (ca. 550 and 350 Ma) do reflect a reset of the U-Pb system of U oxides at these periods of time. This would have occurred through renewed circulation of meteoric and oxidizing fluids during two distinct events precisely dated at 550 Ma and 300 Ma. Such alteration of U0/U1/U2 and alteration by low-T meteoric fluids led ultimately to crystallization of U3 oxides (U3) along redox fronts at the same periods. A specific but unconstrained event of crystallization of a uranium oxide was active at End at ca. 1073 Ma. The compilation of the isotopic U-Pb ages and trace element concentrations for the different mineralization observed in the Kiggavik area indicate that the U system was polyphase and that U was mobilized during more than 1.5 billion years. Such extremely long duration of U events is similar to what has been observed in the Athabasca Basin. Additionally, these similarities between the Athabasca and Thelon Basins demonstrate that they had rather close evolution through time in terms of U systems, moving from relatively high-T magmatic/metamorphic conditions (U0) before 1750 Ma, to moderate-T hydrothermal conditions with basinal brines (U1 and U2) between 1530 to 1270 Ma to low-T meteoric mineralization (U3) after.

5.5 Tectonic stresses driving fracturing events in the Kiggavik area

Fig. 22 displays a synthesis of all oriented mesostructural data that exhibit kinematic indicators. Data are separated into macro/meso-scale observations (field, drill core, Fig. 22A) and micro-scale observations (solution seams and FIPs, Fig. 22B). This allowed to tentatively derive the local tectonic stress prevailing during fracturing/faulting events.

Kinematic indicators associated with f0/U0 are represented by the solution seams oriented NNW-SSE (Fig. 22B). This likely indicates a WSW-ENE trending □1 consistent with what was proposed by Hadlari and Rainbird (2011). However, the number of oriented data is very low which makes it hard to conclude on the tectonic stress even if the result obtained makes sense.

F2 stepped quartz veins and mode-I quartz veins related to U1 indicate a WNW-ESE trending σ1. This direction is also consistent when considering the supposed post-Thelon quartz veins described by Chi et al. (2017). This observation would mean that a regional strike-slip stress regime with a WNW-ESE trending σ1 and NNE-SSW trending σ3 possibly prevailed from the pre-Thelon stage (i.e., when the main Thelon fault developed) to a post-Thelon stage, ultimately until precipitation of U1 from basinal brines, as stepped calcite veins displaying W-E to NW-SE directions would have developed under a similar tectonic stress. Such a stress regime is consistent with type 1 FIPs and type 2 FIPs that display dominant WNW-ESE trends indicating a NNE-SSW to NE-SW trending σ3 during the emplacement of the QB (Fig.23). This WNW-ESE trending σ1 is further consistent with the dextral slip component along E-W to ENE-WSW trending fault relay zones in the QB. This is in agreement with the observations made by Anand and Jefferson (2017) who concluded that re-activation of ENE-WSW, N-dipping extensional faults (such as the TF or the JSF), formed initially during the deposition of the Baker Lake and Wharton Groups, occurred under a ~N110-140° trending σ1. We propose that this local tectonic stress is related to the Thelon-Taltson (2100-1930 Ma) and Trans-Hudsonian orogenies (1900-1800 Ma), when the whole Churchill craton was under roughly E-W compression; however at 1500-1300 Ma (U1 mineralizing stage), the Racklan orogeny (ca. 1600-1380 Ma; Cook 1992; Cook and MacLean 1995; Thorkelson 2000), to the west of the Kiggavik area) would be at the origin of the WNW-ESE shortening, as proposed by Anand and Jefferson (2017).

F6 neoformed and reactivated hematized fault zones underwent either sinistral and/or reverse movements (Fig. 22A). Sinistral reactivation of the ENE-WSW JSF overprinted the dextral motion on this fault that offsets the Schultz Lake Intrusive Complex (map scale observation, Fig. 2). These observations, together with the NE-SW crack-seal calcite (Ca2) veins (f6) coated with U2 spherulitic pitchblende support a local stress regime with NE-SW to ENE-WSW trending σ1 and NW-SE to NNW-SSE trending σ3 for the tectonic event associated with U2. This stress regime accounts for the secondary NE-SW to ENE-WSW trends of type 2 FIPs (Fig. 22B) within magmatic quartz from 85W associated to a second episode of circulation of basinal brines. The regional meaning of this stress regime still remains poorly understood.

Finally, the post-U1 and U2 faults (f7) which drove hot (~300°C), likely acidic fluids that strongly clay altered host rocks and offset U mineralisation, display two main trends: WNW-ESE with dextral to dextral-normal slip component and NNW-SSE with sinistral slip component. Combined with the dominant dip-slip component observed on some WNW-ESE faults observed at Bong, we infer a transtensional stress regime with σ1 trending NW-SE and σ3 trending NE-SW. This faulting event would be responsible for down-drop offset of the U orebodies at Bong, End and Kiggavik Main Zones (example in Fig. 13D). The NW-SE trending σ1 and NE-SW trending σ3 would also account for the latest sinistral offset of the Judge Sisson fault and Thelon fault by NNW-SSE faults, observed in the field and on aeromagnetic maps (Tschirhart et al. 2017). Such NNW-SSE faults were likely reopened during the emplacement of the Mackenzie dikes. The inferred NW-SE trending σ1 and main NE-SW trending σ3 is consistent with a regional-scale compressional stress active on the southeast margin of the Canadian Shield (Hou et al. 2010) at ca. 1270 Ma. Weak reactivation of the fracture network occurred at ca. 500 and 300 Ma, driving circulation of meteoric fluid, remobilizing and/or altering previously formed U oxides and precipitating U3. Such reactivation is probably linked to a far field stress associated with the breakup of West Rodinia supercontinent (ca.500 Ma, Bond et al. 1984) and the Appalachian Orogen (ca. 350 Ma, Hatcher, 2002), and is also observed in Athabasca (Dieng et al. 2013).

The structural evolution proposed in this study differs from the Riedel shear system of Anand and Jefferson (2017), although not incompatible with it. They proposed that the entire fracture network evolved mainly under a ~N110-N140 trending σ1 from ca. 1800 Ma to 1540 Ma. In their model, the different fault zones (ENE-WSW, NNW-SSE, NS, NE-SW, E-W) are part of a Riedel system (i.e., analogue to the P, T, X, R', R shears).

6. Metallogenic model of the Kiggavik area

The combination of all structural, mineralogical, fluid inclusion, dating and geochemical characteristics of the different U deposits and prospects from the Kiggavik area allows proposing for the first time a structurally-controlled metallogenic model of U mineralization in the Kiggavik area. The main fracturing events, their associated tectonic stress and fracture network evolution are presented in synthetic block diagrams (Fig. 23 to 27) for Bong, Kiggavik

Main Zone (both located on ~ENE-WSW faults), Andrew Lake and Contact (both located on ~NE-SW faults), together with the associated types of fluids, conditions and timing of their circulation and related mineralization type.

Pre-Thelon Basin fracturing events and the first stage of U mineralization

(f0, U0): the first U mineralizing event, characterized for the first time in this study, was observed in all major deposits in the Kiggavik area. Hydrothermal rutile cementing microfractures and coated with pitchblende at Contact (Grare et al. 2018a) are relicts of this first mineralizing stage. F0/U0 is crosscut by quartz veins of the QB (formed at ca. 1750 Ma) and is usually better preserved in deep-seated, less altered parts of the deposits (like in End, footwall of the QB). Major faults (ALF, JSF, MZF, probably TF) were active at that time (Fig. 23A), probably under a WSW-ENE σ1 and NNW-SSE σ3 (Fig. 23B), and mineralized.

Analyzed U-bearing minerals for this stage under EMPA come from End only; however, the same chemistry (several percent of thorium) was also described by Weyer (1989) at Kiggavik Main Zone. Thorium content in pitchblende and brannerite characterizes a relatively high temperature fluid (>400°C), along with presence of rutile and temperatures returned by chlorite geothermometer (>350°C). Mineralized microfractures and the characteristic solution seams were also described by Miller, (1980) and Lecheminant et al. (1979) in their study of the Kazan Fall U mineralization, and like unaltered chlorite observed within the cement of the mineralized microbreccia in the Kiggavik area, the chlorite in the Kazan Fall microbreccia returned temperatures around 300-350 °C.

This U mineralization event likely occurred in the Thelon-Baker Lake area at the end of the Trans-Hudsonian orogeny (ca. 1830 Ma), in response to retro-arc extension with deposition of the Baker Lake formation and emplacement of U-rich peralkaline magmas of the Dubawnt igneous suite (Cuney 2014; Cuney et al. 2015). Such mineralizing event is plausible in the Kiggavik area even as located far from the formations of the Baker Lake Basin, since a breccia pipe of the Christopher Island formation (ca. 1827 Ma) was observed in the eastern part of the Kiggavik area, along with ultrapotassic minette and bostonite dikes (Anand and Jefferson 2017) of the Dubawnt igneous suite (ca. 1830 Ma). These rocks are enriched in U (LeCheminant et al. 1987; Miller and Blackwell 1992; Peterson et al. 2011) and could also represent a good source of U.

This mineralizing event, that predates deposition of the Thelon Basin, is the first U mineralizing event in the Kiggavik area and is likely of magmatic/volcanic origin. Mineralisation occurred within major fault zones and form the first significant "stock" of U oxides in the Kiggavik area. This stock will be later remobilize to form the younger mineralization.

(QB, f2): Intense quartz brecciation related to the QB event occurred along major fault zones in the Kiggavik area and also South of the Kiggavik area (Baudemont and Reilly 1997; Turner et al. 2001). FIs in quartz of the QB were characterized by several authors (Pagel 1995; Turner et al. 2001; Riegler 2013; Chi et al. 2017; this study). Most of the quartz belongs to the QB event, as characterized by cathodoluminescence and textural observations on quartz by Grare et al. (2018b). They are characterized by high temperature/low salinity fluids (Pagel et al. 1995). They are also characterized by trends of monophase FIs in concentric zones of quartz. QB crosscut Nueltin granites of the ca. 1750 Ma Kivalliq igneous suite and predates deposition of the Thelon Basin. Textural characteristics and fluid inclusion data from different locations in the Kiggavik area attest for a regional magmatic event associated with massive and likely repeated influx of silica rich fluids of likely igneous origin (Grare et al. 2018b). This event is therefore likely linked to magmatism of the Kivalliq igneous suite dated at ca. 1750 Ma. Fluid circulation was focused along major faults and relay zones (Fig. 24A), silicifying/overprinting previously formed fault rocks. QB formed under a WNW-ESE trending $\sigma1$ and NNE-SSW trending $\sigma3$ (Fig 24B). This silicificationevent likely controlled, at least partly, later fracturing and fluid circulation, depending on the thickness of the quartz breccia: U mineralization is usually stronger in the hanging wall of the structure (e.g., for End and Contact).

(Syn?) Post-Thelon Basin fracturing events: second and third stages of URU-type U mineralization

(f5, U1): this stage is characterized by monometallic to polymetallic mineralization within reduced narrow fault zones (Fig. 25A). Illite is the main alteration product but sudoite was observed in altered mineralized fault rocks at Jane (Miller 1997), End (Lida 1997), Bong, (Riegler et al. 2014; Sharpe et al. 2015) and Kiggavik Main Zone (Pacquet 1993a). APS, synchronous with U mineralization, were observed at 85W (this study), and by Riegler et al. (2016) at Bong.

U1 postdates quartz veins and dolomite veins precipitated from typical basin-derived and highly saline brines (Chi et al. 2017; and Riegler, 2013; respectively), and is synchronous with the first generation of calcite veins. Fluid inclusions in calcite at End were studied by Chi et al. (2017). This calcite was not characterized under cathodoluminescence, but it is probable that Chi et al. (2017) studied fluid inclusions of the first generation of calcite (Ca1 as defined in our study) as veins of the second generation are usually too thin to study fluid inclusions. This first generation of calcite also precipitated from Thelon-derived highly saline basinal brines. This synchronicity also allows deducing that fracturing stage f5 associated with U1 formed in response to a stress regime with WNW-ESE $\sigma 1$ and NNE-SSW $\sigma 3$ (Fig. 22B).

ENE-WSW, N-dipping extensional faults formed earlier during the deposition of the Baker Lake and Wharton Groups were reactivated at that stage with a dextral-normal kinematics, favoring the circulations of the NaCl-rich basinal brines from the Thelon Basin to the basement rocks and the probable formation of $CaCl_2$-and U-rich mineralizing brines (U1). The oldest ages were obtained by Farkas et al., (1984) and Sharpe et al., (2015) at 1403±10 Ma and 1520±79 Ma respectively. Local heating and circulations of hydrothermal fluid associated with emplacement of the Kuungmi lavas at ca. 1540±30 Ma (Chamberlain et al. 2010) are described as one possible first event of URU-type mineralisation in the Kiggavik area (Sharpe et al. 2015). This age was observed throughout the Thelon-Baker Lake area ((Turner et al. 2003; Bridge et al. 2013)). Ages at 1500-1400 Ma are comparable to ages obtained on oldest URU mineralization in Athabasca (1514±18 Ma, Cumming and Krstic 1992; 1519±22 Ma, Fayek et al. 2002; 1540±19 Ma, Alexandre et al. 2009). The time frame defined by age-dating studies and the reconstructed stress regime are consistent with the Racklan orogeny (ca. 1600-1380 Ma; Cook 1992; Cook and MacLean 1995; Thorkelson 2000).

Minerals that fingerprint highly saline basinal brines (sudoite, APS), fluid inclusion characteristics (high salinity, Ca-rich, Th between 100 and 220°C), and the REE bell shape pattern of uranium oxides, along with the timing of the mineralizing event (post-Thelon formation), allow concluding that U1 precipitated from Thelon (or Baker Lake)-derived basinal brines, and thus is of unconformity-related type, like the U deposits in the Athabasca Basin.

(f6, U2): this stage is characterized by monometallic mineralization within oxidized wide fault zones (Fig. 26A), formed under a ~NE-SW trending $\sigma 1$ and ~NW-SE trending $\sigma 3$ (Fig. 26B). This fracturing event formed new fractures while likely reactivating the complex, pre-existing fracture network of the Kiggavik area. The response of the fracture network to the tectonic stress was obviously different depending on its orientation: at Andrew Lake and Contact, hematized and mineralized damage zones of faults trending NE-SW are well developed in contrast to those associated within ENE-WSW fault zones of the Kiggavik Main Zone deposit (Fig. 26A).

APS minerals were observed in oxidized fault zones at Contact (Grare et al. 2018a) and 85W (this study), and sudoite associated with illite, were described, at Contact (Grare et al. 2018a), Jane (Miller 1997), Kiggavik Main Zone (Hasegawa et al. 1990), End (Lida 1997) and Andrew Lake (Hasegawa et al. 1990; Pacquet 1994). This monometallic mineralizing stage was also described at Andrew Lake (Shabaga et al. 2017).

Like U1, U2 formed in relation to the circulations of basinal brines derived from the Thelon Basin, and is of unconformity-related type. Relative chronology places the formation of U2 after the deposition of the Thelon Formation but before emplacement of the Mackenzie dikes, hence bracketed between 1500 and 1267 Ma. Note however that no available absolute age dating (ca. 1000 Ma, Shabaga et al. 2017; 550-300 Ma, Shabaga et al. 2017; this study) supports this timing. One likely explanation is related to alteration and reset/reprecipitation of U-oxides that accounts for the modified REE bell-shape pattern for U2 oxides (Fig. 16).

Concerning URU-type mineralization in the Kiggavik area, two main differences with the Athabasca Basin are the absence of magnesio-foitite (Mg-tourmaline also called dravite, Mercadier et al. 2012) and a Mg-rich sudoite rather than a Al-Mg sudoite. The absence of Mg-foitite is consistent with the non-detection of Boron in the brines of the Kiggavik area (Fig. 19), a major difference with the brines in the Athabasca Basin (Richard et al. 2016). Potential U sources for U1 and U2 are various and could be the metamorphosed epiclastic rocks of the Puqik Lake formation (Johnstone et al., 2017), rhyolitic flows of the Wharton group (Blake 1980; Peterson et al. 2015), fluorapatite-cemented breccia at the base of the Thelon formation (Davis et al. 2011), ultrapotassic minette and bostonite dikes (LeCheminant et al. 1987; Miller and Blackwell 1992; Peterson et al. 2011) of the Dubawnt igneous suite (ca. 1830 Ma), U-rich pegmatite of the Kivalliq igneous suite (Scott and Peterson 2012) but more specifically the previous U mineralizing stage (U0). U0 is observed in significantly mineralized brecciated rocks, and would have been an efficient and easily available source of U for basinal brines during their circulations in U0-mineralized basement structures. The presence of a pre-Thelon-basin source of uranium is comparable to what is described near the Athabasca basin: volcanic and metasomatic uranium in the western margin (Dieng et al. 2013, 2015) or magmatic and metamorphic uranium described in the eastern margin (Mercadier et al. 2013).

(f7): The last main fracturing event is characterized by strongly desilicified, illitized and bleached fault rocks, also reworking/offsetting previously formed ore bodies along E-W and NW-SE faults (Fig. 27A). Emplacement of a mantle plume triggered the emplacement of Mackenzie mafic dikes swarm at ca. 1267 ± 2 Ma.

Such magmatism intruded the pre-existing extensional fractures which were active under a NE-SW trending σ3 (Fig. 27B). This magmatic event is likely at the origin of circulation of hot (~300°C), probably acidic, fluids during the f7 fracturing stage. This timing is supported by age dating on illite (K-Ar and Ar-Ar) showing an alteration event at ca. 1300 Ma (Fig. 21) at End, Andrew Lake, Bong and Kiggavik Main Zone. The circulation of fluids linked to the extensional event and to the magmatism likely occurred at ca. 1330-1265 Ma, considering age dating of uranium oxides and of MacKenzie dikes. This tectonic/magmatic event ended by the emplacement of the MacKenzie diabase dikes which crosscut orebodies and "seal" the affected faults; they are almost unaltered and fractured. Along these dikes, thermal effect would have locally remobilized and reprecipitated U oxides, resetting the U/Pb isotopic system. Such strong clay alteration has previously been described as synchronous with U alteration (Hasegawa et al. 1990; Riegler et al. 2014; Shabaga et al. 2017), but this study shows that white clay illitization post-date U0/U1/U2.

Post Mackenzie dikes minor fracturing events and U mineralization/reprecipitation

Several ages were previously obtained at Kiggavik area on U oxides at ca. 1000 Ma and ca. 800 Ma (Fig. 21). These ages, not measured in the present study, could correspond to far-field tectonic activity associated with the Grenville orogeny (Gordon and Hempton 1986) and the initial rifting event of Rodinia, for example (Badger et al. 2010; McClellan and Gazel 2014). It is to date unknown whether these two events have led to the formation of new mineralization or simply caused alteration and reset of existing mineralization. Younger ages at ca. 550 Ma and ca. 350 Ma correspond to reset of the U-Pb isotopic systems of U1 and U2 but also to their dissolution and precipitation of U3. The specific modified bell shape pattern marks the alteration and remobilization of the URU-type U oxides by low-T meteoric fluids, which is consistent with the observation of goethite in these mineralized samples, a low temperature iron oxide (in contrary to hematite observed for stage U2). U3 occurred at a post-Mackenzie stage and does not belong to the unconformity-related type. It likely happened when a significant thickness of Thelon Basin, Wharton Basin and/or basement rocks was definitely eroded, letting supergene, low-temperature oxidizing fluids circulating through the fracture network and remobilizing U.

7. Conclusions

This paper proposes for the first time an integrated structural and metallogenic model of the Kiggavik area based on a multi-scale and multi-disciplinary approach.

The main conclusions of the study are the followings:

- The Kiggavik area is characterized by a polyphased fracture network that evolved in a brittle style from ca. 1830 Ma until the emplacement of the Mackenzie dikes at ca. 1270 Ma. The pre-Thelon U0 mineralization and QB event (f2 at ca. 1750 Ma) highlight the importance of magmatic-related fracturing, fluid circulation and mineralisation controlling subsequent location of URU-type U deposits.

- This stage of fracturing and U0 mineralization is likely linked with the peralkaline magmatism of the Dubawnt minette suite at ca. 1830 Ma. Such mineralized breccia constituted a first significant stock of U available for reconcentration through later circulation of oxidized basinal brines. This first mineralization is of magmatic-related type.

- After deposition of the Thelon and Lookout Point formations, a first circulation in basement structures of highly-saline basinal brines derived from the Thelon Basin occurred under a WNW-ESE $\sigma 1$ and NNE-SSW $\sigma 3$. This event precipitated U1 in fault relay zones (End, Kiggavik Main Zone) and/or in zones where faults were the Quartz Breccia was present (e.g., Bong, Contact, Andrew Lake, End). Fracturing and renewed circulations of basinal brines occurred under a NE-SW $\sigma 1$ and NW-SE $\sigma 3$ with transpressional reactivation of the previously formed fault/fracture network to form U2. U mineralization preferentially developed in moderately altered damage zones of fault zones. U1 and U2 mineralization belong to the unconformity-related type, as characterized in the Athabasca Basin. They formed before the MacKenzie dike event, i.e. between 1530 and 1270 Ma, in relative similar conditions and timing than URU-type mineralization in the Athabasca Basin.

- Circulations of basinal brines occurred through a fault/fracture network that evolved though time in response to the changing local/far-field tectonic stress. This caused changes in the fluid pathways hence in fluid-rock interaction (changing characteristics of the fluid such as fO_2 and pH) and led to slightly different U mineralization (polymetallic reduced U1 vs monometallic oxidized U2).

- The initial NaCl-rich basinal brines reacted with basement rocks to form CaCl2- and metal-rich mineralizing brines at the origin of U1 and U2. The chemistry and physico-chemical characteristics of the CaCl2-rich brines in the Kiggavik area are similar to those measured for mineralizing $CaCl_2$-rich brines in the Athabasca Basin, indicating rather common processes for the two sedimentary basins and related U mineralization.

- Late faulting and associated strong clay alteration and bleaching of the host rock occurred at ca. 1300 Ma in response to local NE-SW extension and regionally NW-SE far-field $\sigma 1$. This fracturing event, barren of U mineralization, caused the offset of previously formed orebodies and accounts for the formation in the Kiggavik area of strongly altered areas disconnected of any U mineralization.
- Post Mackenzie dikes weak reactivation of the fracture network induced circulation of low-T meteoric fluids, remobilizing/reprecipitating U oxides (U3) and altering their geochemical signature at two different times, ca. 550 and 350 Ma, presumably linked to changing far-field stress associated with continent break-up and assembly. Other events of fluid circulations likely happened at ca. 1000 and 700 Ma in relation similar process. A mineralization event with specific physico-chemical characteristics was dated at 1073 Ma, its origin and related processes remain unknown.
- U mineralization in the Kiggavik area are therefore of a mixed type, combining magmatic, URU type and meteoric-related ("roll-front") mineralization, rather than being purely of URU type, like what is actually described in the Athabasca Basin. This area demonstrates more than 1.5 billion years of uranium mobility.

Acknowledgments

The authors thank Orano and Orano Canada for the full financial support and access to the Kiggavik camp and exploration data. We thank Orano for the permission to publish these results. Special thanks to Dr. Kathryn Bethune for her in-depth review, senior petrographist M. Brouand, senior geoscientist D. Quirt, ARC geologists R. Zerff, R. Hutchinson, K. Martin, and D. Hrabok for their help and enriching discussions during field work and data interpretation. Thanks to P. Martz for his help on studying fluid inclusions. We are grateful to N. Bouden, J. Villeneuve and E. Deloule at CRPG (Vandoeuvre-lès-Nancy) for SIMS analyses, and to A. Lecomte and O. Rouer at SCMEM (GeoRessources, Vandoeuvre-lès-Nancy) for data acquisition. Thanks to J.M. Vergeau and P-C. Guiollard at Bessines-sur-Gartempe Areva site for help and access to historical data and samples.

References

Alexandre P, Kyser K, Layton-Matthews D, et al (2015) Chemical Compositions of Natural Uraninite. Can Mineral 53:595–622. doi: 10.3749/canmin.1500017

Alexandre P, Kyser K, Thomas D, et al (2009) Geochronology of unconformity-related uranium deposits in the

Athabasca Basin, Saskatchewan, Canada and their integration in the evolution of the basin. Miner Depos 44:41–59. doi: 10.1007/s00126-007-0153-3

Allan MM, Yardley BW, Forbes LJ, et al (2005) Validation of LA-ICP-MS fluid inclusion analysis with synthetic fluid inclusions. Am Mineral 90:1767–1775

Anand A, Jefferson CW (2017) Reactivated fault systems and their effects on outcrop patterns of thin-skinned early thrust imbrications in the Kiggavik uranium camp, Nunavut

Ashcroft GS, Fayek M, Quirt D, et al (2017) The geochemistry and geochronology of the End Deposit, NE Thelon region, Nunavut Canada: An insight to the Athabasca basin's closest relative. 1

Badger RL, Ashley KT, Cousens BL (2010) Stratigraphy and geochemistry of the Catoctin volcanics: Implications for mantle evolution during the breakup of Rodinia. In: Tollo RP, Bartholomew MJ, Hibbard JP, Karabinos PM (eds) From Rodinia to Pangea: The Lithotectonic Record of the Appalachian Region. Geological Society of America

Battaglia S (2004) Variations in the chemical composition of illite from five geothermal fields: a possible geothermometer. Clay Miner 39:501–510. doi: 10.1180/0009855043940150

Baudemont D, Reilly B (1997) Thelon Project - 1997: Reconnaissance Mapping and Structural Geology. 43

Benedicto A, Schultz RA (2010) Stylolites in limestone: Magnitude of contractional strain accommodated and scaling relationships. J Struct Geol 32:1250–1256. doi: https://doi.org/10.1016/j.jsg.2009.04.020

Blake DH (1980) Volcanic rocks of the Paleohelikian Dubawnt Group in the Baker Lake - Angikuni Lake area, District of Keewatin, N.W.T., bulletin 3

Bodnar RJ (2003) Introduction to aqueous-electrolyte fluid inclusions. Fluid inclusions Anal Interpret 32:81–100

Bond GC, Nickeson PA, Kominz MA (1984) Breakup of a supercontinent between 625 Ma and 555 Ma: new evidence and implications for continental histories. Earth Planet Sci Lett 70:325–345. doi: https://doi.org/10.1016/0012-821X(84)90017-7

Bonhoure J, Kister P, Cuney M, Deloule E (2007) Methodology for Rare Earth Element Determinations of Uranium Oxides by Ion Microprobe. Geostand Geoanalytical Res 31:209–225. doi: 10.1111/j.1751-908X.2007.00865.x

Bourdelle F, Cathelineau M (2015) Low-temperature chlorite geothermometry: a graphical representation based on a T?R2? ?Si diagram. Eur J Mineral 27:617–626. doi: 10.1127/ejm/2015/0027-2467

Breemen O van, Peterson TD, Sandeman HA (2005) U– Pb zircon geochronology and Nd isotope geochemistry of

Proterozoic granitoids in the western Churchill Province: intrusive age pattern and Archean source domains. Can J Earth Sci 42:339–377. doi: 10.1139/e05-007

Bright S, Conner G, Turner A, Vearncombe J (2014) Drill core, structure and digital technologies. Appl Earth Sci 123:47–68. doi: 10.1179/1743275814Y.0000000051

Burma BH, Riley CM (1955) Two unusual occurrences of microstylolite. J Sediment Res 25:38–40. doi: 10.1306/D42697EC-2B26-11D7-8648000102C1865D

Caine JS, Evans JP, Forster CB (1996) Fault zone architecture and permeability structure. Geology 24:1025–1028

Cathelineau M (1988) Cation Site Occupancy in Chlorites and Illites as a Function of Temperature. Clay Miner - CLAY Min 23:471–485

Cathelineau M, Boiron MC, Holliger P, Poty B (1990) Metallogenesis of the French part of the Variscan orogen. Part II: Time-space relationships between U, Au and Sn□W ore deposition and geodynamic events — mineralogical and U□Pb data. Tectonophysics 177:59–79. doi: https://doi.org/10.1016/0040-1951(90)90274-C

Chamberlain KR, Schmitt AK, Swapp SM, et al (2010) In situ U–Pb SIMS (IN-SIMS) micro-baddeleyite dating of mafic rocks: Method with examples. Precambrian Res 183:379–387. doi: 10.1016/j.precamres.2010.05.004

Chester FM, Logan JM (1986) Implications for mechanical properties of brittle faults from observations of the Punchbowl fault zone, California. pure Appl Geophys 124:79–106. doi: 10.1007/BF00875720

Chi G, Haid T, Quirt D, et al (2017) Petrography, fluid inclusion analysis, and geochronology of the End uranium deposit, Kiggavik, Nunavut, Canada. Miner Depos 52:211–232. doi: 10.1007/s00126-016-0657-9

Chu H, Chi G (2016) Thermal profiles inferred from fluid inclusion and illite geothermometry from sandstones of the Athabasca basin: Implications for fluid flow and unconformity-related uranium mineralization. Ore Geol Rev 75:284–303. doi: https://doi.org/10.1016/j.oregeorev.2015.12.013

Cook DG, MacLean BC (1995) The intracratonic Paleoproterozoic Forward orogeny, and implications for regional correlations, Northwest Territories, Canada. Can J Earth Sci 32:1991–2008. doi: 10.1139/e95-152

Cook FA (1992) Racklan Orogen. Can J Earth Sci 29:2490–2496. doi: 10.1139/e92-195

Corrigan D, Pehrsson S, Wodicka N, de Kemp E (2009) The Palaeoproterozoic Trans-Hudson Orogen: a prototype of modern accretionary processes. Geol Soc London, Spec Publ 327:457–479. doi: 10.1144/SP327.19

Cumming GL, Krstic D (1992) The age of unconformity-related uranium mineralization in the Athabasca Basin, northern Saskatchewan. Can J Earth Sci 29:1623–1639. doi: 10.1139/e92-128

Cuney M (2014) Felsic magmatism and uranium deposits. Bull la Soc Geol Fr 185:75–92

Cuney M, Kyser K (2009) Recent and Not-So-Recent Developments in Uranium Deposits and Implications for Exploration. Econ Geol 104:600–601

Cuney M, Kyser TK, Mineralogical Association of Canada (2015) The geology and geochemistry of uranium and thorium deposits

Curtis L, Miller AR (1980) Uranium geology in the Amer-Dubawnt-Yathkyed-Baker Lakes region, Keewatin district, NWT Canada. Proc Int Uranium Symp Pine Creek Geosyncline 22

Davis WJ, Gall Q, Jefferson CW, Rainbird RH (2011) Fluorapatite in the Paleoproterozoic Thelon Basin: Structural-stratigraphic context, in situ ion microprobe U-Pb ages, and fluid-flow history. GSA Bull 123:1056–1073

Davis WJ, Hanmer S, Tella S, et al (2006) U–Pb geochronology of the MacQuoid supracrustal belt and Cross Bay plutonic complex: Key components of the northwestern Hearne subdomain, western Churchill Province, Nunavut, Canada. Precambrian Res 145:53–80. doi: https://doi.org/10.1016/j.precamres.2005.11.016

Depiné M, Frimmel HE, Emsbo P, et al (2013) Trace element distribution in uraninite from Mesoarchaean Witwatersrand conglomerates (South Africa) supports placer model and magmatogenic source. Miner Depos 48:423–435. doi: 10.1007/s00126-013-0458-3

Derome D, Cathelineau M, Cuney M, et al (2005) Mixing of Sodic and Calcic Brines and Uranium Deposition at McArthur River, Saskatchewan, Canada: A Raman and Laser-Induced Breakdown Spectroscopic Study of Fluid Inclusions. Econ Geol 100:1529–1545. doi: 10.2113/gsecongeo.100.8.1529

Dieng S, Kyser K, Godin L (2013) Tectonic history of the North American shield recorded in uranium deposits in the Beaverlodge area , northern Saskatchewan , Canada. Precambrian Res 224:316–340. doi: 10.1016/j.precamres.2012.09.011

Dieng S, Kyser K, Godin L (2015) Genesis of Multifarious Uranium Mineralization in the Beaverlodge Area, Northern Saskatchewan, Canada. Econ Geol 110:209–240

Donald Bloss F (1954) Microstylolites in a Rhyolite Porphyry. J Sediment Res - J SEDIMENT RES Vol. 24:

Dubacq B, Vidal O, De Andrade V (2010) Dehydration of dioctahedral aluminous phyllosilicates: Thermodynamic modelling and implications for thermobarometric estimates. Contrib to Mineral Petrol 159:159–174

Dubessy J, Pagel M, Beny J, et al (1988) Radiolysis evidenced by Hz-O2 and Hz-bearing fluid inclusions in three uranium deposits. 52:

Dubessy J, Poty B, Ramboz C (1989) Advances in C-O-H-N-S fluid geochemistry based on micro-Raman spectrometric analysis of fluid inclusions. Eur J Mineral 1:517–534. doi: 10.1127/ejm/1/4/0517

Eglinger A, André-Mayer A-S, Vanderhaeghe O, et al (2013) Geochemical signatures of uranium oxides in the Lufilian belt: From unconformity-related to syn-metamorphic uranium deposits during the Pan-African orogenic cycle. Ore Geol Rev 54:197–213. doi: https://doi.org/10.1016/j.oregeorev.2013.04.003

Farkas A (1984) Lone Gull Deposit Mineralogy and Host Rock Alteration. 191

Faulkner DR, Jackson CAL, Lunn RJ, et al (2010) A review of recent developments concerning the structure, mechanics and fluid flow properties of fault zones. J Struct Geol 32:1557–1575. doi: 10.1016/j.jsg.2010.06.009

Fayek M, Kyser TK, Riciputi LR (2002) U and Pb isotope analysis of uranium minerals by ion microprobe and the geochronology of McArthur River and Sue Zone Uranium deposits, Saskatchewan, Canada. Can Mineral 40:1553. doi: 10.2113/gscanmin.40.6.1553

Fayek M, Quirt D, Jefferson CW, et al (2017) The Kiggavik-Andrew Lake structural trend uranium deposits : An overview. 4

Fossen H, Rotevatn A (2016) Fault linkage and relay structures in extensional settings-A review. Earth-Science Rev 154:14–28. doi: 10.1016/j.earscirev.2015.11.014

Friedrich G, Weyer HJ, Bectel A, Ballhorn RK (1989) The Lone Gull uranium deposit - New geochemical and petrological data as evidence for the nature of the ore bearing solutions. IAEA, Tech Comm Metallog uranium Depos 293–305

Frimmel HE, Schedel S, Brätz H (2014) Uraninite chemistry as forensic tool for provenance analysis. Appl Geochemistry 48:104–121. doi: https://doi.org/10.1016/j.apgeochem.2014.07.013

Fuchs HD, Hilger W (1989) Kiggavik (Lone Gull): An unconformity related uranium deposit in the Thelon basin, northwest territories, Canada

Fuchs HD, Hilger W, Prosser E (1986) Geology and Exploration History of the Lone Gull Property

Gall Q, Peterson TD, Donaldson J (1992) A proposed revision of Early Proterozoic stratigraphy of the Thelon and Baker Lake basins, Northwest Territories. Geol Surv Canada Curr Res 92–1c:129–137

Golding HG, Conolly JR (1962) Stylolites in volcanic rocks. J Sediment Res 32:534–538. doi: 10.1306/74D70D12-2B21-11D7-8648000102C1865D

Gordon MB, Hempton MR (1986) Collision-induced rifting: The Grenville Orogeny and the Keweenawan Rift of

North America. Tectonophysics 127:1–25. doi: https://doi.org/10.1016/0040-1951(86)90076-4

Grare A, Benedicto A, Lacombe O, et al (2018a) The Contact uranium prospect, Kiggavik project, Nunavut (Canada): Tectonic history, structural constraints and timing of mineralization. Ore Geol Rev 93:141–167. doi: https://doi.org/10.1016/j.oregeorev.2017.12.015

Grare A, Lacombe O, Mercadier J, et al (2018b) Fault Zone Evolution and Development of a Structural and Hydrological Barrier: The Quartz Breccia in the Kiggavik Area (Nunavut, Canada) and Its Control on Uranium Mineralization. Minerals 8:319. doi: 10.3390/min8080319

Gueguen Y, Palciauskas V, Jeanloz R (1995) Introduction to Physics of Rocks. Phys Today - PHYS TODAY 48:

Guillong M, Meier DL, Allan MM, Yardley BWD (2008) SILLS: A MATLAB-based program for the reduction of laser ablation ICP-MS data of homogeneous materials and inclusions. In: Laser ablation ICP-MS in the Earth sciences: current practices and outstanding issues, vol 40. Mineralogical Association of Canada Short Course Series, Sylvester. Vancouver, pp 328–333

Hadlari T, Rainbird RH (2011) Retro-arc extension and continental rifting : a model for the Paleoproterozoic Baker Lake Basin ,. doi: 10.1139/E11-002

HadlariT., RainbirdR.H. (2011) Retro-arc extension and continental rifting: a model for the Paleoproterozoic Baker Lake Basin, Nunavut1Geological Survey of Canada Contribution 20100436. Can J Earth Sci 48:1232–1258. doi: 10.1139/e11-002

Hasegawa K, Davidson GI, Wollenberg P, Lida Y (1990) Geophysical Exploration for Unconformity-related uranium deposits in the Northeastern part of the Thelon basin, Northwest territories, Canada. Kozan Chishitsu 40:83–94

Hatcher Robert D. J (2002) Alleghanian (Appalachian) orogeny, a product of zipper tectonics: Rotational transpressive continent-continent collision and closing of ancient oceans along irregular margins. In: Catalán JRM, Hatcher Robert D. J, Arenas R, García FD (eds) Variscan-Appalachian dynamics: The building of the late Paleozoic basement. Geological Society of America

Heaman LM, LeCheminant AN (1993) Paragenesis and U-Pb systematics of baddeleyite (ZrO_2). Chem Geol 110:95–126. doi: http://dx.doi.org/10.1016/0009-2541(93)90249-I

Hiatt EE, Kyser K, Dalrymple RW (2003) Relationships among sedimentology, stratigraphy, and diagenesis in the Proterozoic Thelon Basin, Nunavut, Canada: Implications for paleoaquifers and sedimentary-hosted mineral deposits. J Geochemical Explor 80:221–240. doi: 10.1016/S0375-6742(03)00192-4

Hoeve J, Quirt DH (1984) Mineralization and host rock alteration in relation to clay mineral diagenesis and evolution of the Middle-Proterozoic, Athabasca Basin, Northern Saskatchewan, Canada

Hoffman PF (1988) United Plates of America, The Birth of a Craton: Early Proterozoic Assembly and Growth of Laurentia. Annu Rev Earth Planet Sci 16:543–603. doi: 10.1146/annurev.ea.16.050188.002551

Hou G, Kusky TM, Wang C, Wang Y (2010) Mechanics of the giant radiating Mackenzie dyke swarm: A paleostress field modeling. J Geophys Res Solid Earth 115:n/a-n/a. doi: 10.1029/2007JB005475

Hunt PA, Roddick JC (1988) A compilation of K-Ar ages: Report 18. In: Radiogenic Age and Isotopic Studies: Report 2, Paper 88-2. Geological Survey of Canada, pp 127–153

Hunt PA, Roddick JC (1992a) A compilation of K-Ar ages: Report 21. In: Radiogenic Age and Isotopic Studies: Report 5, Paper 91-2. Geological Survey of Canada, pp 207–261

Hunt PA, Roddick JC (1992b) A compilation of K-Ar and 40Ar-39Ar ages: Report 22. In: Radiogenic Age and Isotopic Studies: Report 6, Paper 92-2. Geological Survey of Canada, pp 179–226

J. Bridge N, Banerjee N, Pehrsson S, et al (2013) Lac Cinquante Uranium Deposit, Western Churchill Province, Nunavut, Canada. Explor Min Geol 21:27–50

Jefferson C, Pehrsson S, Peterson T, et al (2011) Northeast Thelon region geoscience framework - new maps and data for uranium in Nunavut. 288791. doi: 10.4095/288791

Jefferson CW, Thomas DJ, Gandhi SS, et al (2007) Unconformity-associated uranium deposits of the Athabasca Basin, Saskatchewan and Alberta. Bull Surv Canada 588:23

Johnstone D Geology , tectonics and setting of uranium mineralization in the central Rae craton of Laurentia

Jowett EC (1991) Fitting iron and magnesium into the hydrothermal chlorite geothermometer. In: GAC/MAC/SEG Joint Annual Meeting, Toronto, May 27-29, 1991, Program with Abstracts 16

Kim Y-S, Peacock DCP, Sanderson DJ (2004) Fault damage zones. J Struct Geol 26:503–517. doi: https://doi.org/10.1016/j.jsg.2003.08.002

Kotzer TG, Kyser TK (1995) Petrogenesis of the Proterozoic Athabasca Basin, northern Saskatchewan, Canada, and its relation to diagenesis, hydrothermal uranium mineralization and paleohydrogeology. Chem Geol 120:45–89. doi: https://doi.org/10.1016/0009-2541(94)00114-N

Kranidiotis P, MacLean WH (1987) Systematics of chlorite alteration at the Phelps Dodge massive sulfide deposit, Matagami, Quebec. Econ Geol 82:1898–1911. doi: 10.2113/gsecongeo.82.7.1898

Lach P (2012) Signature géochimique des éléments des terres rares dans les oxydes d'uranium et minéraux associés dans les gisements d'uranium : analyse par ablation laser couplée à l'ICP-MS et étude géochronologique. Thèse de doctorat en Géosciences Sous la direction de Jean Dubessy et de Michel Cuney, Université de Lorraine, 320 p.

Lach P, Mercadier J, Dubessy J, et al (2013) In Situ Quantitative Measurement of Rare Earth Elements in Uranium Oxides by Laser Ablation-Inductively Coupled Plasma-Mass Spectrometry. Geostand Geoanalytical Res 37:277–296. doi: 10.1111/j.1751-908X.2012.00161.x

LeCheminant AN, Heaman LM (1989) Mackenzie igneous events, Canada: Middle Proterozoic hotspot magmatism associated with ocean opening. Earth Planet Sci Lett 96:38–48. doi: http://dx.doi.org/10.1016/0012-821X(89)90122-2

LeCheminant AN, Miller AR, Booth GW, et al (1979) Geology of the Tebesjuak lake map area - a progress report with notes on uranium and Base metal mineralization. 30

LeCheminant AN, Miller AR, LeCheminant GM (1987) Early Proterozoic Alkaline Igneous Rocks, District of Keewatin, Canada: Petrogenesis and Mineralization. Geol Soc London, Spec Publ 33:219–240. doi: 10.1144/GSL.SP.1987.033.01.16

Leisen M, Boiron M-C, Richard A, Dubessy J (2012) Determination of Cl and Br concentrations in individual fluid inclusions by combining microthermometry and LA-ICPMS analysis: Implications for the origin of salinity in crustal fluids. Chem Geol 330–331:197–206. doi: https://doi.org/10.1016/j.chemgeo.2012.09.003

Lespinasse M (1999) Are fluid inclusion planes useful in structural geology? J Struct Geol 21:1237–1243. doi: https://doi.org/10.1016/S0191-8141(99)00027-9

Lespinasse M, Désindes L, Fratczak P, Petrov V (2005) Microfissural mapping of natural cracks in rocks: Implications for fluid transfers quantification in the crust. Chem Geol 223:170–178. doi: https://doi.org/10.1016/j.chemgeo.2005.05.009

Lespinasse M, Pêcher A (1986) Microfracturing and regional stress field: a study of the preferred orientations of fluid-inclusion planes in a granite from the Massif Central, France. J Struct Geol 8:169–180. doi: https://doi.org/10.1016/0191-8141(86)90107-0

Lida Y (1997) Geochemical and Mineralogical studies - 1997 Sissons Project. 169

Ludwig K (2007) Isoplot/Ex version 3.41b, a geochronological toolkit for Microsoft Excel. Berkeley Geochronol Cent Spec Publ

Martz P, Cathelineau M, Mercadier J, et al (2017) C-O-H-N fluids circulations and graphite precipitation in reactivated Hudsonian shear zones during basement uplift of the Wollaston-Mudjatik Transition Zone: Example of the Cigar Lake U deposit. Lithos 294–295:222–245. doi: https://doi.org/10.1016/j.lithos.2017.10.001

Martz P, Mercadier J, Cathelineau M, et al (2018) Formation of U-rich mineralizing fluids through basinal brine migration within basement-hosted shear zones: A large-scale study of the fluid chemistry around the unconformity-related Cigar Lake U deposit (Saskatchewan, Canada). Chem Geol. doi: https://doi.org/10.1016/j.chemgeo.2018.05.042

McClellan E, Gazel E (2014) The Cryogenian intra-continental rifting of Rodinia: Evidence from the Laurentian margin in eastern North America. Lithos 206–207:321–337. doi: https://doi.org/10.1016/j.lithos.2014.08.006

Mercadier J, Annesley IR, McKechnie CL, et al (2013) Magmatic and Metamorphic Uraninite Mineralization in the Western Margin of the Trans-Hudson Orogen (Saskatchewan, Canada): A Uranium Source for Unconformity-Related Uranium Deposits? Econ Geol 108:1037. doi: 10.2113/econgeo.108.5.1037

Mercadier J, Cuney M, Cathelineau M, Lacorde M (2011a) U redox fronts and kaolinisation in basement-hosted unconformity-related U ores of the Athabasca Basin (Canada): Late U remobilisation by meteoric fluids. Miner Depos 46:105–135. doi: 10.1007/s00126-010-0314-7

Mercadier J, Cuney M, Lach P, et al (2011b) Origin of uranium deposits revealed by their rare earth element signature. Terra Nov 23:264–269. doi: 10.1111/j.1365-3121.2011.01008.x

Mercadier J, Richard A, Boiron MC, et al (2010) Migration of brines in the basement rocks of the Athabasca Basin through microfracture networks (P-Patch U deposit, Canada). Lithos 115:121–136. doi: 10.1016/j.lithos.2009.11.010

Mercadier J, Richard A, Cathelineau M (2012) Boron- and magnesium-rich marine brines at the origin of giant unconformity-related uranium deposits: δ11B evidence from Mg-tourmalines. Geology 40:231. doi: 10.1130/G32509.1

Miller AR (1980) Uranium geology of the eastern Baker lake basin, district of keewatin, northwest territories. Geological Survey of Canada, bulletin 330

Miller AR (1982) Alteration and Mineralization types: Amer-Thelon Area, NTS 66G, H District of Keewatin, N.W.T. Pref to Res Doc #1 Westmin Resour Ltd

Miller AR (1995) Polymettalic unconformity-related uranium veins in lower Proterozoic Amer Group, Pelly Lake map area, northern Thelon Basin, Churchill Province, Northwest territories. Curr Res 1995-C; Geol Surv Canada 151–161

Miller AR (1997) Petrography and Mineral Chemistry of the Jane Prospect : A platinum group element-bearing basement-hosted unconformity-related uranium deposit type. 128

Miller AR, Blackwell GW (1992) Petrology of Alkaline Rare Earth Element - Bearing Plutonic Rocks, Enekatcha Lake [65e/15] and Carey Lake [65l/7] map - Areas, District of Mackenzie. Geol Surv Canada, Open File 2484 129–134. doi: https://doi.org/10.4095/133336

Miller AR, LeCheminant AN (1985) Geology and uranium metallogeny of Proterozoic supracrustal successions, central district of Keewatin. 19

Miller AR, Stanton RA, Cluff GR, Male MJ (1986) Uranium deposits and prospects of the Baker Lake Basin and subbasins, Central District of Keewatin, Northwest Territories. Uranium Depos Canada, CIM Spec Vol 33 23

Ng R, Alexandre P, Kyser K (2013) Mineralogical and Geochemical Evolution of the Unconformity-Related McArthur River Zone 4 Orebody in the Athabasca Basin, Canada: Implications of a Silicified Zone*. Econ Geol 108:1657. doi: 10.2113/econgeo.108.7.1657

Pacquet A (1993a) Report 8493 Canada Kiggavik Main Zone D.H. 306 (93-UGC-92-01) - Petrography and XRD analysis. 19

Pacquet A (1993b) Report 8494 - Canada - Sissons Schultz South - End Grid DH END 42 - Petrography and XRD analysis. 14

Pacquet A (1993c) Report 8556 - XRD - Andrew Lake Centre (Lower Lens) DH SW 78. 2

Pacquet A (1994) Report 8549 - Canada (NWT) Andrew Lake DH SW 73 - Petrography and XRD. 12

Pagel M (1975) Cadre géologique des gisements d’uranium dans la structure de Carswell (Saskatchewan, Canada). Etudes des phases fluides. Thèse de 3ème cycle, Université de Nancy, Nancy, France. 171

Pagel M (1995) Etude des inclusions fluides dans les quartz des gisements U de l’Athabasca et du Thelon.pdf. 1–10

Pascal M, Ansdell K, Annesley I (2015) Graphite-bearing and Graphite-depleted Basement Rocks in the Dufferin Lake Zone, South-central Athabasca Basin, Saskatchewan. 83–92

Pehrsson SJ, Berman RG, Eglington B, Rainbird R (2013) Two Neoarchean supercontinents revisited : The case for a Rae family of cratons. Precambrian Res 232:27–43. doi: 10.1016/j.precamres.2013.02.005

Percival JA, Tschirhart V (2017) Trans-Hudsonian far-field deformation effects in the Rae foreland: An integrated geological-3D magnetic model. Tectonophysics 699:82–92. doi: 10.1016/j.tecto.2017.01.021

Peterson TD (2006) Geology of the Dubawnt Lake area, Nunavut-Northwest Territories. Bull Geol Surv Canada 580:

Peterson TD (2015) Geological setting and geochemistry of the ca. 2.6 Ga Snow island Suite in the central Rae Domain of the Western Churchill Province, Nunavut. Geol Surv Canada Open File 7841:

Peterson TD, Breemen O Van, Sandeman H, Cousens B (2002) Proterozoic (1.85–1.75 Ga) igneous suites of the Western Churchill Province: granitoid and ultrapotassic magmatism in a reworked Archean hinterland. Precambrian Res 119:73–100. doi: https://doi.org/10.1016/S0301-9268(02)00118-3

Peterson TD, Scott JMJ, Jefferson CW (2011) Uranium-rich bostonite-carbonatite dykes in Nunavut : recent observations Geological Survey of Canada Current Research 2011-11. 12

Peterson TD, Scott JMJ, LeCheminant AN, et al (2015) The Kivalliq Igneous Suite: Anorogenic bimodal magmatism at 1.75Ga in the western Churchill Province, Canada. Precambrian Res 262:101–119. doi: 10.1016/j.precamres.2015.02.019

Pinheiro RVL, Holdsworth RE (1997) Reactivation of Archaean strike-slip fault systems, Amazon region, Brazil. J Geol Soc London 154:99–103. doi: 10.1144/gsjgs.154.1.0099

Polito PA, Kyser TK, Rheinberger G, Southgate PN (2005) A Paragenetic and Isotopic Study of the Proterozoic Westmoreland Uranium Deposits, Southern McArthur Basin, Northern Territory, Australia. Econ Geol 100:1243–1260. doi: 10.2113/gsecongeo.100.6.1243

Potter E, M Wright D (2015) TGI-4 Unconformity-related uranium deposits synthesis: tools to aid deep exploration and refine the genetic model. Bull Geol Surv Canada Open File:1–13

Rainbird RH, Davis WJ (2007) U-Pb detrital zircon geochronology and provenance of the late Paleoproterozoic Dubawnt Supergroup: Linking sedimentation with tectonic reworking of the western Churchill Province, Canada. GSA Bull 119:314. doi: 10.1130/B25989.1

Rainbird RH, Davis WJ, Pehrsson SJ, et al (2010) Early Paleoproterozoic supracrustal assemblages of the Rae domain, Nunavut, Canada: Intracratonic basin development during supercontinent break-up and assembly. Precambrian Res 181:167–186. doi: https://doi.org/10.1016/j.precamres.2010.06.005

Rainbird RH, Davis WJ, Stern RA, et al (2006) Ar-Ar and U-Pb Geochronology of a Late Paleoproterozoic Rift Basin: Support for a Genetic Link with Hudsonian Orogenesis, Western Churchill Province, Nunavut, Canada. J Geol 114:1–17. doi: 10.1086/498097

Rainbird RH, Hadlari T, Aspler LB, et al (2003) Sequence stratigraphy and evolution of the paleoproterozoic intracontinental Baker Lake and Thelon basins, western Churchill Province, Nunavut, Canada. Precambrian Res 125:21–53. doi: 10.1016/S0301-9268(03)00076-7

Ramaekers P, Jefferson CW, Yeo GM, et al (2007) Revised geological map and stratigraphy of the Athabasca group, Saskatchewan and Alberta. Bull Geol Surv Canada 588:155–191

Renac C, Kyser TK, Durocher K, et al (2002) Comparison of diagenetic fluids in the Proterozoic Thelon and Athabasca Basins, Canada: implications for protracted fluid histories in stable intracratonic basins. Can J Earth Sci 39:113–132. doi: 10.1139/e01-077

Richard A (2017) Radiolytic (H2, O2) and other Trace Gases (CO2, CH4, C2H6, N2) in Fluid Inclusions from Unconformity-related U Deposits. Procedia Earth Planet Sci 17:273–276. doi: https://doi.org/10.1016/j.proeps.2016.12.053

Richard A, Banks DA, Mercadier J, et al (2011a) An evaporated seawater origin for the ore-forming brines in unconformity-related uranium deposits (Athabasca Basin, Canada): Cl/Br and δ37Cl analysis of fluid inclusions. Geochim Cosmochim Acta 75:2792–2810. doi: https://doi.org/10.1016/j.gca.2011.02.026

Richard A, Boulvais P, Mercadier J, et al (2013) From evaporated seawater to uranium-mineralizing brines : Isotopic and trace element study of quartz – dolomite veins in the Athabasca system. Geochim Cosmochim Acta 113:38–59. doi: 10.1016/j.gca.2013.03.009

Richard A, Cathelineau M, Boiron M-C, et al (2016) Metal-rich fluid inclusions provide new insights into unconformity-related U deposits (Athabasca Basin and Basement, Canada). Miner Depos 51:249–270

Richard A, Cauzid J, Cathelineau M, et al (2012) Synchrotron-XRF and XANES investigation of fluid inclusions from unconformity-related uranium deposits

Richard A, Kendrick MA, Cathelineau M (2014) Noble gases (Ar, Kr, Xe) and halogens (Cl, Br, I) in fluid inclusions from the Athabasca Basin (Canada): Implications for unconformity-related U deposits. Precambrian Res 247:110–125. doi: https://doi.org/10.1016/j.precamres.2014.03.020

Richard A, Pettke T, Cathelineau M, et al (2010) Brine – rock interaction in the Athabasca basement (McArthur

River U deposit , Canada): consequences for fluid chemistry and uranium uptake. 303–308. doi: 10.1111/j.1365-3121.2010.00947.x

Richard A, Rozsypal C, Mercadier J, et al (2011b) Giant uranium deposits formed from exceptionally uranium-rich acidic brines. Nat Geosci 5:142–146. doi: 10.1038/ngeo1338

Riegler T (2013) Système d’altération et minéralisation en uranium le long du faisceau structural Kiggavik - Andrew Lake (Nunavut, Canada) : modèle génétique et guides d’exploration. Poitiers

Riegler T, Lescuyer J-L, Wollenberg P, et al (2014) Alteration related to uranium deposits in the Kiggavik-Andrew Lake structural trend, Nunavut, Canada: new insights from clay mineralogy and petrography. Can Mineral 52:27–45. doi: 10.3749/canmin.52.1.27

Riegler T, Quirt D, Beaufort D (2016) Spatial distribution and compositional variation of APS minerals related to uranium deposits in the Kiggavik-Andrew Lake structural trend, Nunavut, Canada. Miner Depos 51:219–236. doi: 10.1007/s00126-015-0595-y

Romberger SB (1984) Transport and deposition of uranium in hydrothermal systems at temperatures up to 300{\textdegree}C: geological implications. In: De Vivo B, Ippolito F, Capaldi G, Simpson PR (eds) Uranium geochemistry, mineralogy, geology, exploration and resources. Springer Netherlands, Dordrecht, pp 12–17

Rotevatn A, Bastesen E (2014) Fault linkage and damage zone architecture in tight carbonate rocks in the Suez Rift (Egypt): implications for permeability structure along segmented normal faults. Geol Soc London, Spec Publ 374:79–95. doi: 10.1144/SP374.12

Roy R, Benedicto A, Grare A, et al (2017) Three-dimensional gravity modelling applied to the exploration of uranium unconformity-related basement-hosted deposits: the Contact prospect case study, Kiggavik, northeast Thelon region (Nunavut, Canada). Can J Earth Sci 54:869–882. doi: 10.1139/cjes-2016-0225

Rutter EH (1983) Pressure solution in nature, theory and experiment. J Geol Soc London 140:725–740. doi: 10.1144/gsjgs.140.5.0725

Schorscher HD, Shea ME (1992) The regional geology of the Poços de Caldas alkaline complex: mineralogy and geochemistry of selected nepheline syenites and phonolites. J Geochemical Explor 45:25–51. doi: https://doi.org/10.1016/0375-6742(92)90121-N

Scott J, Peterson TD (2012) U, Th, and REE occurrences within Nueltin granite at Nueltin Lake, Nunavut: recent observations. Geol Surv Canada Curr Res 2012–1:

Scott JMJ, Peterson TD, Jefferson CW, Cousens BL (2015) Petrology and geochronology of Paleoproterozoic intrusive rocks, Kiggavik uranium camp, Nunavut. Can J Earth Sci 518:1–80. doi: 10.1139/cjes-2014-0153

Shabaga BM, Fayek M, Quirt D, et al (2017) Mineralogy, geochronology, and genesis of the Andrew Lake uranium deposit, Thelon Basin, Nunavut, Canada. Can J Earth Sci 54:850–868. doi: 10.1139/cjes-2017-0024

Sharpe R, Fayek M, Quirt D, Jefferson CW (2015) Geochronology and genesis of the bong uranium deposit, Thelon Basin, Nunavut, Canada. Econ Geol 110:1759–1777. doi: 10.2113/econgeo.110.7.1759

Stacey JS, Kramers JD (1975) Approximation of terrestrial lead isotope evolution by a two-stage model. Earth Planet Sci Lett 26:207–221. doi: https://doi.org/10.1016/0012-821X(75)90088-6

Thorkelson D (2000) Geology and mineral occurrences of the Slats Creek, Fairchild Lake and "Dolores Creek" areas, Wernecke Mountains, Yukon Territory (106 D/16, 106 C/13, 106 C/14). Geol Miner Occur Slats Creek, Fairchild Lake Dolores Creek Areas 10:

Tschirhart P, Morris WA, Jefferson CW (2013) Geophysical modelling of the Neoarchean Woodburn Lake and Paleoproterozoic Ketyet River groups , and plutonic rocks in central Schultz Lake map area , Nunavut Geophysical modelling of the Neoarchean Woodburn Lake and Paleoproterozoic Ketyet River groups ,. Curr Res

Tschirhart V, Jefferson CW, Morris WA (2017) Basement geology beneath the northeast Thelon Basin, Nunavut: insights from integrating new gravity, magnetic and geological data. Geophys Prospect 65:617–636. doi: 10.1111/1365-2478.12430

Turner W, Richards J, Nesbitt B, et al (2001) Proterozoic low-sulfidation epithermal Au-Ag mineralization in the Mallery Lake area, Nunavut, Canada. Miner Depos 36:442–457. doi: 10.1007/s001260100181

Turner WA, Heaman LM, Creaser RA (2003) Sm–Nd fluorite dating of Proterozoic low-sulfidation epithermal Au–Ag deposits and U–Pb zircon dating of host rocks at Mallery Lake, Nunavut, Canada. Can J Earth Sci 40:1789–1804. doi: 10.1139/e03-061

Velde B (ed) (1985) III-General Phase Diagrams for Some Clay Mineral Assemblages. In: Clay Minerals. Elsevier, pp 257–357

W Jefferson C, Thomas DJ, S Gandhi S, et al (2007) Unconformity-associated uranium deposits of the Athabasca Basin, Saskatchewan and Alberta. Bull. Geol. Surv. Canada 588:23–67

Weyer HJ, Friedrich G, Bechtel A, Ballhorn RK (1987) The Lone Gull Uranium deposit - New geochemical and petrological data as evidence for the nature of the ore bearing solutions. 14

Wibberley CAJ, Yielding G, Di Toro G (2008) Recent advances in the understanding of fault zone internal structure: A review. Intern Struct Fault Zo Implic Mech Fluid-Flow Prop 299:5–33. doi: 10.1144/SP299.2

Williams JH, Johnson CD (2004) Acoustic and optical borehole-wall imaging for fractured-rock aquifer studies. J Appl Geophys 55:151–159. doi: https://doi.org/10.1016/j.jappgeo.2003.06.009

Zang W, Fyfe WS (1995) Chloritization of the hydrothermally altered bedrock at the Igarap{é} Bahia gold deposit, Caraj{á}s, Brazil. Miner Depos 30:30–38. doi: 10.1007/BF00208874

Fig. 1 Geological map of the Thelon-Baker Lake area (after Curtis and Miller 1980; Rainbird et al. 2003). Small insert depicts the main geological units of the Churchill-Wyoming craton and the location of the Thelon Basin (cross section built and modified after Jefferson et al. 2011; Hadlari and Rainbird 2011; Pehrsson et al. 2013).

Fig. 2 Simplified geological map of the Kiggavik area (Orano internal document) and cross section from the Thelon fault to the Judge Sissons fault. Deposits and prospects are indicated with red and yellow circles, respectively.

Fig. 3 Orientations of faults and breccias for each fracturing stage and for main deposits and prospects of the Kiggavik area, where available. The presence of each fracturing stage is relative to the same fracture set or to the same deposit/prospect. The chronology of the fracturing events was presented by Grare et al. (2018a). Schmidt's lower hemisphere stereoplots.

Fig. 4 Drill core photographs (DCP) for different U deposits and prospects of the Kiggavik area. Numbers on the core boxes quantify the radioactivity (in count per second). **a** Uranium mineralized microbreccia (U0) crosscut by a quartz vein (yellow outline) of the QB. **b** Microbrecciated, uranium mineralized (U0) and unaltered psammo-pelitic gneiss of the Woodburn Lake Grp. **c** Various examples of uranium mineralized, grey-greenish altered fault zones of U2. White arrows on the picture from End locate mineralisation in fractures and parallel to foliation. **d** Disseminated U1 mineralization in 85W granite.

Fig. 5 DCP for different U deposits and prospects of the Kiggavik area. **a** Spherulitic pitchblende (U2) in hematized, clay altered microgranite. **b** Strongly clay altered, hematized fault rock (f6) from Sleek (top). Vein cemented with hematite and uranium oxides (second stage of uranium mineralization-U2, bottom). **c** Spherulitic pitchblende (U2, white arrows) leaking out from Ca2 veinlet (top). Spherulitic pitchblende and syngenetic hematite (bottom). **d** U2 mineralized, hematized fault damage zone. **e** Strongly clay altered, bleached but unmineralized fault zones (fault core highlighted in yellow, limits of the fault zone are delimited in green). **f** white clay altered fault zone (in yellow) crosscutting a U2 mineralized fault zone. **g** Top and bottom: White clay altered cataclastic fault rock bearing small relict of spherulitic pitchblende (white arrow, unidentified generation). **h** Mackenzie diabase dike (black outline) crosscutting a uranium mineralized fault zone (red outline). The fresh diabase dike is not mineralized and weakly fractured.

Fig. 6 Three examples of redox fronts with goethite (orange) remobilizing uranium oxides (grey-black products) from End, Kiggavik Main Zone and 85W.

Fig. 7 a DCP from the 85W prospect, Kiggavik area. Stepped subvertical, ENE-WSW quartz vein coated with uranium oxides showing evidence of dextral motion. **b** Field picture (FP). Stepped subvertical, NW-SE quartz vein displaying evidence of sinistral motion. **c** FP from the 85W area, Kiggavik area. Network of Mode I quartz veins (f2) trending ESE-WNW. **d** Oriented data and kinematic of quartz veins, collected on outcrops. The St-Tropez area is located 20 km to the NNE of Kiggavik Main Zone. Schmidt's lower hemisphere stereoplots.

Fig. 8 a DCP from the Kiggavik Main Zone, Kiggavik area. Stepped veins of the first generation of calcite (Ca1) coated with uranium oxides (U1, red zones). **b** Oriented data and kinematics of Ca1 veins from drillcores. Schmidt's lower hemisphere plots.

Fig. 9 a FP. NE-SW hematized fault zone (f6) displaying dextral kinematics. **b** FP. ENE-WSW hematized fault-relay zone (f6)displaying evidence of sinistral strike-slip kinematics. **c** Oriented data and kinematic of faults and microfaults (f6), mainly from field observations but also collected on drillcores (i.e. Contact, Sleek and 85W).

Fig. 10 a FP from End area, Kiggavik area: Quartz veins of the quartz breccia (QB) being crosscut and offset (senestral motion) by late NNW-SSE to NW-SE microfaults. **b** DCP (top) and interpretation (bottom) from 85W prospect, of a uranium oxides (U2) and a clay-cemented vein (orange outline) being crosscut and offset by a NW-SE microfault. Host rock is strongly altered. **c** Oriented data and kinematic of faults and microfaults, from field observations and from drillcores (i.e. Contact and 85W). **d** Simplified NNW-SSE cross-section of the Bong deposit, depicting dip-slip offset of the ore body by E-W oriented faults also driving fluids that strongly clay altered and bleached the host rock.

Fig. 11 Micro-scale observations of U0 breccia from End deposit. **a**, **b**, **c** and **e**: Optical microphotograph (OMP), d and f: SEM pictures. **a** Undulated microstructures cemented with chlorite and uranium oxides. **b** Mineralized microbreccia: corroded clasts (yellow outline) cemented by chlorite and opaque minerals (sulfide, uranium oxides and rutile indicated by white arrow). **c** Mineralized microbreccia crosscut by a quartz (qtz) vein of QB. **d** SEM microphotograph and element mapping of U-S-Ti compounds. **e** Microbreccia with chlorite (Chl, dark green) crosscut by a quartz vein of QB and altered to sudoite (Sud, light green). **f** SEM microphotograph. Anhedral rutile (Rt), uraniferous titanate (Ti-U) and pitchblende (Pch).

Fig. 12 SEM microphotographs of different U mineralization from the Kiggavik area: **a** Microbreccia cemented with uranium oxides and subhedral brannerite and uraniferous titanate (Ti-U). **b** Anhedral uraniferous titanate coating rutile grains with pitchblende micro-inclusions (U). **c** Magmatic quartz displaying a micro-fracture cemented with colloform pitchblende and anhedral rutile. **d** Uraninite displaying various state of alteration, cemented by calcite. **e** Quartz vein showing traces of dissolution and colloform pitchblende. **f** Ni-bearing pyrite (bravoite) and pyrite (Py) with concentric uranium growth zone. **g** Quartz vein crosscut by Galena (Gal)-Ag-U cemented microfracture. **h** Pitchblende displaying micro-inclusions of gold. **i** Aluminum-phosphate-sulfate (APS) embedded in anhedral pitchblende and pyrite, in f5 fault zone. **j** APS observed in altered and oxidized granite proximal to f6 fault. **k** U2-f6 stage: Anhedral pitchblende cementing anastomosing fracture. **l** U3 pitchblende coating quartz and clay minerals.

Fig. 13 Cathodoluminescence microphotograph (CLMP) and OMP **a**. Dolomite (Dol) corroded and coated with pitchblende and a first generation of calcite (Ca1). The calcite (Ca1) cements a distinct area separating pitchblende (U1) and dolomite. **b** Microbreccia cemented with calcite (Ca1) and synchronous pitchblende (U1). **c** Pitchblende (U1) within a matrix of calcite (Ca1). **d** Dolomite brecciated and cemented by calcite (Ca1) and synchronous pitchblende (U1). **e** Pitchblende (U1) crosscut by calcite micro veinlet. **f** Same picture as **e** observed under cathodoluminescence, the typical crack-seal texture of the second generation of calcite Ca2 is observable.

Fig. 14 a Chemiographic representation of chlorites analysed from different locations in the Kiggavik area (Jane, Contact, 85W, Andrew Lake). **b** Chemiographic representation of chlorite grains formed during U0 mineralizing stage and their later hydrothermal alteration. Structural formulas of chlorites were plotted in a MR3-2R3-3R2 diagram (Velde 1985). **c** OMP of a U0 microbreccia cemented with unaltered dioctahedral chlorite (1. dark green), altered to light green di-trioctahedral chlorite (2. sudoite). Opaque minerals are ore minerals. Numbers localize the point analysed under EMPA, which results are plotted in B. **d** Electron microprobe analysis of chlorites from the U0 mineralized microbreccia, and calculated temperatures after several techniques.

Fig. 15 a Analyzed white mica plotted on a ternary diagram of the average compositional fields of dioctahedral mica-like phases, after Dubacq et al. (Dubacq et al. 2010). Pr: pyrophillite; Cel: celadonite; Ms: muscovite; Pg:

paragonite. **b** Pre-ore white mica in a fracture cemented by white mica in link with U1. **c** Pre-ore white mica in a micro-fracture reopened and cemented by white mica in link with U2. **d** Reworked clasts of ore minerals with second stage white mica, in a matrix cemented by late ore white mica. **e** Temperatures deduced from the composition of various generations of white mica (EMPA).

Fig. 16 Chondrite-normalized REE patterns for pitchblende and uraninite from 8 different samples from Andrew Lake (Top left), End (Top right) and 85W (bottom right). Each curve corresponds to an *in situ* SIMS or LA-ICP-MS REE analysis in a selected U-oxide of the studied samples. Ages for the samples were obtained in this study (see also Fig. 17), except for sample 9568-38 and 9568-39, obtained by Lach (2011). The grey zones corresponds to the unconformity-related uranium oxide reference chondrite-normalised REE patterns from the Mc Arthur River and Sue deposit (Mercadier et al. 2011b), Kalongwe deposit (Eglinger et al. 2013), Centennial and Millenium deposits (Alexandre et al. 2015).

Fig. 17 $^{206}Pb/^{238}U$- $^{207}Pb/^{235}U$ Concordia diagram showing the isotopic composition of uranium oxides (pitchblende and uraninite) from six samples coming from End (9568-38), Andrew Lake (9850, 9851, And-15-01-04, And-15-01-05) and 85W (85W-10-04). Analytical data are available as complementary material.

Fig. 18 Thick section pictures. **a** Magmatic quartz from the granite of 85W displaying monophase FIPs (red) crosscut by aqueous FIPs (blue). **b** Monophase fluid inclusion displaying negative crystal shape. **c** Biphase aqueous fluid inclusion. **d** Triphase aqueous fluid inclusion with halite crystal. **e** Monophase FIPs (red dotted lines) and aqueous FIP (blue dotted line). Monophase FIs are obliterated at the intersections between monophase and aqueous FIPs.

Fig. 19 Concentration (ppm) in several metals for selected secondary fluid inclusions in the Kiggavik area. Comparison is made with data from the Athabaca basin (grey bars, Richard et al. 2016).

Fig. 20 Directions for type 1 (red) and type 2 (blue) FIPs, for 85W (left) and Contact (right). Mean granitic gneiss foliation at Contact is given. The general dip for the FIPs is sub-vertical.

Fig. 21 Scheme summarizing ages obtained within the Thelon/Baker-Lake area, through U-Pb isotopes on uranium oxides (Farkas 1984; Miller et al. 1986; J. Bridge et al. 2013; Lach et al. 2013; Sharpe et al. 2015b; Chi et al. 2017; Shabaga et al. 2017; This study), Ar-Ar ages on illite (Friedrich et al. 1989; Riegler 2013; Ashcroft et al. 2017; Shabaga et al. 2017), Ar-Ar on muscovite (Ashcroft et al. 2017; Shabaga et al. 2017), K-Ar on illite (Friedrich et al. 1989) and whole rock analysis (Hunt and Roddick 1988, 1992a, b).

Fig. 22 Synthesis of oriented data with kinematic indicators and derived paleostress interpretation (black arrows). **a**

macro scale data. **b** micro scale data

Fig. 23 Pre-Thelon basin first stage of micro-brecciation and uranium mineralization in the Kiggavik area associated with magmatism of the Kivalliq igneous suite. **a** bloc diagram. **b** Map view of the fracture network at this stage.

Fig. 24 F2/QB. Pre-Thelon hydraulic quartz breccia linked to magmatism of the Kivalliq igneous suite (ca. 1750 Ma). ESE-WNW oriented $\sigma 1$ and NNE-SSW oriented $\sigma 3$. **a** bloc diagram. **b** Map view of the fracture network at this stage.

Fig. 25 F5/U1. Syn-Post Thelon circulation of basinal brines. ESE-WNW oriented $\sigma 1$ and NNE-SSW oriented $\sigma 3$. **a** bloc diagram. **b** Map view of the fracture network at this stage.

Fig. 26: F6/U2. Post-Thelon renewed circulation of basinal brines. ENE-WSW oriented $\sigma 1$ and NNW-SSE oriented $\sigma 3$. **a** bloc diagram. **b** Map view of the fracture network at this stage.

Fig. 27: Post ore, Pre Mackenzie dikes (1267 Ma) illitization and desilicification, local remobilization and offsetting of orebodies. NNE-SSW oriented $\sigma 3$. **a** bloc diagram. **b** Map view of the fracture network at this stage.

Table 1 selected representative chlorite analysis from different deposits/prospects of the Kiggavik area.

Table 2 Summary of microthermometric fluid inclusions data obtained in this study for aqueous biphase and triphase fluid inclusions (type 2 FIP). Te: Temperature of eutectic. Tm ice: melting temperature of the last crystal of ice. Ts NaCl: Fusion temperature of the crystal of halite. Classification of fluid inclusions (after Derome et al. 2005).

Table 1

Location	End U0	End U0*	Contact U2	Jane U1	Jane U2	End	Kiggavik MZ U2	85W U1
SiO_2	27,05	36,33	36,97	36,02	35,23	36,49	34,59	35,29
Al_2O_3	20,21	28,81	34,45	33,98	35,74	30,09	35,17	32,31
K_2O	0,02	0,54	0,88	0,74	0,25	0,27	1,96	0,92
CaO	0,03	0,1	0,15	0,17	0,02	0,04	0,15	0,18
FeO	26,5	4,17	0,96	0,12	0,17	2,24	0,5	0,86
MgO	15,61	16,93	12,28	14,72	15,04	17,13	13,41	15,87
MnO	0,35	0,03	0,02	0	0	0,06	0	0,03
TiO_2	0,11	0	0	0	0	0	0	0
Na_2O	0,06	0,02	0,04	0	0,04	0,08	0	0,06
Total	90,08	86,96	85,81	85,75	86,49	86,46	85,78	85,52

Table 1: selected representative chlorite analysis from different deposits/prospects of the Kiggavik area.

Table 2

FI type			% vapor phase	Microthermometric data (°C)				Salinity (Wt% NaCl+CaCl2)
				Te	Tm ice	Ts NaCl	Th	
85W	Lw'	Range	10-50	-85 to -66	-45,4 to -30,6	207 to 223	100 to 215	25,0 to 29,3
		Mode		-70				28,1
		n		5	6	2	6	6
	Lwh'	Range	5-40	-80 to -60	-45,8 to -22,8	121 to 222	62 to 136	24,4 to 29,4
		Mode		-70	-38,5			27,6
		n		17	19	11	8	19
	Lw''	Range	5-90	-65 to -38	-23,9 to -1,4		208 to 215	2,3 to 22,3
		Mode		-60				
		n		9	16			16
Contact	Lw1	Range	10-30	-77	-28,9 to -25,9			23,2 to 24,4
		n		1	2			2
	Lw'	Range	10	-75	-31,4		92,0	25,3
		n		1	1		1	1
	Lwh'	Range	10			155 to 168	81,8 to 117,7	
		n				3	4	
	Lw''	Range	30		-16,6			19,8
		n			1			1

Figure 1

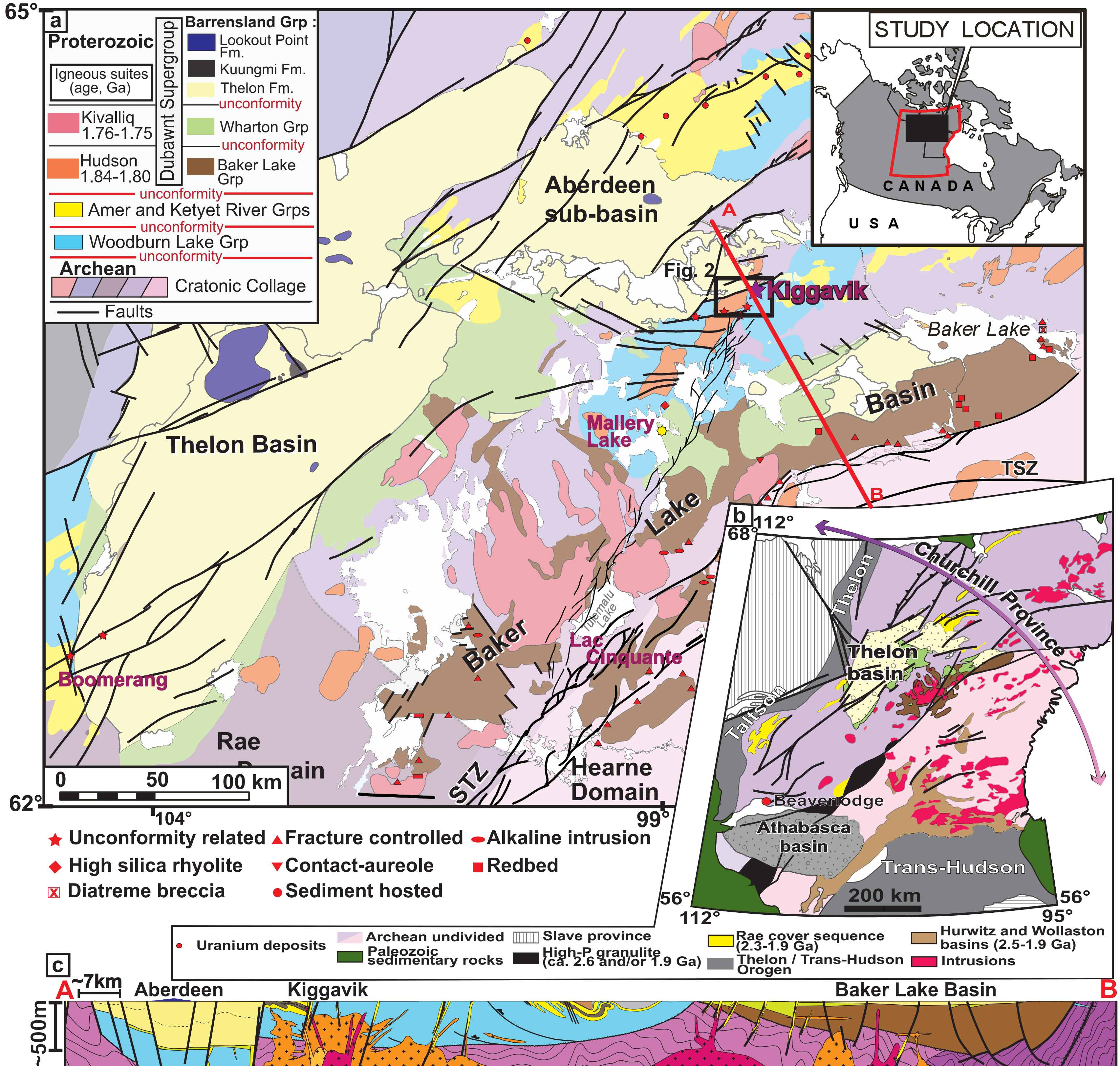

a
Proterozoic
Igneous suites (age, Ga)
Kivalliq 1.76-1.75
Hudson 1.84-1.80
Dubawnt Supergroup
Barrensland Grp :
Lookout Point Fm.
Kuungmi Fm.
Thelon Fm.
unconformity
Wharton Grp
unconformity
Baker Lake Grp
unconformity
Amer and Ketyet River Grps
unconformity
Woodburn Lake Grp
unconformity
Archean
Cratonic Collage
Faults
STUDY LOCATION
CANADA
USA
Aberdeen sub-basin
Thelon Basin
Fig. 2
Kiggavik
Baker Lake
Basin
Lake
Baker
Mallery Lake
Lac Cinquante
Boomerang
Rae Domain
Hearne Domain
STZ
TSZ
A
B
65°
62°
104°
99°
0 50 100 km
Unconformity related
Fracture controlled
Alkaline intrusion
High silica rhyolite
Contact-aureole
Redbed
Diatreme breccia
Sediment hosted
b
112°
68°
Churchill Province
Thelon
Thelon basin
Taltson
Beaverlodge
Athabasca basin
Trans-Hudson
200 km
56°
112°
56°
95°
Uranium deposits
Archean undivided
Paleozoic sedimentary rocks
Slave province
High-P granulite (ca. 2.6 and/or 1.9 Ga)
Rae cover sequence (2.3-1.9 Ga)
Thelon / Trans-Hudson Orogen
Hurwitz and Wollaston basins (2.5-1.9 Ga)
Intrusions
c
A
~7km
Aberdeen
Kiggavik
Baker Lake Basin
B
~500m

Figure 2

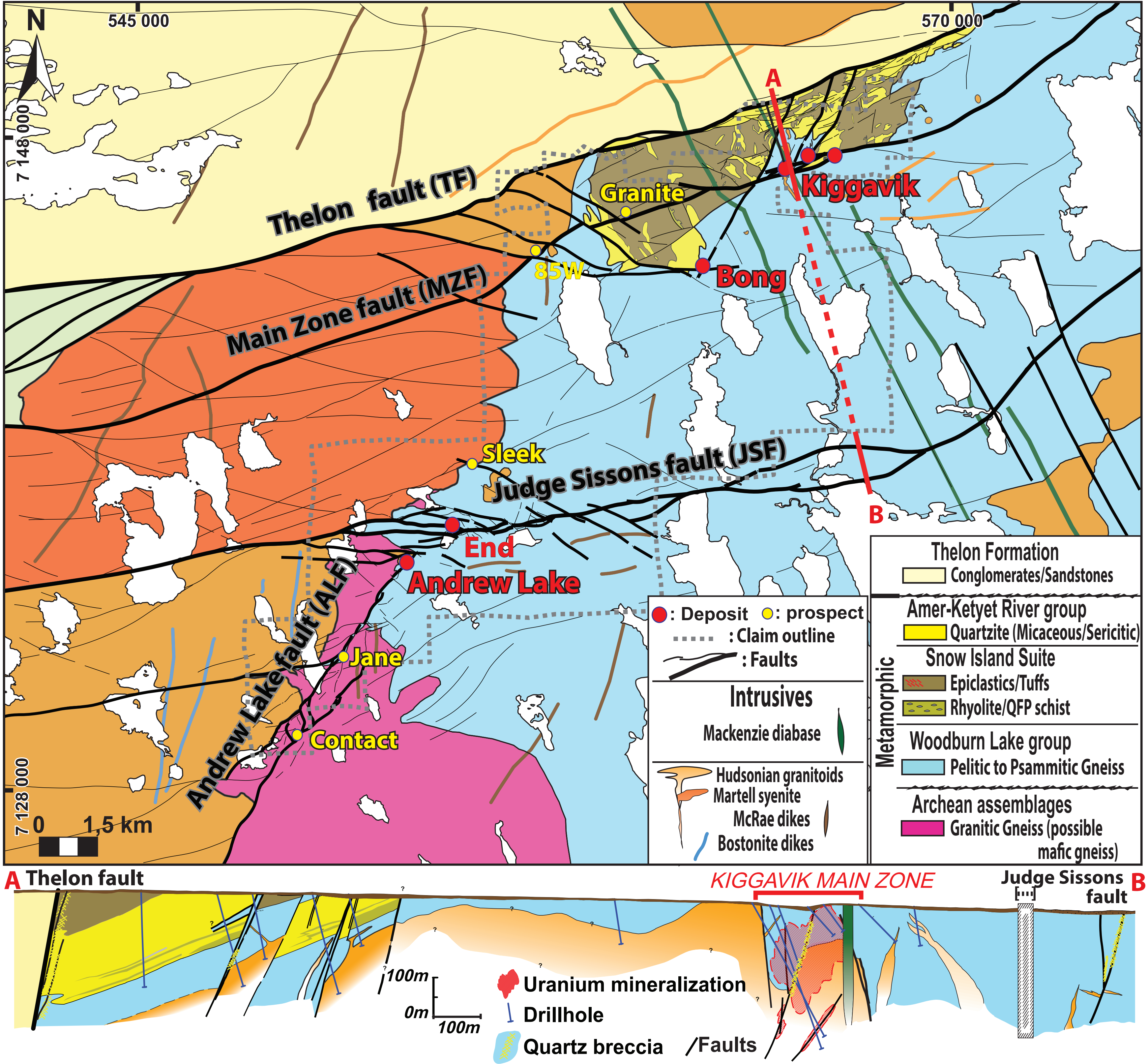

N
545 000
570 000
7 148 000
7 128 000
0
1,5 km
Thelon fault (TF)
Main Zone fault (MZF)
Judge Sissons fault (JSF)
Andrew Lake fault (ALF)
Granite
85W
Bong
Kiggavik
Sleek
End
Andrew Lake
Jane
Contact
A
B
: Deposit
: prospect
: Claim outline
: Faults
Intrusives
Mackenzie diabase
Hudsonian granitoids
Martell syenite
McRae dikes
Bostonite dikes
Thelon Formation
Conglomerates/Sandstones
Amer-Ketyet River group
Quartzite (Micaceous/Sericitic)
Snow Island Suite
Epiclastics/Tuffs
Rhyolite/QFP schist
Woodburn Lake group
Pelitic to Psammitic Gneiss
Archean assemblages
Granitic Gneiss (possible mafic gneiss)
Metamorphic
A Thelon fault
KIGGAVIK MAIN ZONE
Judge Sissons fault B
100m
0m
100m
Uranium mineralization
Drillhole
Quartz breccia
Faults

Figure 3

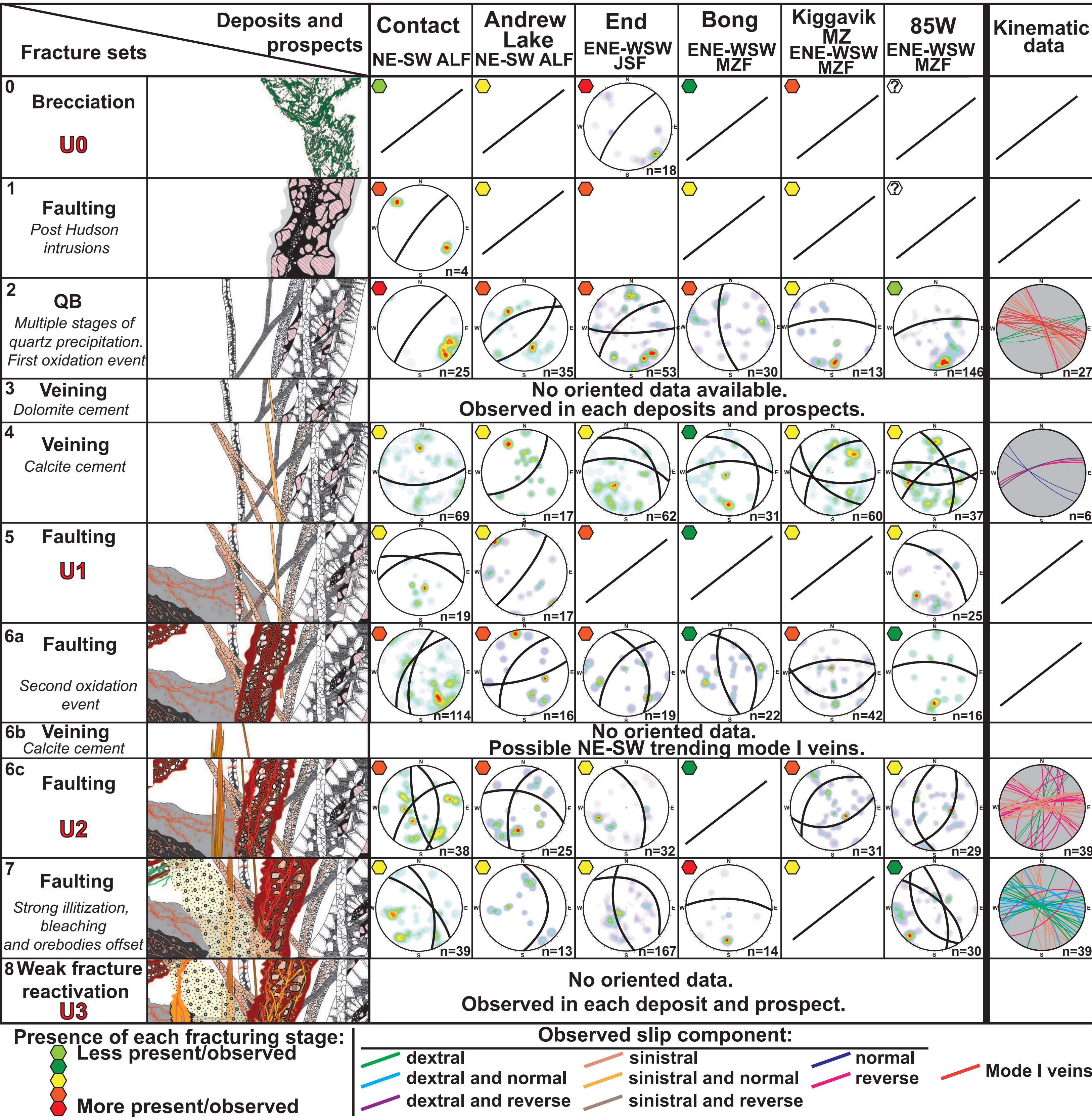
Deposits and prospects
Fracture sets
Contact
NE-SW ALF
Andrew Lake
NE-SW ALF
End
ENE-WSW JSF
Bong
ENE-WSW MZF
Kiggavik MZ
ENE-WSW MZF
85W
ENE-WSW MZF
Kinematic data
0 Brecciation
U0
n=18
1 Faulting
Post Hudson intrusions
n=4
2 QB
Multiple stages of quartz precipitation.
First oxidation event
n=25
n=35
n=53
n=30
n=13
n=146
n=27
3 Veining
Dolomite cement
No oriented data available.
Observed in each deposits and prospects.
4 Veining
Calcite cement
n=69
n=17
n=62
n=31
n=60
n=37
n=6
5 Faulting
U1
n=19
n=17
n=25
6a Faulting
Second oxidation event
n=114
n=16
n=19
n=22
n=42
n=16
6b Veining
Calcite cement
No oriented data.
Possible NE-SW trending mode I veins.
6c Faulting
U2
n=38
n=25
n=32
n=31
n=29
n=39
7 Faulting
Strong illitization, bleaching and orebodies offset
n=39
n=13
n=167
n=14
n=30
n=39
8 Weak fracture reactivation
U3
No oriented data.
Observed in each deposit and prospect.
Presence of each fracturing stage:
Less present/observed
More present/observed
Observed slip component:
dextral
dextral and normal
dextral and reverse
sinistral
sinistral and normal
sinistral and reverse
normal
reverse
Mode I veins

Figure 4

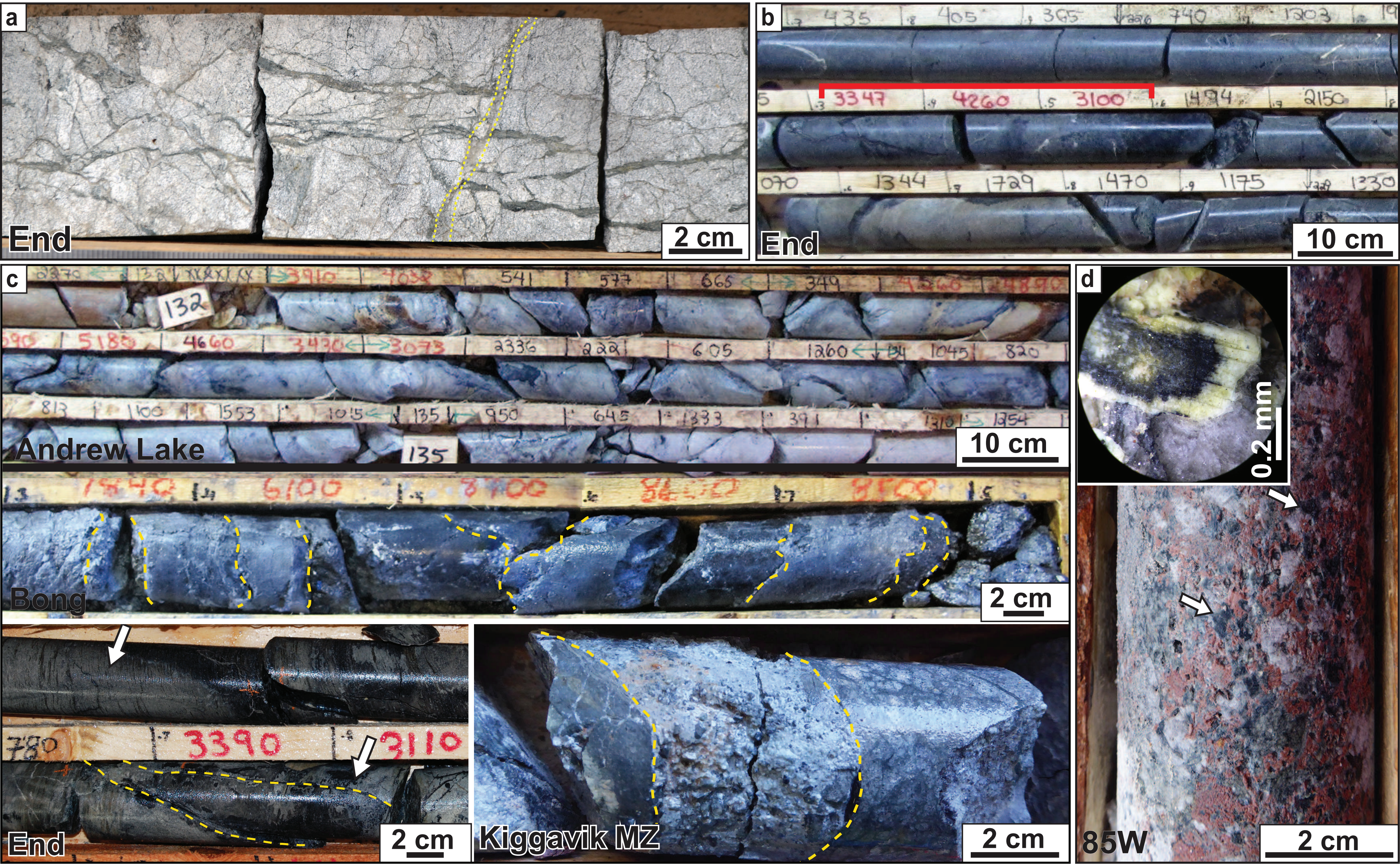
a
End
2 cm
b
End
10 cm
c
Andrew Lake
10 cm
Bong
2 cm
End
2 cm
Kiggavik MZ
2 cm
d
0.2 mm
85W
2 cm

Figure 5


a
85W
2 cm
b
Sleek
2 cm
Andrew Lake
2 cm
c
Andrew Lake
2 cm
End
2 cm
d
Andrew Lake
10 cm
e
Kiggavik MZ
10 cm
f
End
10 cm
g
Bong
2 cm
Andrew Lake
1 cm
h
Kiggavik MZ
10 cm

Figure 6

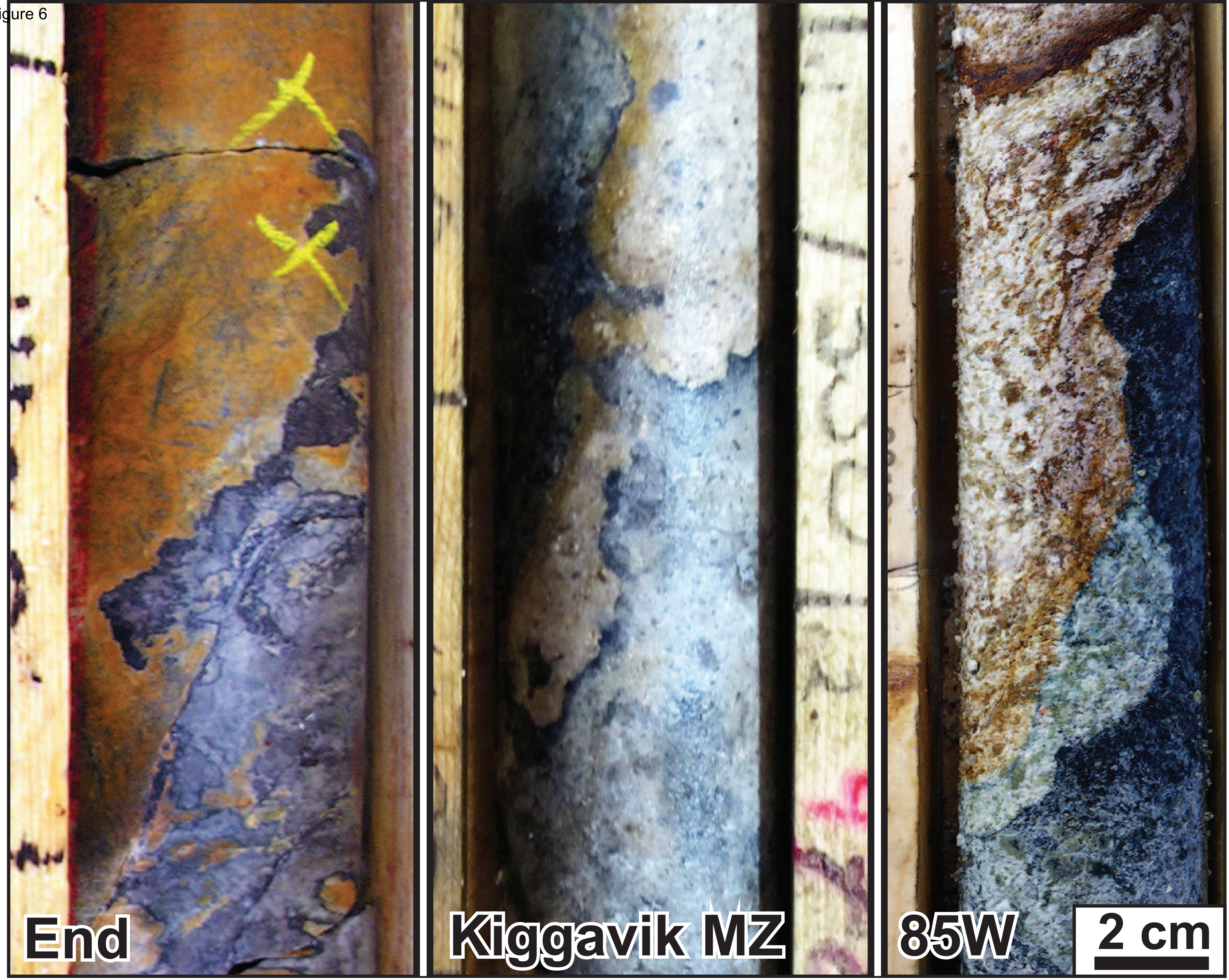

Figure 7

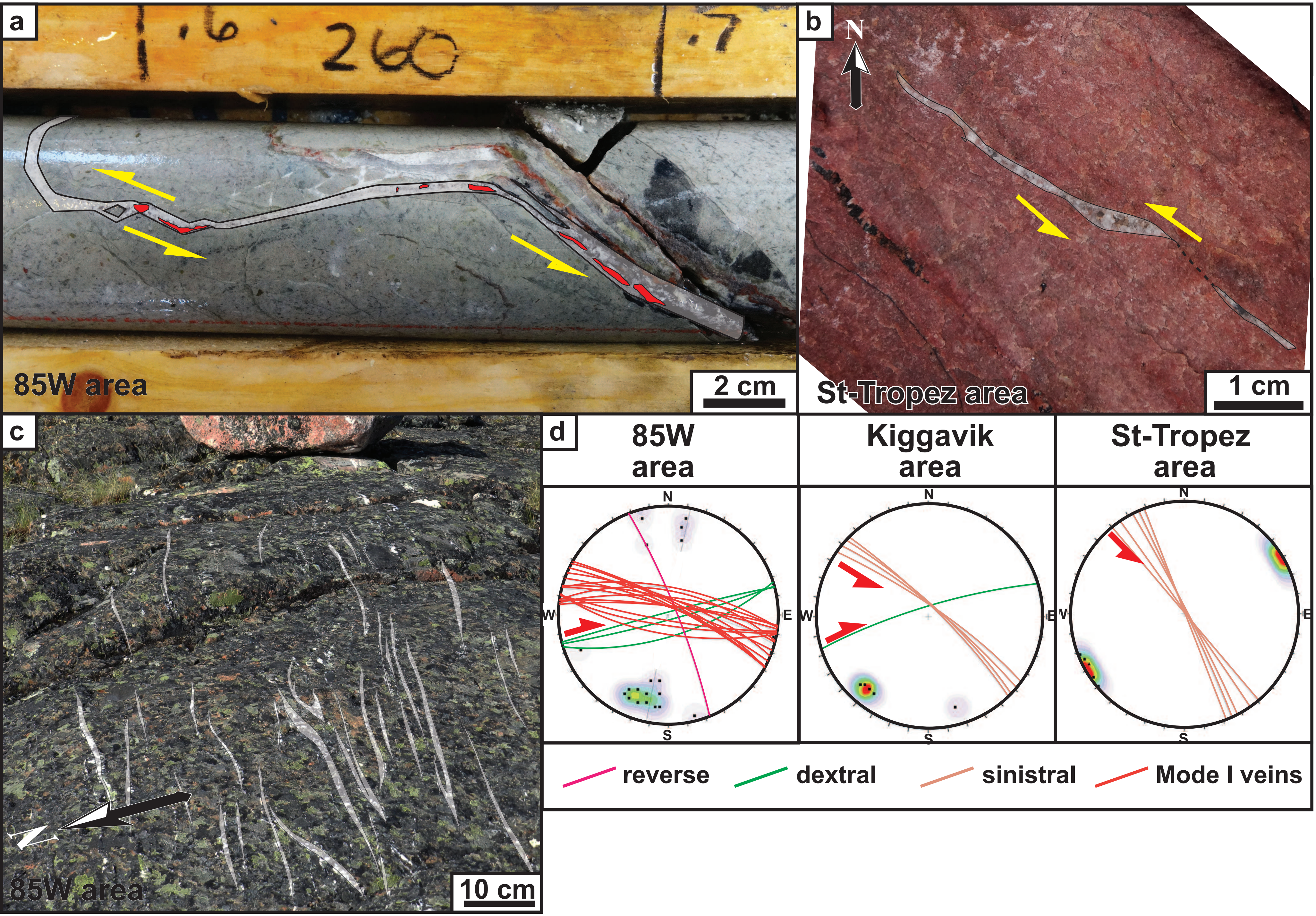

a
1.6
260
.7
85W area
2 cm
b
N
St-Tropez area
1 cm
c
85W area
10 cm
d
85W area
Kiggavik area
St-Tropez area
N
W
E
S
reverse
dextral
sinistral
Mode I veins

Figure 8

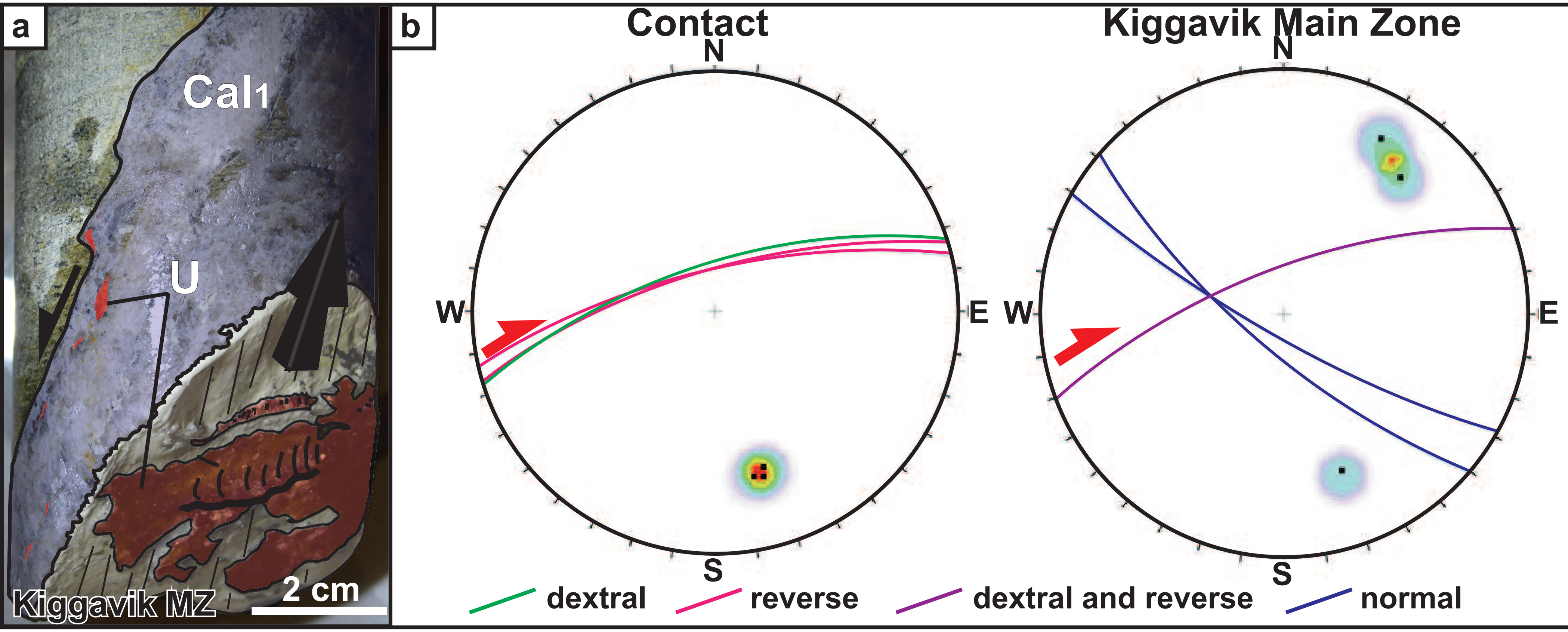

a
Cal1
U
Kiggavik MZ
2 cm
b
Contact
N
W
E
S
Kiggavik Main Zone
N
W
E
S
dextral
reverse
dextral and reverse
normal

Figure 9

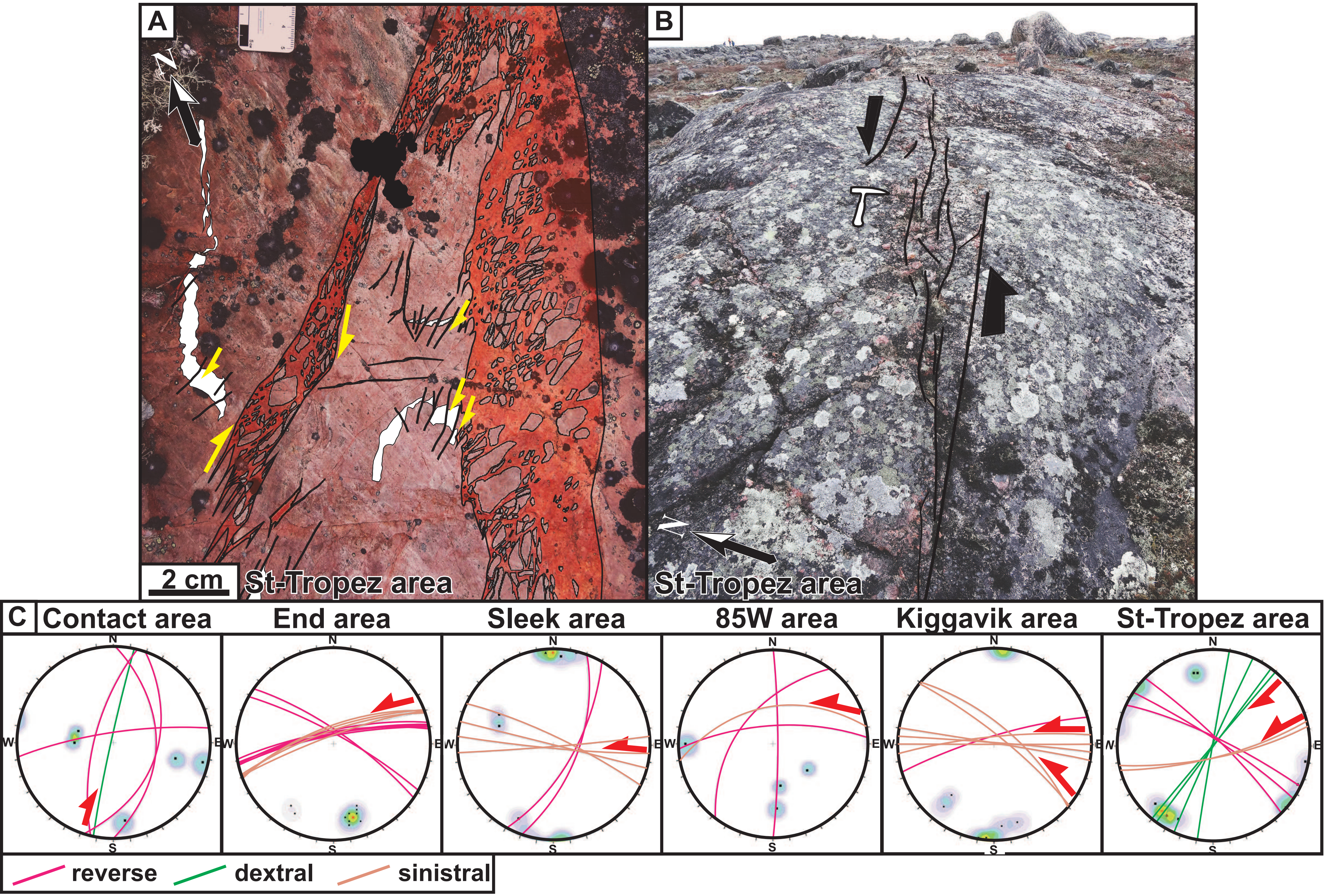

A
N
2 cm
St-Tropez area
B
St-Tropez area
C
Contact area
End area
Sleek area
85W area
Kiggavik area
St-Tropez area
N
S
W
E
reverse
dextral
sinistral

Figure 10

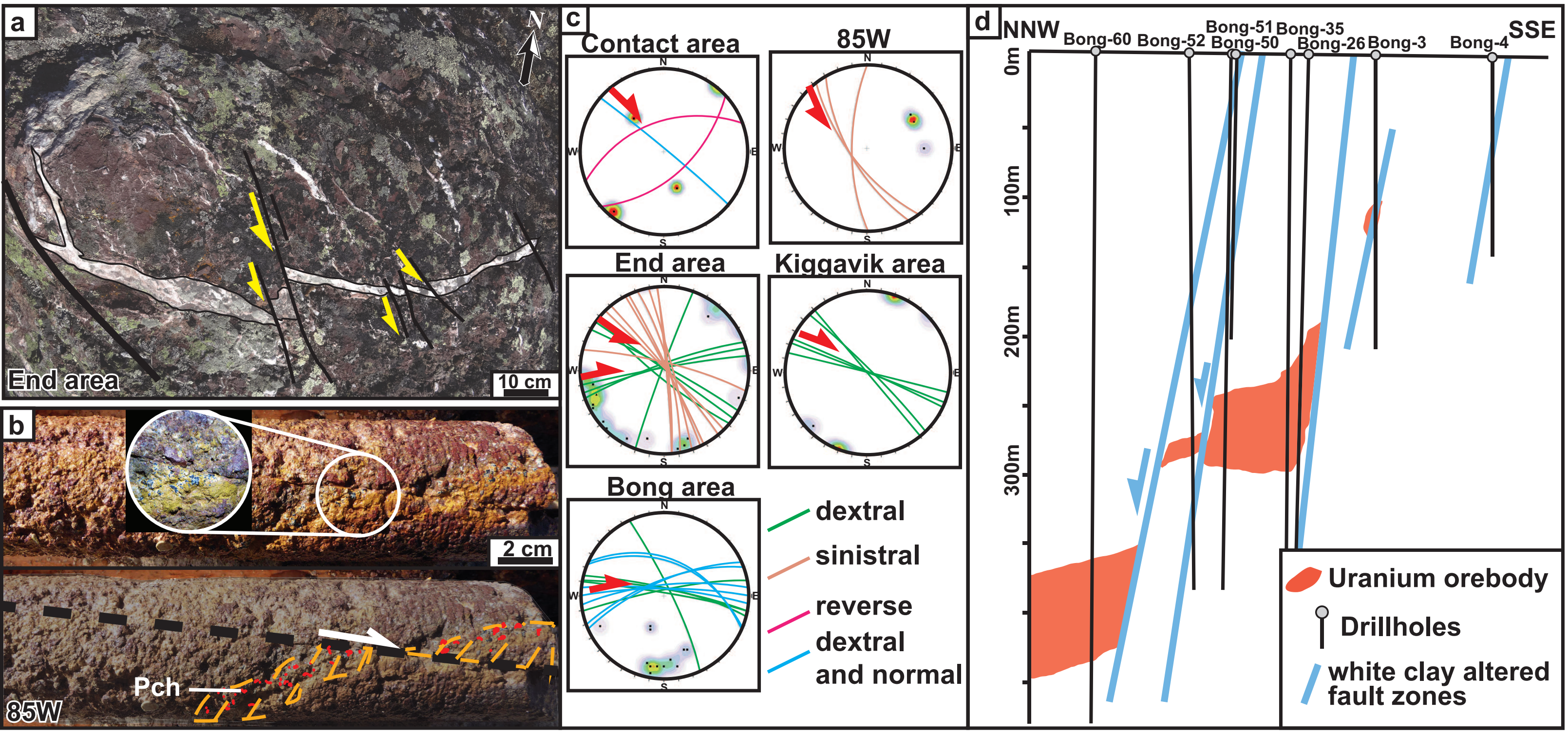

a
N
End area
10 cm
b
2 cm
Pch
85W
c
Contact area
85W
End area
Kiggavik area
Bong area
dextral
sinistral
reverse
dextral
and normal
d
NNW
SSE
Bong-60
Bong-52
Bong-51
Bong-50
Bong-35
Bong-26
Bong-3
Bong-4
0m
100m
200m
300m
Uranium orebody
Drillholes
white clay altered
fault zones

Figure 11

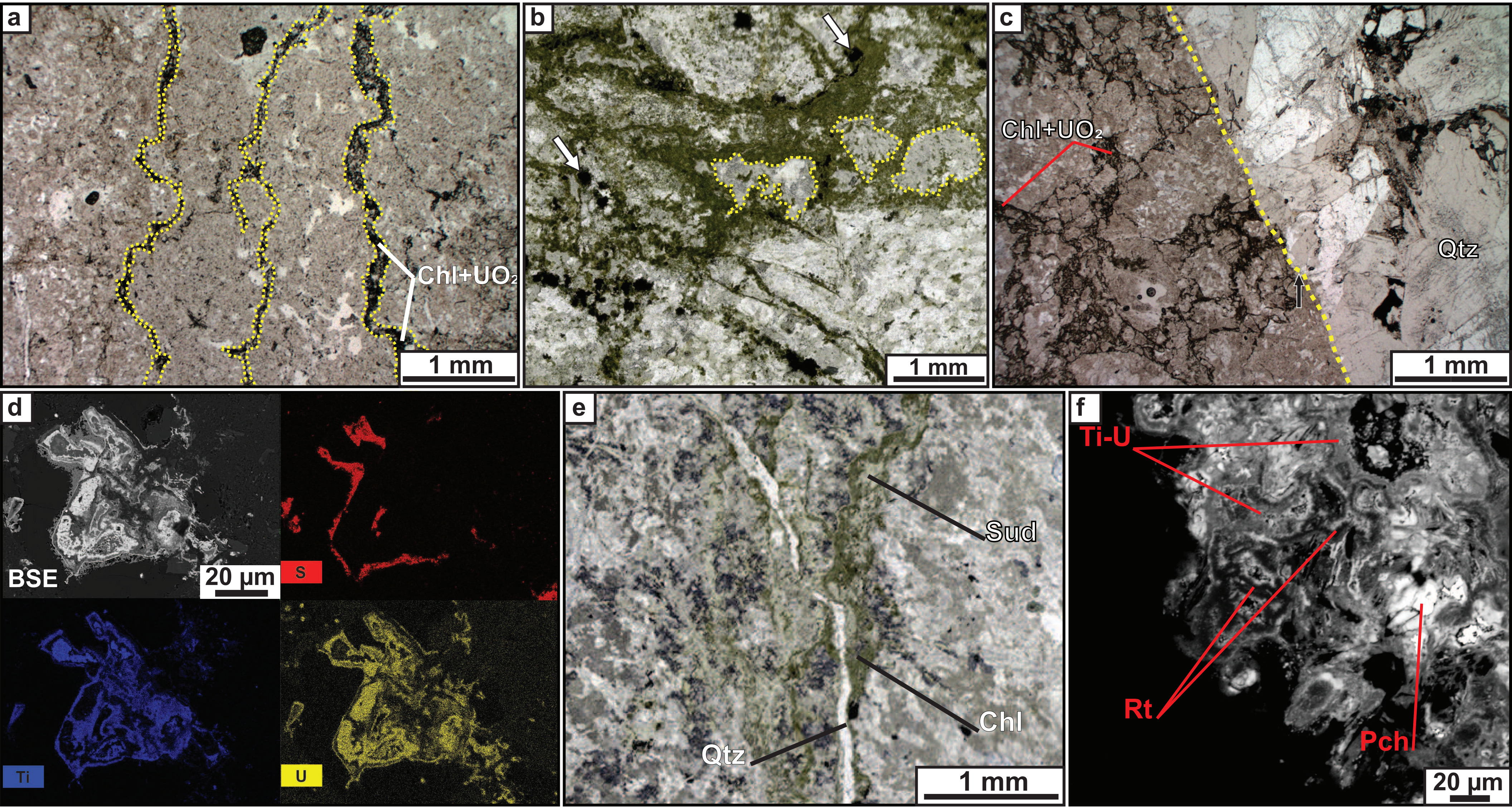
a
Chl+UO2
1 mm
b
1 mm
c
Chl+UO2
Qtz
1 mm
d
BSE
20 µm
S
Ti
U
e
Sud
Chl
Qtz
1 mm
f
Ti-U
Rt
Pch
20 µm

Figure 12

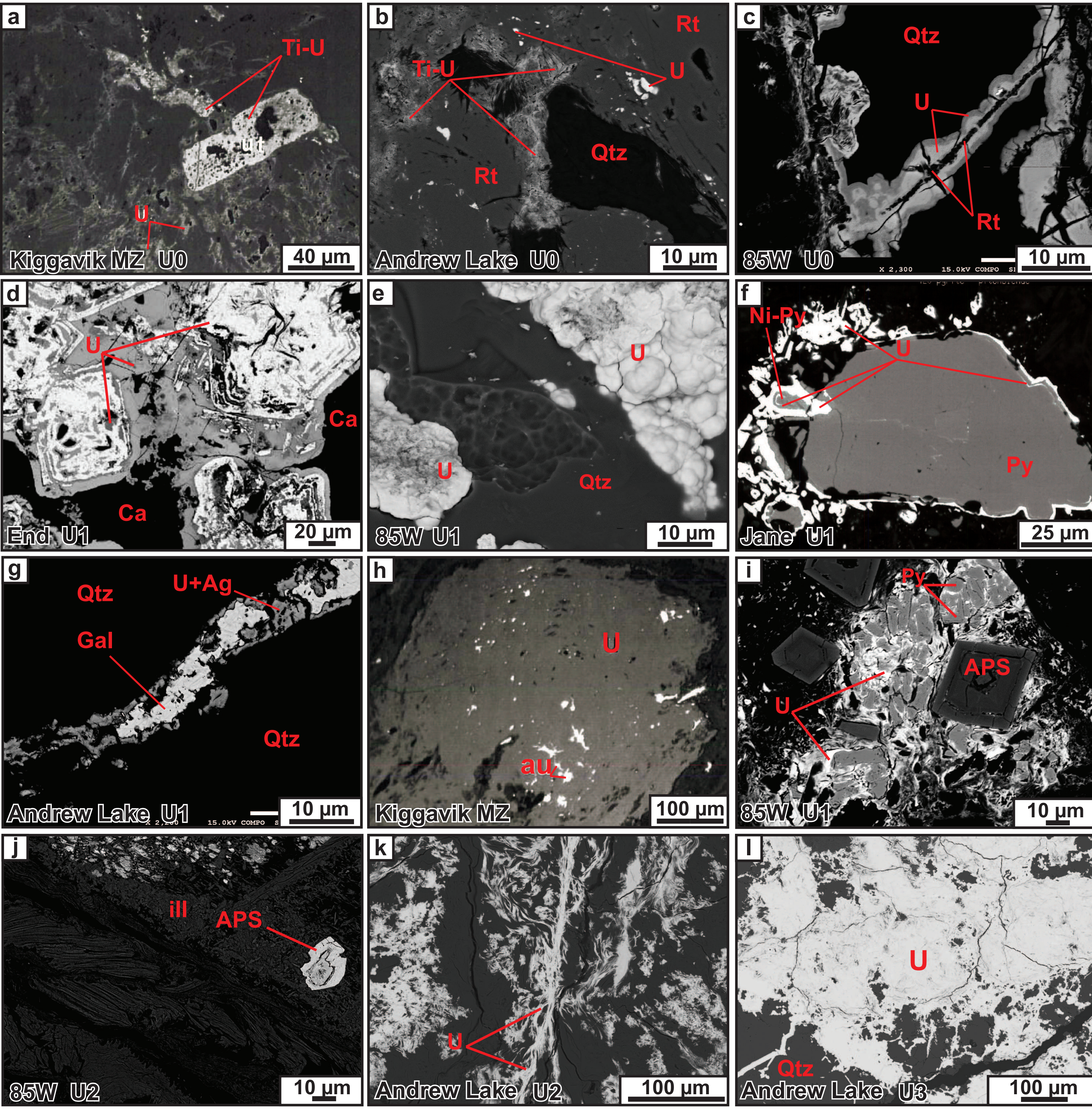
a
Ti-U
U
Kiggavik MZ U0
40 µm
b
Rt
Ti-U
U
Qtz
Rt
Andrew Lake U0
10 µm
c
Qtz
U
Rt
85W U0
10 µm
d
U
Ca
Ca
End U1
20 µm
e
U
U
Qtz
85W U1
10 µm
f
Ni-Py
U
Py
Jane U1
25 µm
g
Qtz
U+Ag
Gal
Qtz
Andrew Lake U1
10 µm
h
U
au
Kiggavik MZ
100 µm
i
Py
APS
U
85W U1
10 µm
j
ill
APS
85W U2
10 µm
k
U
Andrew Lake U2
100 µm
l
U
Qtz
Andrew Lake U3
100 µm

Figure 13

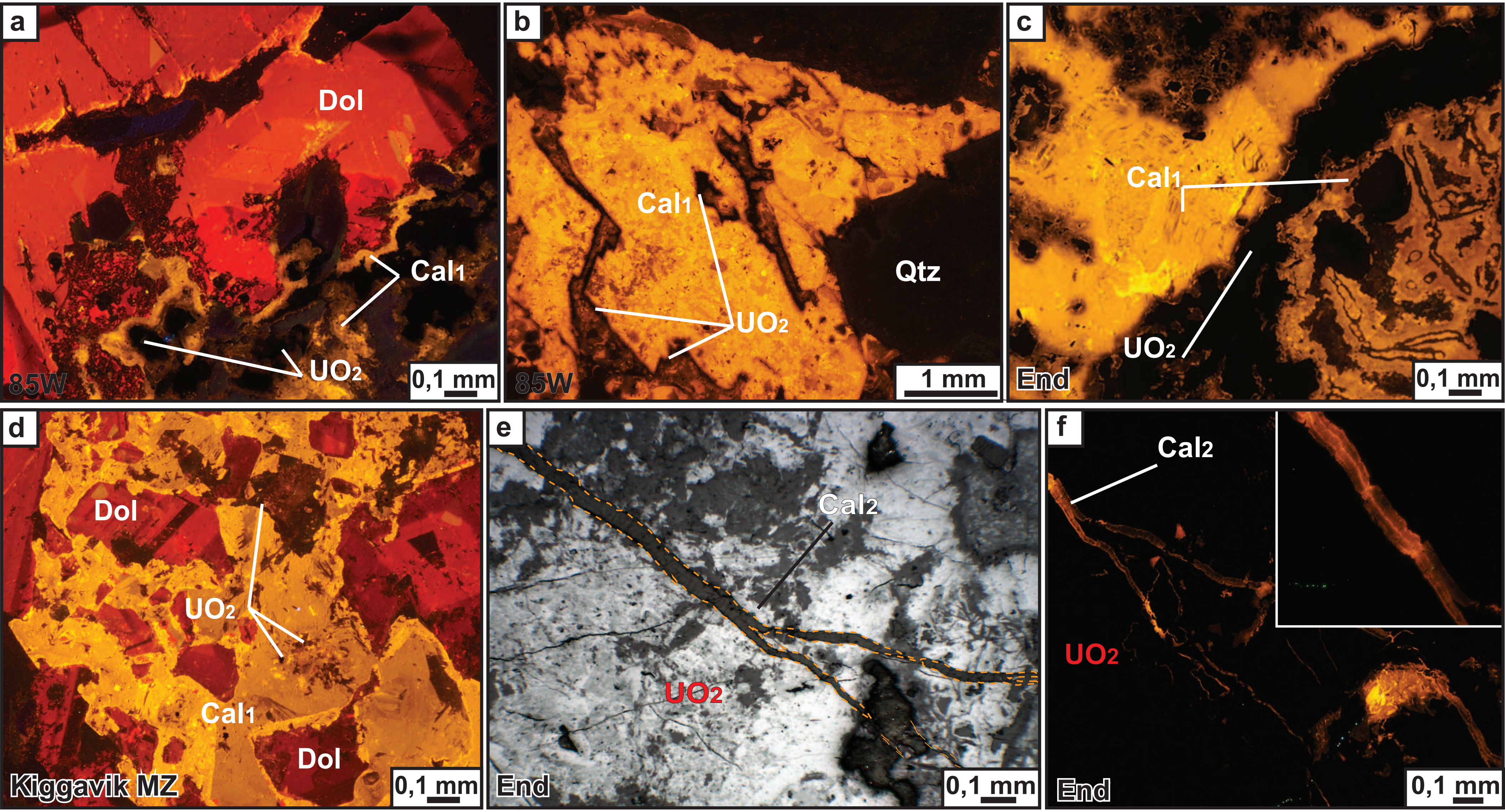
a
Dol
Cal1
UO2
85W
0,1 mm
b
Cal1
Qtz
UO2
85W
1 mm
c
Cal1
UO2
End
0,1 mm
d
Dol
UO2
Cal1
Dol
Kiggavik MZ
0,1 mm
e
Cal2
UO2
End
0,1 mm
f
Cal2
UO2
End
0,1 mm

Figure 14

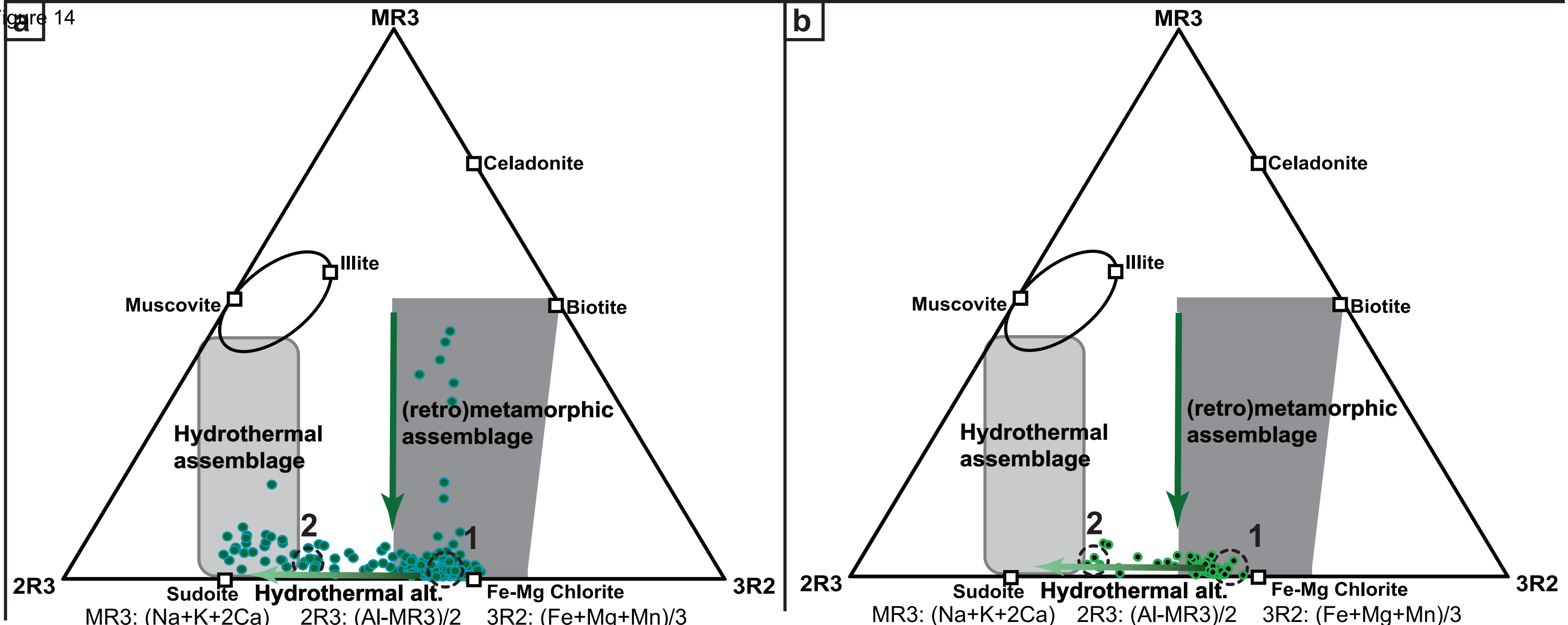

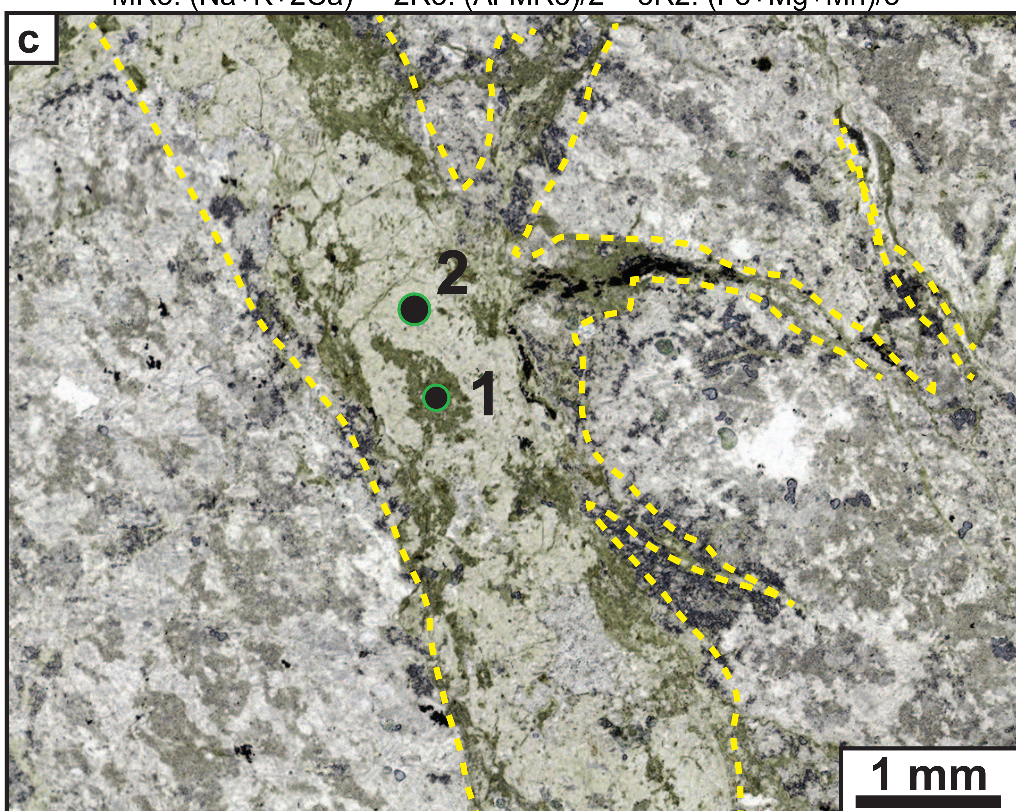

d

	Unaltered (U0) chlorite				
Sample	8561-9	8561-9	8561-9	8494-8	8548-14
Al_{total}	2,36	2,23	2,52	2,42	2,51
Al^{IV}	1,23	1,17	1,33	1,20	1,14
Al^{VI}	1,13	1,07	1,19	1,22	1,37
Mg	2,62	2,87	2,39	2,37	2,38
Fe	2,18	2,08	2,43	2,34	2,07
Occ	5,94	6,02	6,01	5,94	5,82
XFe:Fe/(Fe+Mg)	0,45	0,42	0,50	0,50	0,47
Calculated T°C of formation					
Cathelineau, 1988	333	314	366	324	306
Jowett, 1991	322	303	355	313	295
Kranidiotis, 1987	148	142	159	145	139
Zang & Fyfe, 1995	137	134	143	130	127

Figure 15

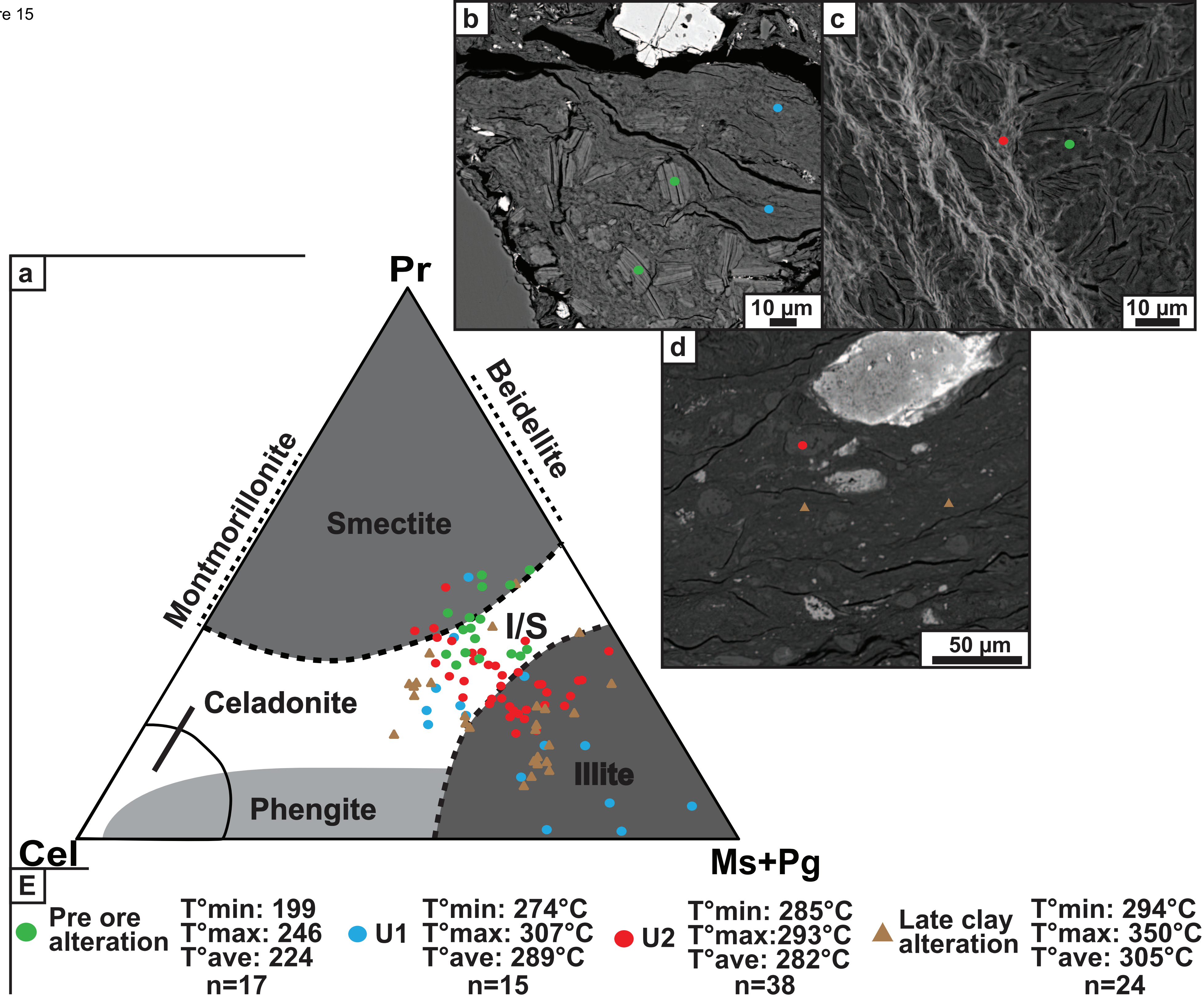
a
b
c
d
Pr
Cel
Ms+Pg
Montmorillonite
Beidellite
Smectite
I/S
Celadonite
Phengite
Illite
10 µm
10 µm
50 µm
E
Pre ore alteration
T°min: 199
T°max: 246
T°ave: 224
n=17
U1
T°min: 274°C
T°max: 307°C
T°ave: 289°C
n=15
U2
T°min: 285°C
T°max:293°C
T°ave: 282°C
n=38
Late clay alteration
T°min: 294°C
T°max: 350°C
T°ave: 305°C
n=24

Figure 16

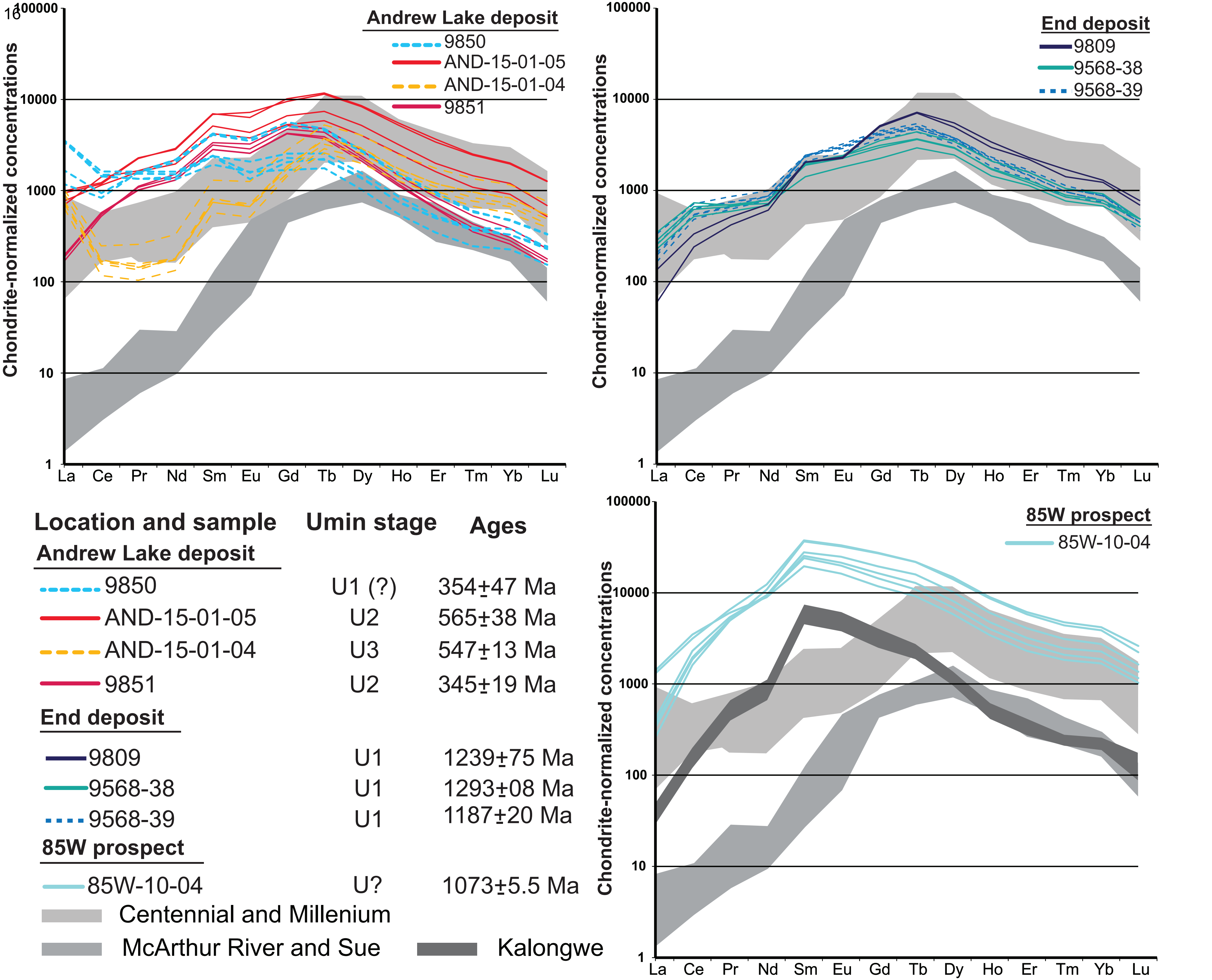
Andrew Lake deposit
9850
AND-15-01-05
AND-15-01-04
9851
End deposit
9809
9568-38
9568-39
85W prospect
85W-10-04
Chondrite-normalized concentrations
100000
10000
1000
100
10
1
La Ce Pr Nd Sm Eu Gd Tb Dy Ho Er Tm Yb Lu
Location and sample
Umin stage
Ages
Andrew Lake deposit
9850 U1 (?) 354±47 Ma
AND-15-01-05 U2 565±38 Ma
AND-15-01-04 U3 547±13 Ma
9851 U2 345±19 Ma
End deposit
9809 U1 1239±75 Ma
9568-38 U1 1293±08 Ma
9568-39 U1 1187±20 Ma
85W prospect
85W-10-04 U? 1073±5.5 Ma
Centennial and Millenium
McArthur River and Sue
Kalongwe

Figure 17

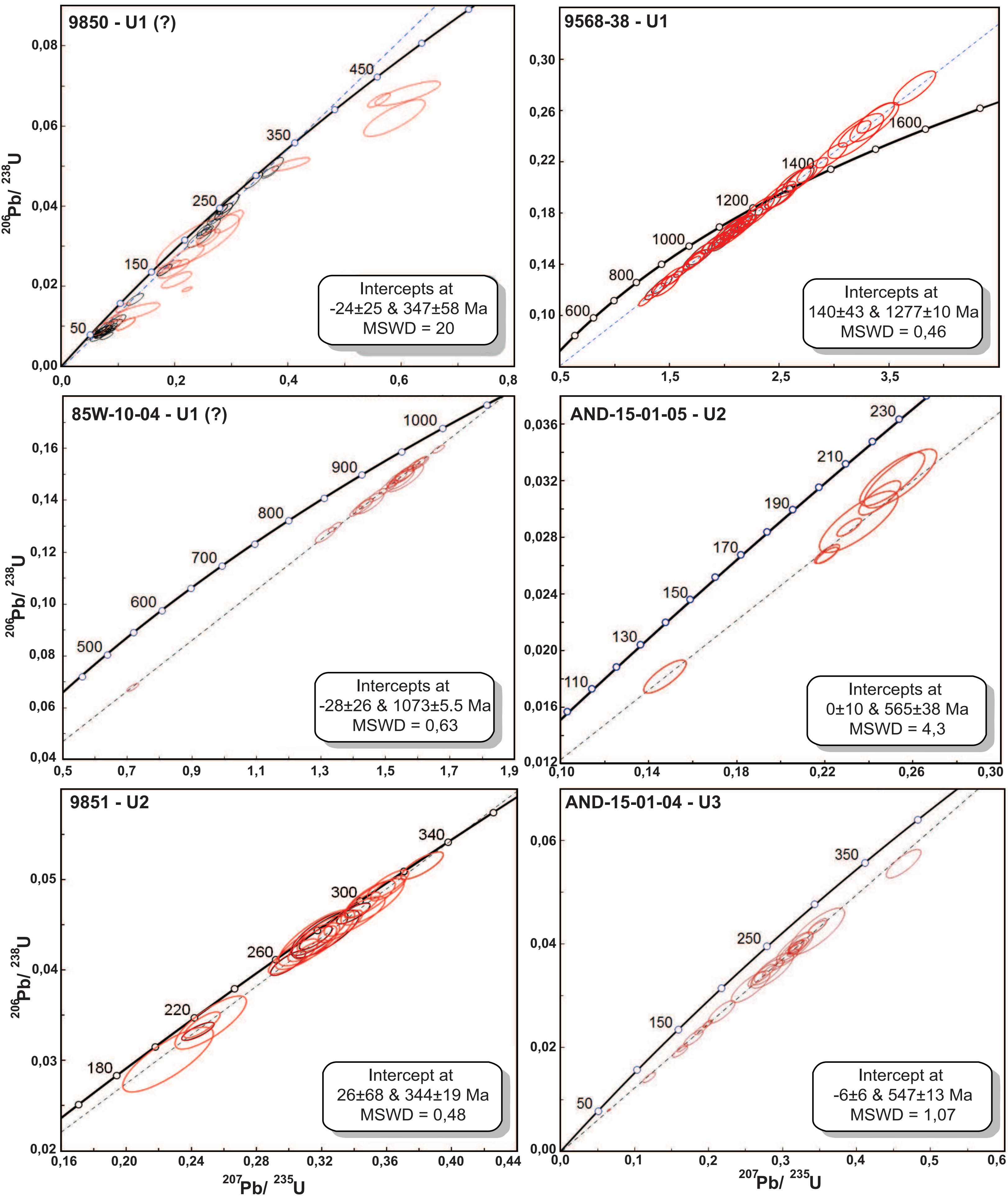
9850 - U1 (?)
Intercepts at
-24±25 & 347±58 Ma
MSWD = 20
9568-38 - U1
Intercepts at
140±43 & 1277±10 Ma
MSWD = 0,46
85W-10-04 - U1 (?)
Intercepts at
-28±26 & 1073±5.5 Ma
MSWD = 0,63
AND-15-01-05 - U2
Intercepts at
0±10 & 565±38 Ma
MSWD = 4,3
9851 - U2
Intercept at
26±68 & 344±19 Ma
MSWD = 0,48
AND-15-01-04 - U3
Intercept at
-6±6 & 547±13 Ma
MSWD = 1,07
206Pb/ 238U
207Pb/ 235U

Figure 18

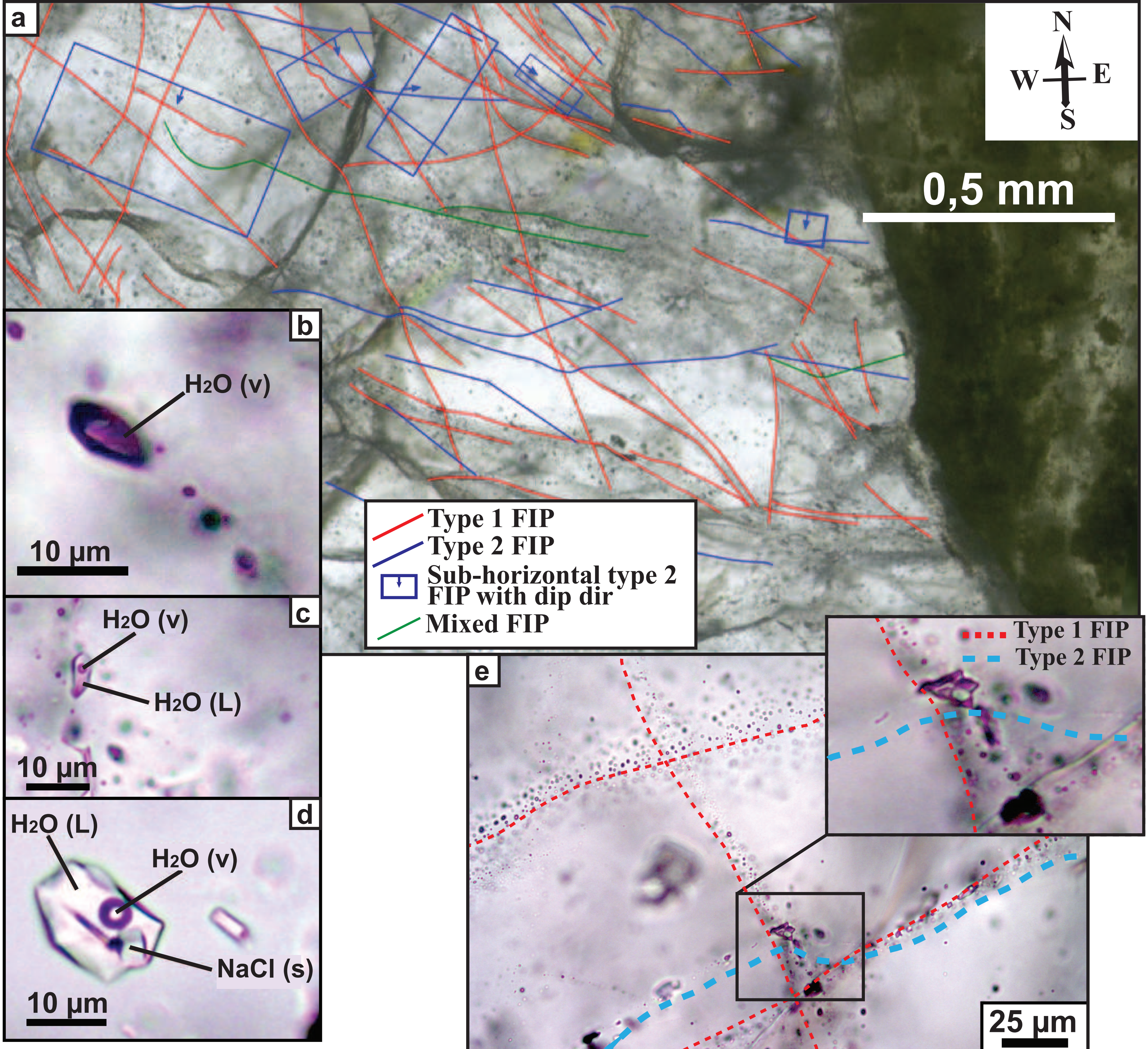

a
N
W
E
S
0,5 mm
Type 1 FIP
Type 2 FIP
Sub-horizontal type 2 FIP with dip dir
Mixed FIP
b
H2O (v)
10 µm
c
H2O (v)
H2O (L)
10 µm
d
H2O (L)
H2O (v)
NaCl (s)
10 µm
e
Type 1 FIP
Type 2 FIP
25 µm

Figure 19

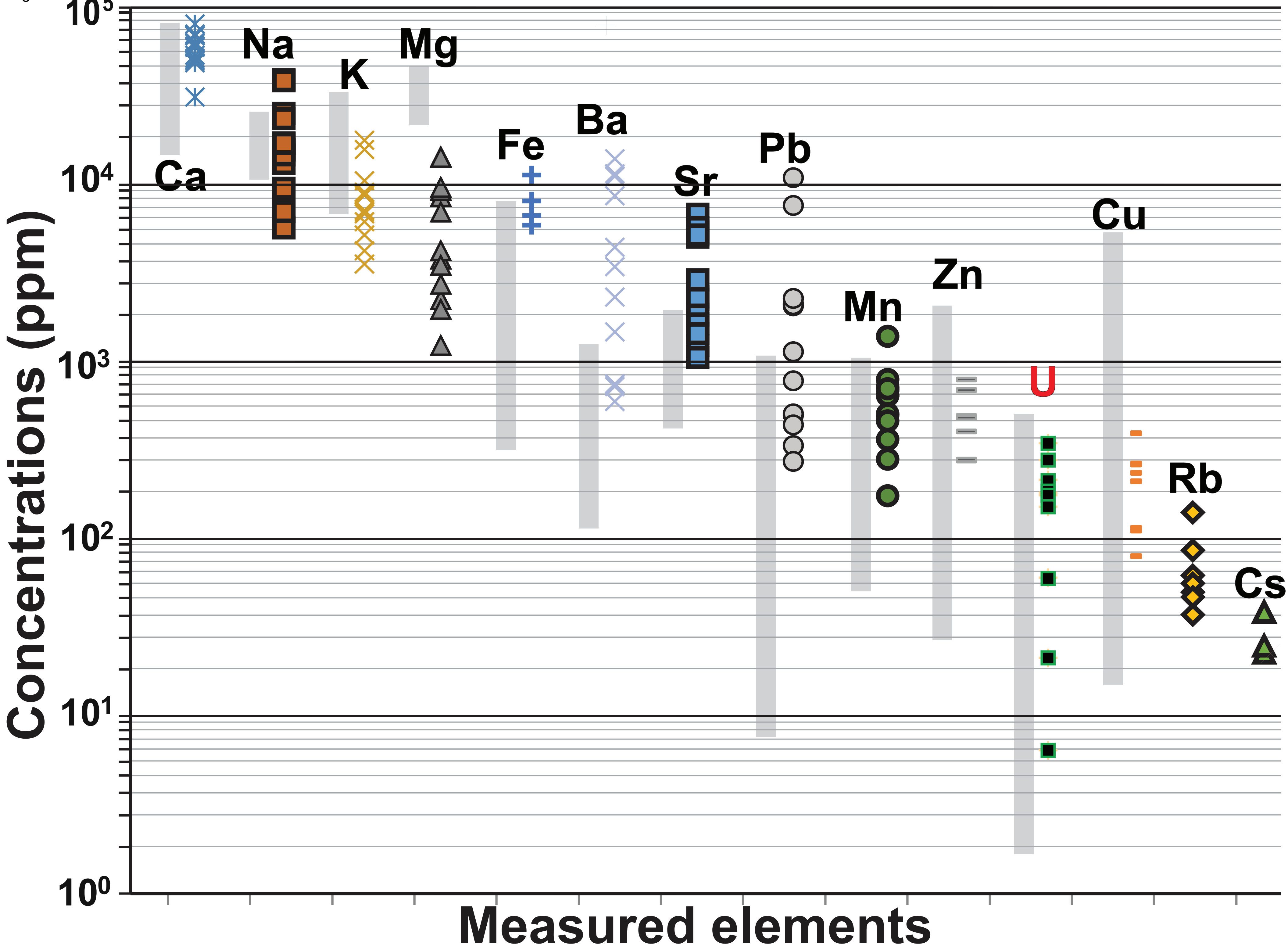

Concentrations (ppm)
10^5
10^4
10^3
10^2
10^1
10^0
Ca
Na
K
Mg
Fe
Ba
Sr
Pb
Mn
Zn
U
Cu
Rb
Cs
Measured elements

Figure 20

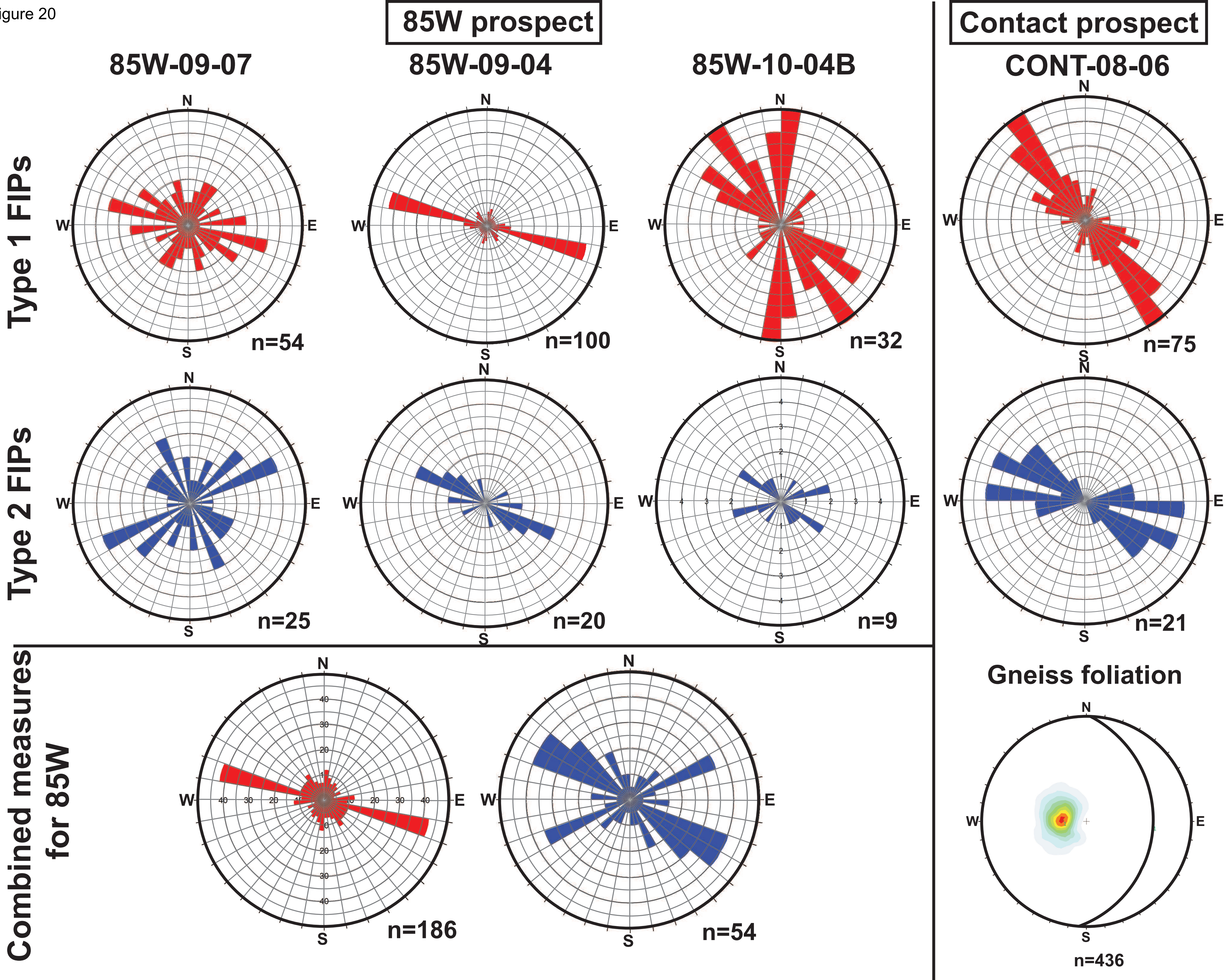
85W prospect
Contact prospect
85W-09-07
85W-09-04
85W-10-04B
CONT-08-06
Type 1 FIPs
Type 2 FIPs
Combined measures for 85W
N
S
E
W
n=54
n=100
n=32
n=75
n=25
n=20
n=9
n=21
n=186
n=54
Gneiss foliation
n=436

Figure 21

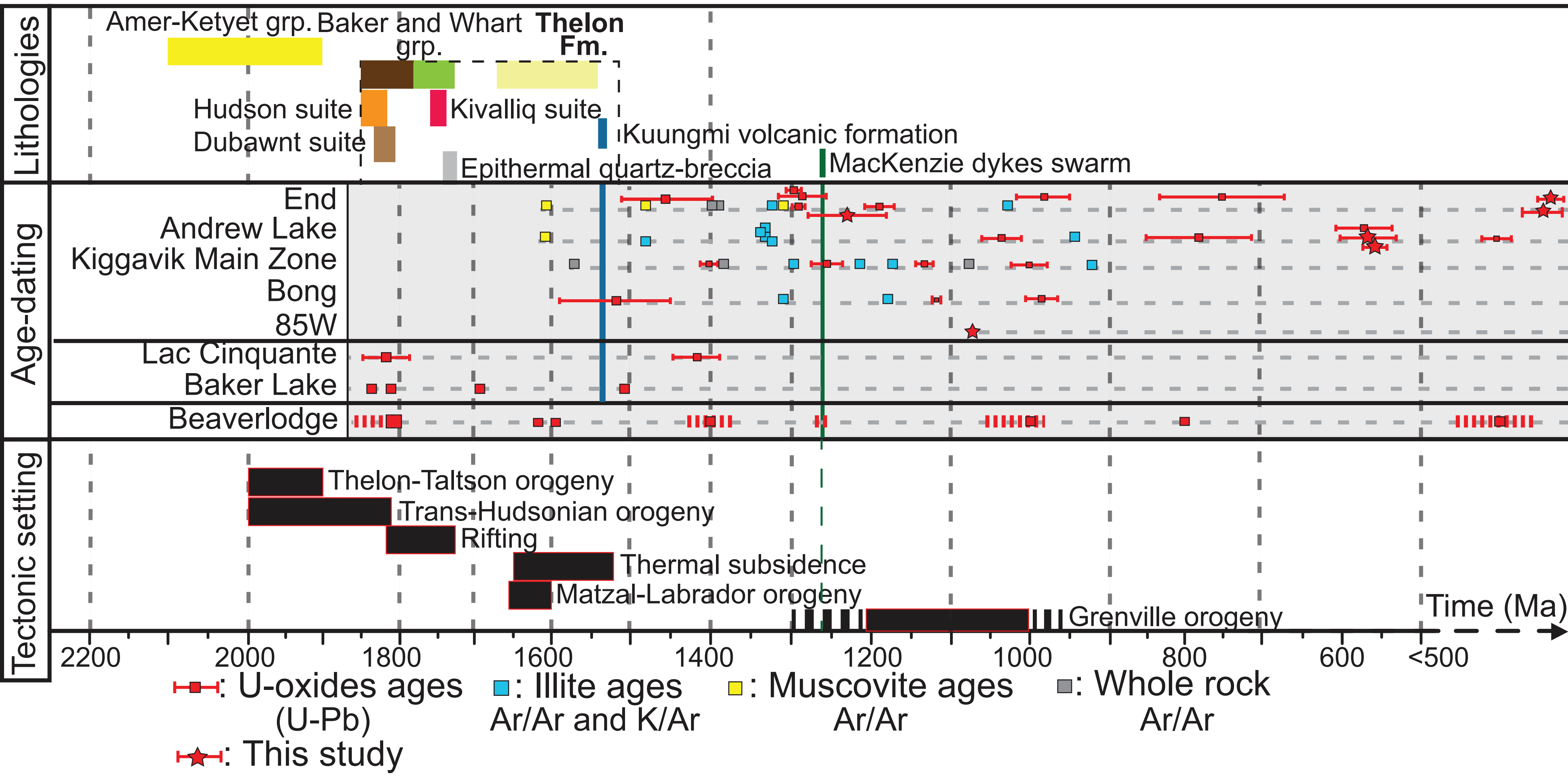
Lithologies
Amer-Ketyet grp.
Baker and Whart grp.
Thelon Fm.
Hudson suite
Kivalliq suite
Dubawnt suite
Kuungmi volcanic formation
Epithermal quartz-breccia
MacKenzie dykes swarm
Age-dating
End
Andrew Lake
Kiggavik Main Zone
Bong
85W
Lac Cinquante
Baker Lake
Beaverlodge
Tectonic setting
Thelon-Taltson orogeny
Trans-Hudsonian orogeny
Rifting
Thermal subsidence
Matzal-Labrador orogeny
Grenville orogeny
Time (Ma)
2200
2000
1800
1600
1400
1200
1000
800
600
<500
: U-oxides ages (U-Pb)
: Illite ages Ar/Ar and K/Ar
: Muscovite ages Ar/Ar
: Whole rock Ar/Ar
: This study

Figure 22

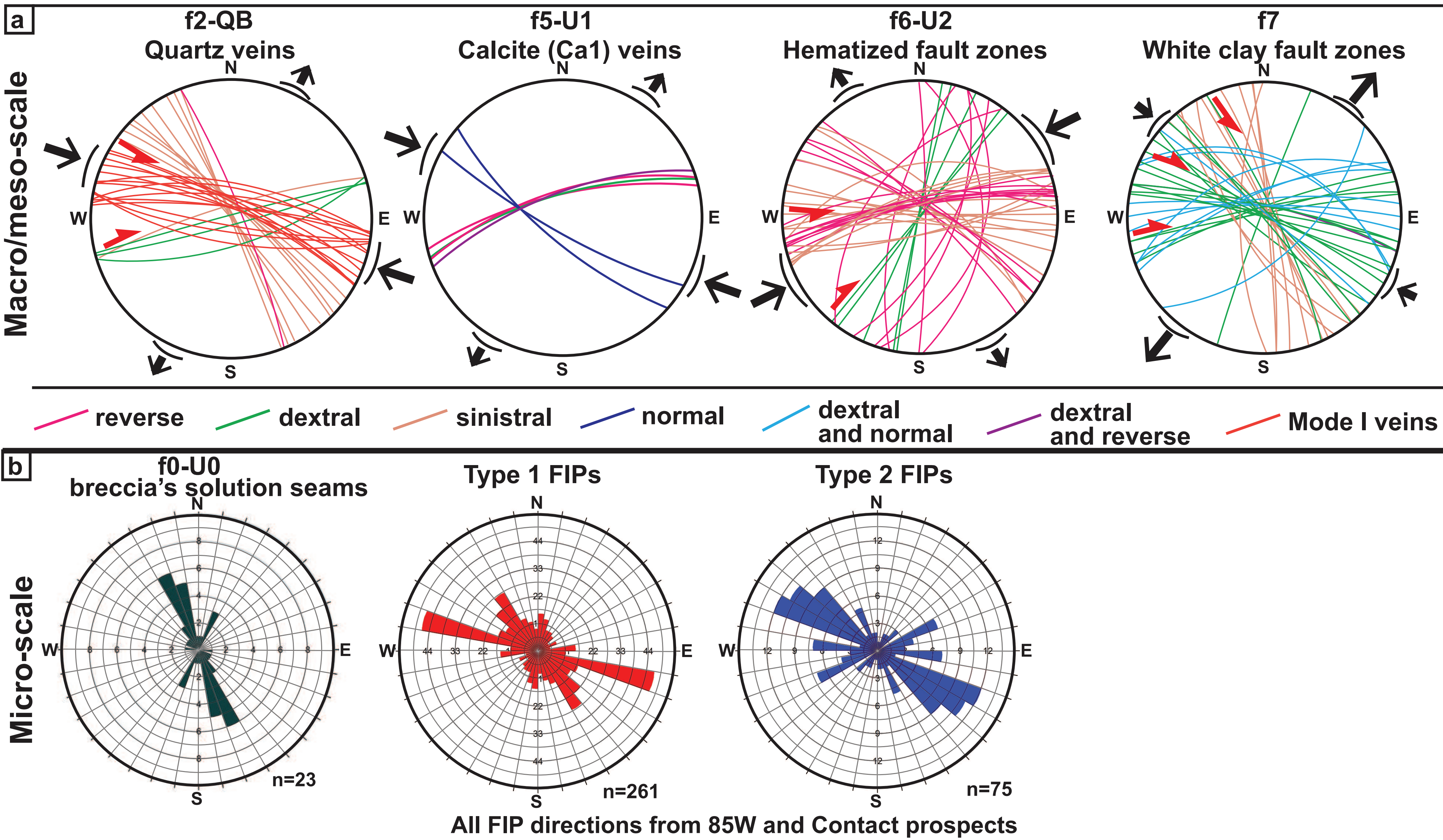
a
f2-QB
Quartz veins
f5-U1
Calcite (Ca1) veins
f6-U2
Hematized fault zones
f7
White clay fault zones
N
S
E
W
Macro/meso-scale
reverse
dextral
sinistral
normal
dextral and normal
dextral and reverse
Mode I veins
b
f0-U0
breccia's solution seams
Type 1 FIPs
Type 2 FIPs
Micro-scale
n=23
n=261
n=75
All FIP directions from 85W and Contact prospects

Figure 23

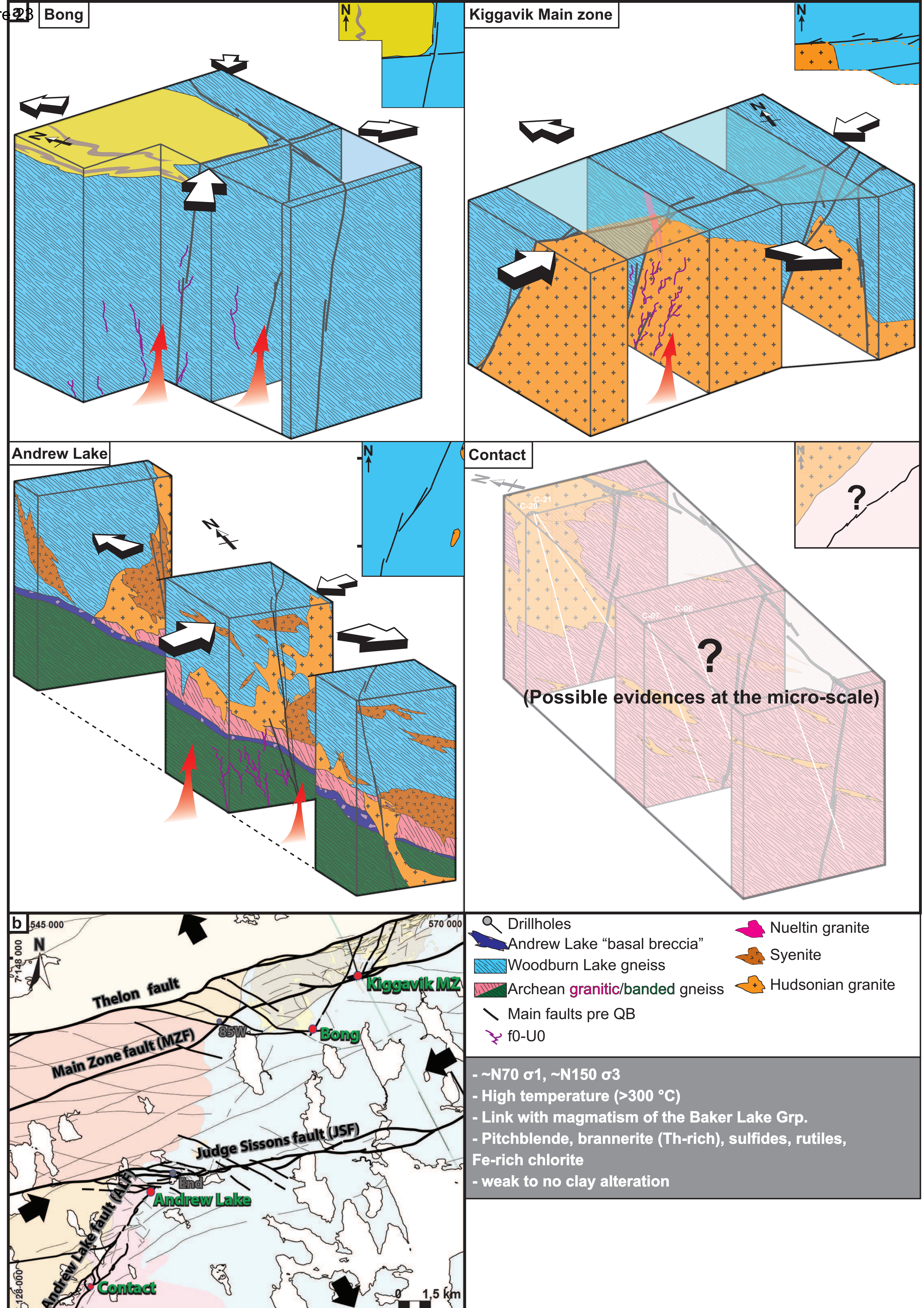
a
Bong
N
Kiggavik Main zone
N
Andrew Lake
N
Contact
N
?
C-20
C-21
?
(Possible evidences at the micro-scale)
b
545 000
570 000
7 148 000
7 128 000
N
Thelon fault
Kiggavik MZ
85W
Bong
Main Zone fault (MZF)
Judge Sissons fault (JSF)
End
Andrew Lake
Andrew Lake fault (ALF)
Contact
0
1,5 km
Drillholes
Andrew Lake "basal breccia"
Woodburn Lake gneiss
Archean granitic/banded gneiss
Main faults pre QB
f0-U0
Nueltin granite
Syenite
Hudsonian granite
- ~N70 σ1, ~N150 σ3
- High temperature (>300 °C)
- Link with magmatism of the Baker Lake Grp.
- Pitchblende, brannerite (Th-rich), sulfides, rutiles, Fe-rich chlorite
- weak to no clay alteration

Figure 24

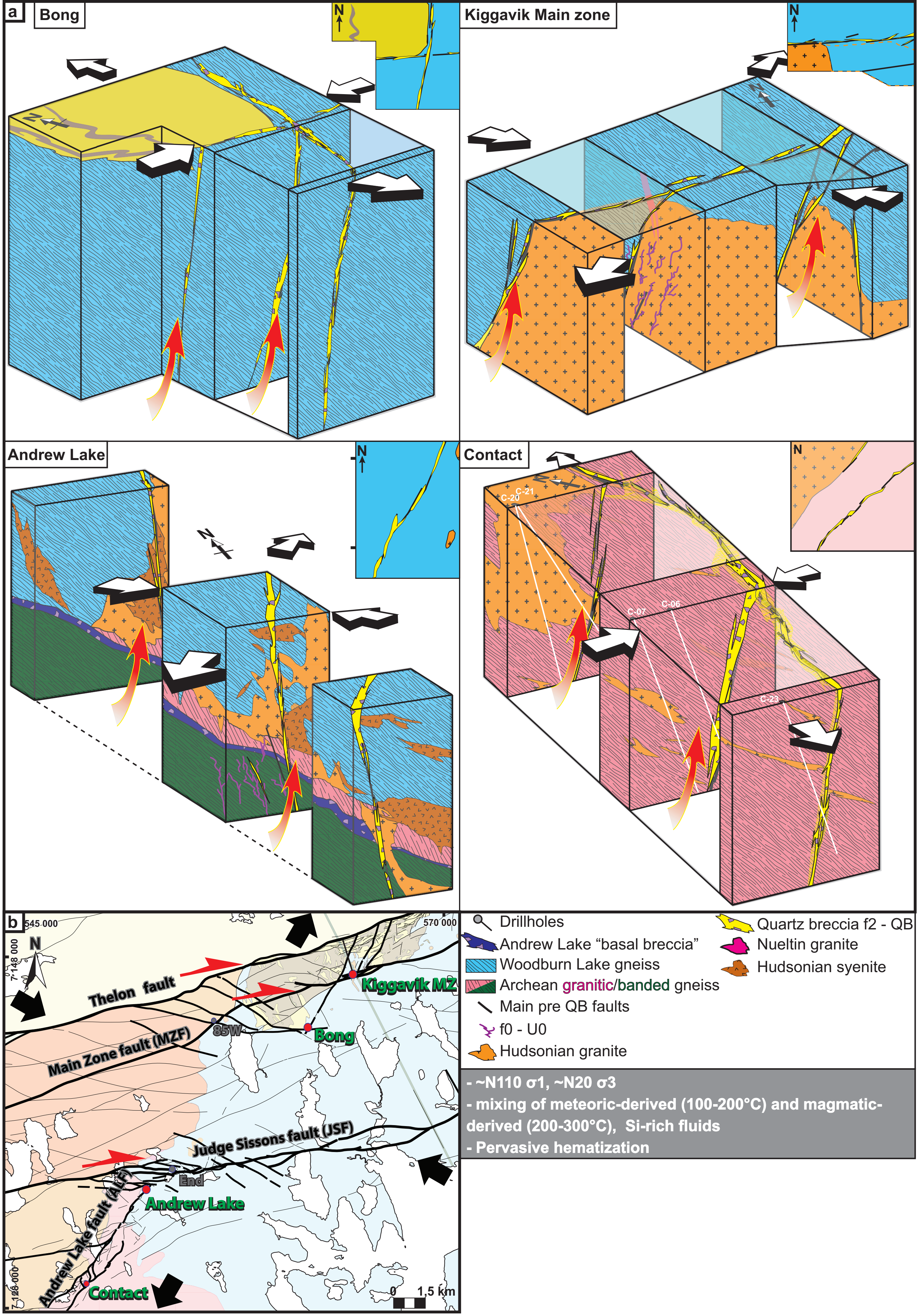

a
Bong
Kiggavik Main zone
Andrew Lake
Contact
N
C-20
C-21
C-07
C-06
C-23
b
545 000
570 000
7 148 000
7 128 000
Thelon fault
Main Zone fault (MZF)
85W
Bong
Kiggavik MZ
Judge Sissons fault (JSF)
End
Andrew Lake
Andrew Lake fault (ALF)
Contact
0
1,5 km
Drillholes
Andrew Lake "basal breccia"
Woodburn Lake gneiss
Archean granitic/banded gneiss
Main pre QB faults
f0 - U0
Hudsonian granite
Quartz breccia f2 - QB
Nueltin granite
Hudsonian syenite
- ~N110 σ1, ~N20 σ3
- mixing of meteoric-derived (100-200°C) and magmatic-derived (200-300°C), Si-rich fluids
- Pervasive hematization

Figure 25

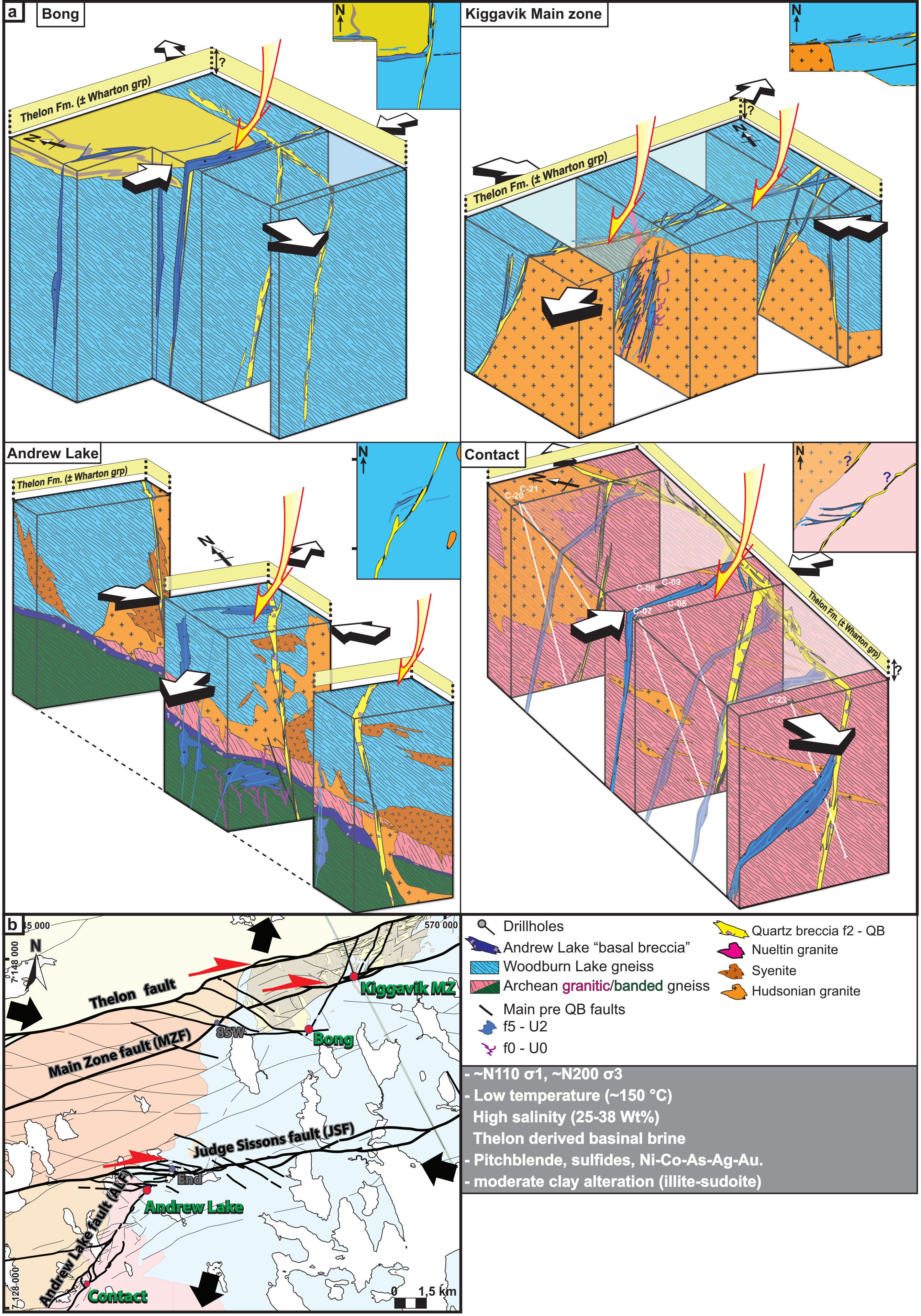

a
Bong
Thelon Fm. (± Wharton grp)
?
N
Kiggavik Main zone
Thelon Fm. (± Wharton grp)
Andrew Lake
Thelon Fm. (± Wharton grp)
Contact
C-21
C-20
C-08
C-09
C-07
C-06
C-23
Thelon Fm. (± Wharton grp)
b
545 000
570 000
7 148 000
7 128 000
Thelon fault
Kiggavik MZ
85W
Bong
Main Zone fault (MZF)
Judge Sissons fault (JSF)
End
Andrew Lake
Andrew Lake fault (ALF)
Contact
0
1,5 km
Drillholes
Andrew Lake "basal breccia"
Woodburn Lake gneiss
Archean granitic/banded gneiss
Main pre QB faults
f5 - U2
f0 - U0
Quartz breccia f2 - QB
Nueltin granite
Syenite
Hudsonian granite
- ~N110 σ1, ~N200 σ3
- Low temperature (~150 °C)
High salinity (25-38 Wt%)
Thelon derived basinal brine
- Pitchblende, sulfides, Ni-Co-As-Ag-Au.
- moderate clay alteration (illite-sudoite)

Figure 26

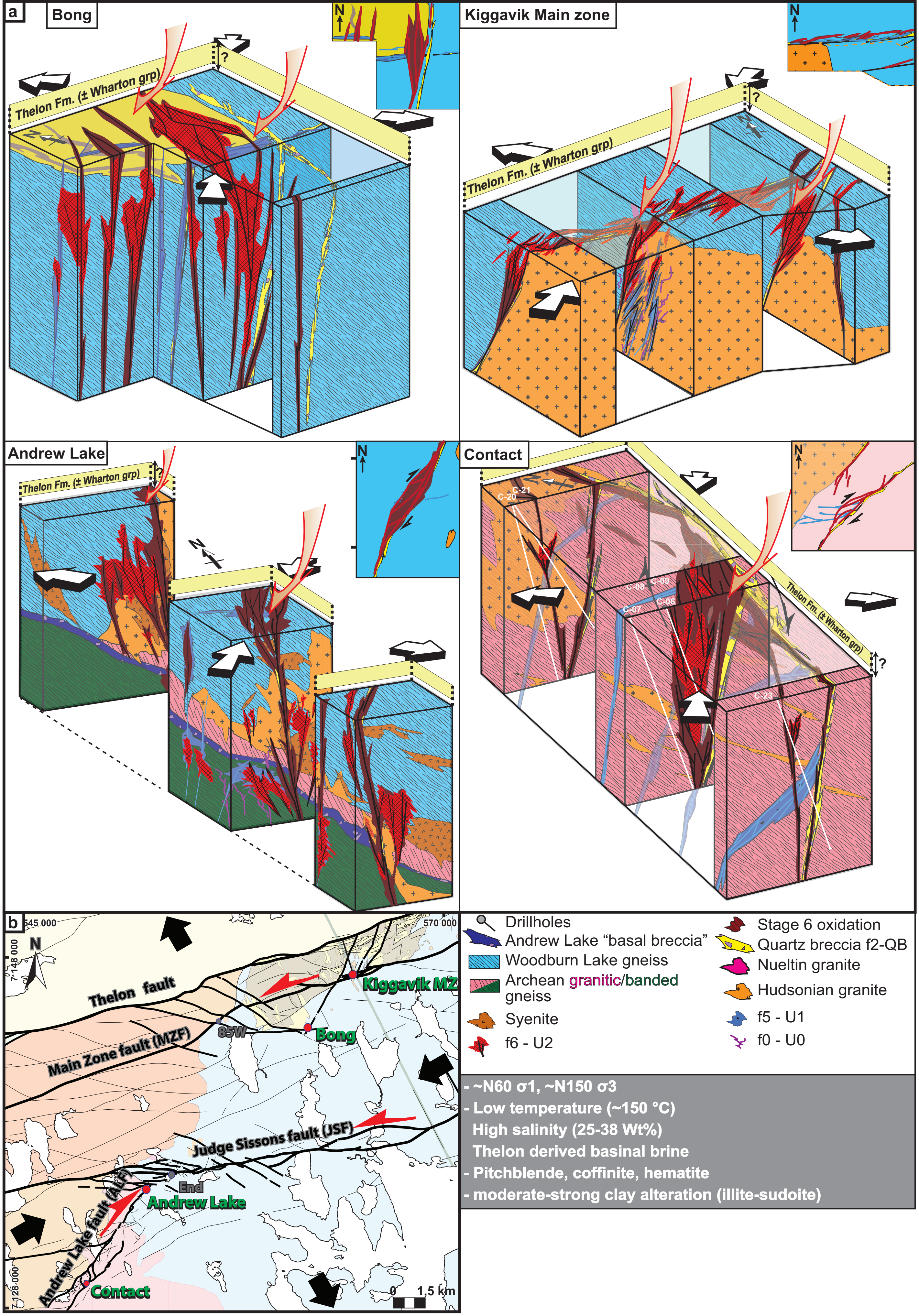
a
Bong
Thelon Fm. (± Wharton grp)
Kiggavik Main zone
Thelon Fm. (± Wharton grp)
Andrew Lake
Thelon Fm. (± Wharton grp)
Contact
Thelon Fm. (± Wharton grp)
C-20
C-21
C-08
C-09
C-07
C-06
C-23
b
545 000
570 000
7 148 000
7 128 000
N
Thelon fault
Kiggavik MZ
85W
Bong
Main Zone fault (MZF)
Judge Sissons fault (JSF)
End
Andrew Lake
Andrew Lake fault (ALF)
Contact
0
1,5 km
Drillholes
Andrew Lake "basal breccia"
Woodburn Lake gneiss
Archean granitic/banded gneiss
Syenite
f6 - U2
Stage 6 oxidation
Quartz breccia f2-QB
Nueltin granite
Hudsonian granite
f5 - U1
f0 - U0
- ~N60 σ1, ~N150 σ3
- Low temperature (~150 °C)
High salinity (25-38 Wt%)
Thelon derived basinal brine
- Pitchblende, coffinite, hematite
- moderate-strong clay alteration (illite-sudoite)

Figure 27

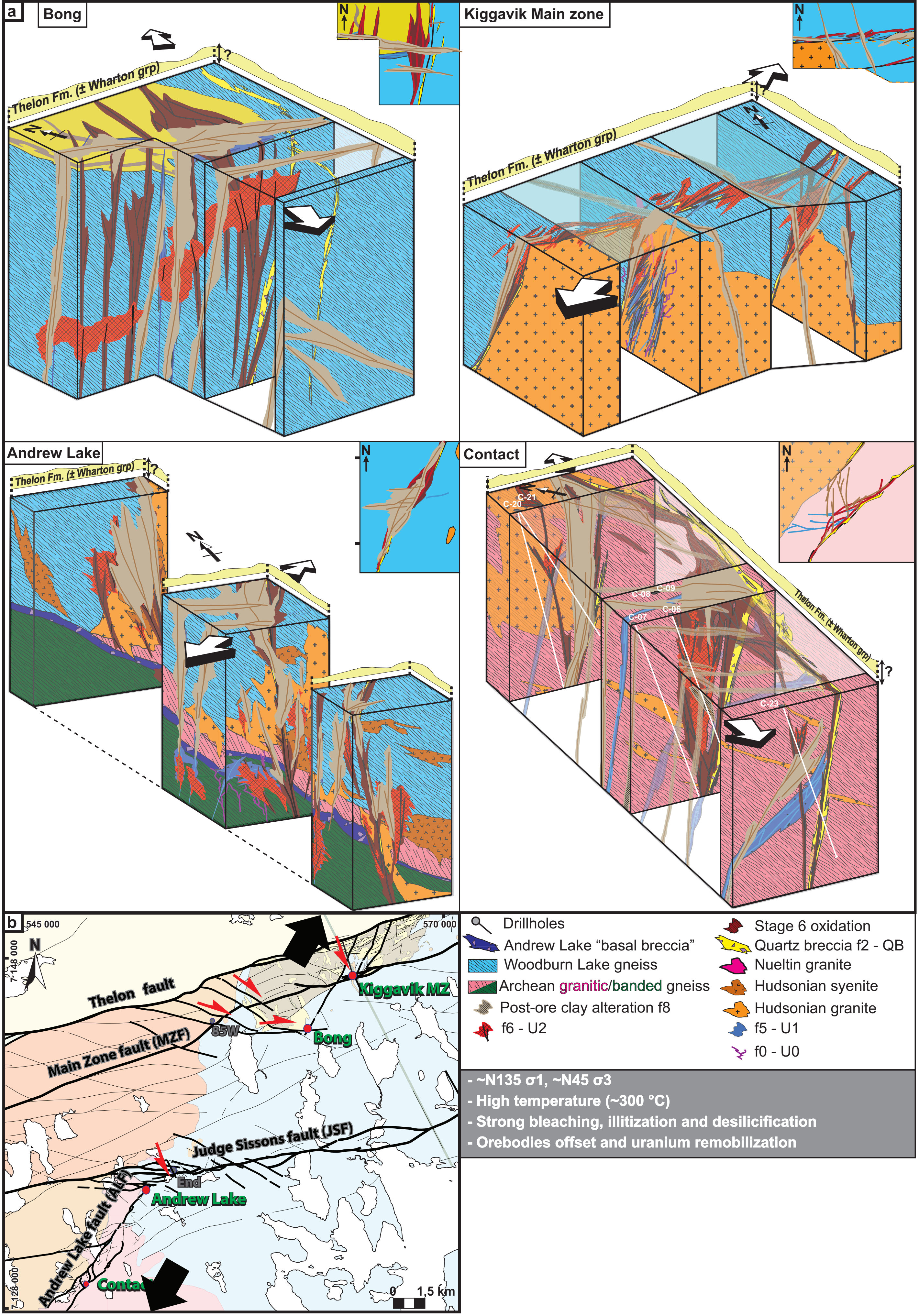
a
Bong
Thelon Fm. (± Wharton grp)
?
N
Kiggavik Main zone
Thelon Fm. (± Wharton grp)
?
N
Andrew Lake
Thelon Fm. (± Wharton grp)
?
N
Contact
C-21
C-20
C-08
C-09
C-07
C-06
C-23
Thelon Fm. (± Wharton grp)
?
N
b
545 000
570 000
7 148 000
7 128 000
Thelon fault
Kiggavik MZ
85W
Bong
Main Zone fault (MZF)
Judge Sissons fault (JSF)
End
Andrew Lake
Andrew Lake fault (ALF)
Contact
0
1,5 km
Drillholes
Andrew Lake "basal breccia"
Woodburn Lake gneiss
Archean granitic/banded gneiss
Post-ore clay alteration f8
f6 - U2
Stage 6 oxidation
Quartz breccia f2 - QB
Nueltin granite
Hudsonian syenite
Hudsonian granite
f5 - U1
f0 - U0
- ~N135 σ1, ~N45 σ3
- High temperature (~300 °C)
- Strong bleaching, illitization and desilicification
- Orebodies offset and uranium remobilization

Supplementary Material 1

Click here to access/download
Supplementary Material
ESM_1.docx

Supplementary Material 2

Click here to access/download
Supplementary Material
ESM_2.docx